Report No. 46

Columbia University
in the City of New York

THE INTERACTION OF A SATELLITE WITH THE IONOSPHERE

by
Stephen M. Call

1969

PLASMA LABORATORY
SCHOOL OF ENGINEERING AND APPLIED SCIENCE
NEW YORK 27, N.Y.

THE INTERACTION OF A SATELLITE WITH THE IONOSPHERE

by
Stephen M. Call
1969

Plasma Laboratory
Report No. 46
School of Engineering and Applied Science
Columbia University
New York, N.Y. 10027

NGR-33-008-007

This research was supported by the National Aeronautics and Space Administration under Contract ~~NsG 302-63~~, and by the Air Force Office of Scientific Research under Contract AF 49(638)-1634.

ABSTRACT

The interaction of a satellite with the ionosphere is studied by solving numerically the Poisson-Vlasov system of equations. The self-consistent electric field is obtained by means of an iteration technique which cycles between the ion density and potential calculations. The current-voltage characteristics are computed as functions of satellite velocity, ion mass, electron temperature, and satellite shape and size. The size of the satellite studied varies over a range extending from 0.2 to 25 Debye lengths. The floating potential and the plasma drag of the satellite are obtained. In addition, the angular distribution of the ion current to a cylindrical satellite is obtained. The detailed structure of the wake is investigated. In particular, the wake length and ion focusing in the wake are studied. The satellite interaction with the ionosphere is examined without the effect of an ambient magnetic field. This interaction is then restudied by considering the inclusion of a uniform magnetic field. It is shown that a magnetic field oriented parallel to the flow velocity has a much greater influence on the subsequent motion of the ions in the wake than a field of equal magnitude oriented perpendicular to the flow velocity.

to Gloria

ACKNOWLEDGEMENT

The author would like to thank Professor Robert A. Gross, Director of the Plasma Physics Laboratory, for suggesting this problem and for his continued guidance and encouragement throughout the course of the research.

To Professor C. K. Chu, Professor R. T. Taussig, and Dr. G. K. Medicus special appreciation is expressed for their many valuable suggestions. The author would also like to acknowledge the many useful discussions he has had with Mr. J. G. Bede. His thanks go also to Mrs. W. E. Whitaker for her excellent editing, Miss M. Strong for her typing, Mr. W. Lewis and his staff for their drafting of the figures, and the Goddard Institute for Space Studies for making its computer facilities available.

A special tribute is due to my wife, Gloria, for her constant support.

The author is grateful to the National Aeronautics and Space Administration (Contract # NsG 302-63) and the Air Force Office of Scientific Research [Contract # AF 49(638)-1634] whose financial support made this research possible.

TABLE OF CONTENTS

CHAPTER I: INTRODUCTION

A. Properties of the Interaction of a Satellite with the Ionosphere

1. Statement of the Problem

The launching of artificial satellites into the earth's ionosphere has created interest in the problem of predicting the interaction of a moving body with the ionospheric plasma. When interparticle collisions are negligible, the steady flow of the plasma around the body is described by the Poisson-Vlasov system of equations. Poisson's equation relates the electric field to the net charge density of the disturbed plasma, and the Vlasov equation describes the distribution functions of the charged particles in an electromagnetic force field. These equations constitute a nonlinear integro-differential system which is of sufficient complexity to require a numerical rather than an analytical solution.

2. Environmental Data of the Ionosphere

The validity of the Poisson-Vlasov system of equations in the ionosphere is based on the properties of the ionospheric plasma. In Table I the reference data for the ionosphere are presented for altitudes ranging from 300 to 3000 km above the surface of the earth. The data are primarily obtained from Johnson[1] and Al'pert *et al.*[2] with some modifications taken from more recent papers.[3,4]

The ionospheric data in the table vary considerably with position and time. The charged particle density, the ion temperature, and the relative importance of the ion

TABLE I

Basic Data of the Ionosphere.

Altitude (km)	300	500	1000	1500	2000	2500	3000
Mean neutral particle density n_o (m^{-3})	9.8×10^{14}	5.4×10^{13}	2.9×10^{11}	5.8×10^{10}	1.1×10^{10}	4.0×10^{8}	1.0×10^{6}
Mean charged-particle density n_e (m^{-3})	6.2×10^{11}	1.4×10^{11}	4.3×10^{10}	1.6×10^{10}	1.3×10^{10}	1.2×10^{10}	1.1×10^{10}
Mean electron temperature T_e (^oK)	1000	1500	2000	2300	2500	2600	2700
Electron thermal speed $V_{T_e} = (kT_e/m_e)^{\frac{1}{2}}$ (m/sec)	1.2×10^{5}	1.5×10^{5}	1.8×10^{5}	1.9×10^{5}	1.9×10^{5}	2.0×10^{5}	2.0×10^{5}
Mean ion molecular weight	20.2	16.7	9.2	3.6	2.9	2.4	2.0
Dominant ion component	O^+	O^+	He^+	He^+	He^+	H^+	H^+
Ion thermal velocity $V_{T_i} = (kT_e/m_i)^{\frac{1}{2}}$ (m/sec)	6.4×10^{2}	8.6×10^{2}	1.4×10^{2}	2.3×10^{3}	2.7×10^{3}	3.0×10^{3}	3.7×10^{3}
Satellite velocity V_{sat} (m/sec)	7.7×10^{3}	7.6×10^{3}	7.4×10^{3}	7.1×10^{3}	6.9×10^{3}	6.7×10^{3}	6.5×10^{3}
Magnetic field H_o (G)	0.44	0.37	0.32	0.27	0.23	0.19	0.15
Mean electron-ion collision frequency ν_{ei} (sec^{-1})	780	230	36	30	24	19	14
Electron-ion mean free path $\lambda_{ei} = (8/\pi)^{\frac{1}{2}} V_{T_e}/\nu_{ei}$ (m)	2.5×10^{2}	1.1×10^{3}	7.8×10^{3}	1.0×10^{3}	1.3×10^{4}	1.7×10^{4}	2.3×10^{4}

species undergo variations which are functions of not only altitude but also latitude, time of day, time of year, and even the 11-year solar cycle (i.e., a variation in the sunspot intensity). Therefore, the data in the table are mean values only.

Density of charged particles. The ionosphere contains both neutral and ionized atoms, and their densities decrease with increasing altitude. However, since the neutral particle density decreases much more rapidly than the charged particle density (due to the larger amount of ionizing radiation at higher altitudes), the influence of the charged particles upon a satellite is dominant at altitudes above 1000 km. Even at lower altitudes of the ionosphere, the charged particle density is sufficiently large to interact with the moving satellite. In this thesis, therefore, the investigation will be limited to the interaction of the satellite with the charged particles of the ionosphere since the interaction with neutral particles is well known.[5]

Influence of electron-ion collisions. In the ionosphere (see Table I) the electron-ion mean free path is much longer than the satellite length. As a result, the plasma flow near the satellite is considered to be collisionless, and the collisional term on the right-hand side of the Boltzmann equation may be neglected. The resulting Vlasov equation describes the behavior of the electrons and ions near the satellite. In the far wake, which is located many body lengths downstream and is comparable in length to the electron-ion collision length, collisional effects must be considered. For example, the collision term of the Boltzmann

equation may be approximated by the Krook model.[6] This thesis, however, will be concerned only with that region in which the distance from the satellite is much less than any collision length. This region is sufficiently large to include most of the phenomena arising from the electromagnetic interaction of the satellite with the plasma.

Electron density. In the ionosphere, the electrons and ions have approximately the same temperature (i.e., $T_e = T_i$). Although this temperature can vary by more than one hundred percent, generally it is not less than $1000^{\circ}K$. Then the electron thermal speed defined as $v_{Te} = (kT_e/m_e)^{\frac{1}{2}}$ is not less than 1.2×10^5 m/sec. The satellite velocity for a stationary orbit depends only upon the altitude; it ranges from 6500 to 7700 m/sec at altitudes of 3000 and 300 km, respectively. Hence, the thermal speeds of electrons are an order of magnitude greater than the satellite speed, and the velocity of the satellite is negligible when compared to the electron thermal speed (see Table II). Consequently, the electrons are assumed to have no net motion relative to the satellite, and the electron distribution function remains a stationary Maxwellian in the satellite frame of reference. Furthermore, the satellite body generally has a negative potential, and the body intercepts and absorbs relatively few electrons. In this case, the electron density is given by the Boltzmann factor as a local function of the potential V:

$$n_e = n_o \exp(eV/kT_e). \tag{1.1}$$

TABLE II

Parameters and dimensionless ratios for the interaction of a satellite with the ionosphere. (See Chaps. II and IV for a discussion of dimensionless quantities.)

Altitude (km)	300	500	1000	1500	2000	2500	3000
Debye length $\lambda_D = (\epsilon_o kT_e/ne^2)^{\frac{1}{2}}$ (cm)	0.28	0.71	1.5	2.6	3.0	3.2	3.5
Dimensionless satellite radius $r_{sat} = R_{sat}/\lambda_D$, where $R_{sat} = 0.5$ m	180	71	34	19	17	16	15
Dimensionless antenna radius $r_{sat} = R_{sat}/\lambda_D$, where $R_{sat} = 1$ cm	3.5	1.4	0.68	0.38	0.33	0.31	0.29
Dimensionless satellite speed $u_s = V_{sat}/V_{T_e}$	6.3×10^{-2}	5.0×10^{-2}	4.2×10^{-2}	3.8×10^{-2}	3.5×10^{-2}	3.3×10^{-2}	3.2×10^{-2}
V_{sat}/V_{T_i}	12	8.9	5.5	3.1	2.6	2.2	1.8
Dimensionless ion kinetic energy $\hat{E}_{KE} = m_i V_{sat}^2/2kT_e$	73	39	15	4.8	3.3	2.5	1.9
Dimensionless magnetic field $B = \lambda_D/r_{ge} = H(\epsilon_o/n_e m_e)^{\frac{1}{2}}$	0.55	0.97	1.5	2.1	2.0	1.7	1.4
λ_D/r_{gi}, where r_{gi} is ion gyroradius	2.9×10^{-3}	5.6×10^{-3}	1.2×10^{-2}	2.6×10^{-2}	2.7×10^{-2}	2.6×10^{-2}	2.3×10^{-2}

Influence of ion thermal motion of wake length. Table II indicates that the thermal speed of the ions of the ionospheric plasma is much less than that of the electrons. In fact, the ion thermal speed is less than the satellite speed. Since the moving satellite sweeps up the ions directly in front of it, the ion density of the immediate wake is much less than the ambient density. Further downstream, the ions fill in the wake because of their thermal motion. Let the radius of the satellite cross section be R_{sat}, the satellite velocity v_{sat}, and the most probable ion speed $v_{pi} = (2kT_e/m_i)^{\frac{1}{2}}$. Then an ion which travels with the most probable speed and with velocity directed toward the wake will intersect the center line of the wake at a distance $d_{thermal}$ downstream of the satellite. This distance,

$$d_{thermal} = R_{sat} v_{sat}/v_{pi} = R_{sat}(m_i v_{sat}^2/2kT_e)^{\frac{1}{2}}, \tag{1.2}$$

can be considered the approximate length of the ion-free near wake.[2] Since the ion speed is less than the satellite speed, this length is several times greater than the satellite radius.

Influence of electric field on wake length. In the disturbed wake, the electron and ion densities are not equal, and the resulting net charge density generates an electric field which may be calculated by means of Poisson's equation. The energy density of the electric field in the ion-free near wake is of the same order of magnitude as the electron pressure $n_e kT_e$ since the field, compensating the lack of ions, prevents all but the most energetic electrons from entering

the wake. Since the field repels electrons, it attracts ions into the wake and assists the filling-in process.

If the influence of the electric field on the ion motion is neglected, then the ion density may be obtained by the well-known methods of rarefied gas dynamics.[5] When these values of the ion density are inserted into Poisson's equation (the electron density being given by the Boltzmann factor), the electric field in the disturbed region may be calculated.[7,8]

This calculated field, however, is not the actual field. The error may be estimated by comparing the length of the ion-free wake with and without the electric field. In Chap. III where the ion thermal energy is neglected, the ion-free wake length is approximately

$$d_{wake}/\lambda_D = 2(R_{sat}/\lambda_D)^{\frac{1}{2}} (m_i v_{sat}/2kT_e)^{\frac{1}{2}},$$

where the Debye length is $\lambda_D = (\epsilon_o kT_e/ne^2)^{\frac{1}{2}}$. In the case of satellites with radii greater than the Debye length, the wake length with electric field is shorter than that without field [estimated above in Eq. (1.2)]. Hence, in certain cases the influence of the field on the ions is more important than the ion thermal motion.

Influence of satellite potential on plasma flow. The electric field which is due to the satellite potential has great influence on certain quantities such as the ion current and drag of a satellite. The potential acquired by a satellite as a result of the unequal electron and ion fluxes is negative and has been estimated to be two to four times the

electron thermal energy.[2,9] When the satellite potential is taken into account, the ion current collected may be 20% more than the swept-up current. A similar increase occurs in the satellite drag.

In certain cases, the influence of the satellite potential on the ion flow is of primary importance. For example, if a long thin antenna is moving perpendicular to the magnetic field of the earth, the induced potential gradient can cause the potential at one end of the antenna to be many times greater than the electron thermal energy.[10] Another example is a Langmuir probe situated on a satellite. In this case the probe may be biased to a highly negative potential relative to the main satellite in order to obtain information about the ionic medium.[11] If the probe is located sufficiently far from the satellite, it can be considered as a small satellite independent of its larger neighbor. In this case, the exact ion current to the probe at high negative potentials is of importance to the experiment. In fact, the detailed flow of the ions about the main satellite is important for the determination of the plasma flow to the probe.

Relation of Debye length to size of disturbed region. In order to estimate the distance over which the electric field (arising from the potential of both wake and satellite) will disturb the ionized medium, the Debye length of the plasma must be compared with the length of the body. In Table II, ratios of satellite radius to Debye length are shown for a satellite of 0.5 m radius (such as Explorer 20) and for an antenna of 1 cm radius. Note that the ratios vary widely from 0.3 to greater than 100.

For the antenna, the body size is comparable to the Debye length. Hence, the electric field disturbs the ion and electron distributions within several body radii of the antenna. Furthermore, any change in the satellite parameters will have a strong effect on the current, drag, and wake development.

In the case where the satellite radius is much larger than the Debye length, the electric field is shielded from the plasma within a distance which is a small fraction of the body radius, at least in front of and to the side of the body where the ion charge density is near its ambient value. In the wake, however, the length of the ion-free region is proportional to the one-half power of the ratio of satellite radius to the Debye length. Hence, the wake, several times larger than the body size, can be many times larger than the Debye length. Nevertheless, the development of the large wake of the satellite is very dependent on the electric field. In both cases, then, the influence of the electric field on the ion-flow field must be taken into account.

Influence of magnetic field on particle motion. In the above discussion, the influence of the geomagnetic field on the particle motion has not been considered. As shown in Table II, the ratio of the Debye length to the electron gyroradius in the geomagnetic field is of the order of unity throughout the ionosphere. Thus, the magnetic field influences significantly the electron trajectories. However, since the electrons maintain their Maxwellian distribution in the magnetic field, the influence of the field on the electron

density may be neglected. Hence, the electron density is given by the Boltzmann factor in Eq. (1.1).[12]

Table II also indicates that the ratio of the Debye length to the ion gyroradius is very small. Therefore, the geomagnetic field is important only when the region of interest is very much larger than the Debye length (e.g., the far wake). Furthermore, when a magnetic field is oriented parallel to the satellite velocity (e.g., in the case of a polar-orbiting satellite located at the magnetic equator), the motion of the ions moving to fill in the ion-free wake is retarded. As a result, the wake is lengthened and may contain spatial variations which correspond to the rotation of ions about the lines of magnetic force.[6]

B. Review of Prior Work

As a first approximation to the solution of the flow of the ionospheric gas around a satellite, the ion component of the plasma is assumed to behave as a free-molecular (collisionless) gas consisting of neutral particles. The electric and magnetic properties of the plasma are entirely ignored, and the problem becomes identical to that of an object moving through a rarified gas. Schaaf and Chambré[5] have reviewed analytical results obtained for symmetric body shapes (flat plate, cylinder, and sphere) in free-molecular flow and have presented data on the drag force and the drag coefficient as a function of Mach number and surface accommodation coefficient. Furthermore, Al'pert et al.[2] solved the particle flow around any arbitrarily shaped body by making use of the fact that the ionospheric flow around satellites is hypersonic, i.e., the Mach number is much larger than unity. Instead of calculating the drag coefficient, Al'pert et al. presented contour plots of particle density around the satellite. Their results showed that the particle density was strongly disturbed in the satellite wake up to a distance $d=(m_i v_{sat}^2/2kT_e)^{\frac{1}{2}} \times R_{sat}$ downstream of the satellite, where R_{sat} is the effective radius of the maximum cross section of the satellite. In addition, the particle density in the region in front of and along the sides of the satellite was quite similar to the ambient particle density. The study also showed that neither the exact shape nor the length of the satellite in the flow direction is important in the process of filling in the wake; the cross-sectional area of the satellite controls this process.

The approximation which assumes that the flowing particles are acting freely can be made more realistic by treating the particles as ions which interact with the earth's magnetic field. Alpert et al.[2] assumed a uniform magnetic field but continued to neglect the electric field. In this case, their plots of ion density show that a magnetic field parallel to the flow velocity will prevent the ion density from attaining its ambient value for an infinitely long distance downstream of the satellite. In reality, collisions or plasma instabilities will provide the mechanism which restores the ion density in the wake to its ambient value. On the other hand, a magnetic field perpendicular to the flow velocity has only a moderate influence on the ion density in the wake. Here, the filling-in process is similar to that without magnetic field.

The case of a conducting satellite moving perpendicularly to a magnetic field was treated by several investigators. By neglecting the influence of the magnetic field on the ions, Beard and Johnson[13] determined the potential gradient induced on a long thin satellite. The results included the distribution of current along the length of the body and the determination of the induction drag resulting from the interaction of the current with the magnetic field. Other investigators[14] determined the portion of the satellite drag which is due to the generation of Alfvén waves. Furthermore, as a result of various estimates of either the potential field or the ion density, several other investigators[15-17] obtained the joint effect of the electric and

magnetic fields on the plasma flow around a spherical satellite. However, in these cases, the obtained electric fields were not self-consistent.

In 1962 Davis and Harris[18] analyzed the case where the ions and electrons of the plasma interact with a self-consistent electric field. They assumed the effect of the earth's magnetic field to be negligible and, moreover, the satellite potential to be sufficiently negative to insure that the electron density is given by the Boltzmann factor, i.e., $n_e = n_o \exp \varphi$, where $\varphi = eV/kT_e$. In order to obtain the total charge density, the ion temperature was assumed to be zero, and the ion density was calculated by means of the equation of continuity. The region was divided into finite elements and therefore Poisson's equation could be approximated with a set of coupled algebraic equations. The self-consistent electric field was obtained by cycling between Poisson's equation and the equation of continuity for the ions. However, since the region of interest was very large compared to the Debye length, the accuracy of their results of the computation of the potential was severely limited. Nevertheless, these investigators were able to verify numerically what had been anticipated from physical arguments, namely, that the charge density is positive in front of the satellite and, for the most part, negative in the wake. In addition, it was discovered that downstream in the wake, considerable ion focusing occurs; this ion focusing is a result of the electric field and, in some cases, can give rise to net positive charge densities on the axis of the normally negative wake. The wake is not limited in length

to the order of a Debye length; actually, it extends many Debye lengths downstream. Of course, in front and at the sides of the satellite, the plasma is disturbed over a distance no longer than a few Debye lengths.

In 1964 Lam and Greenblatt[19,20] devised a technique for solving the flow of the ionospheric plasma around a satellite which is considerably larger than a Debye length. Rather than make use of the finite-difference method employed by Davis and Harris and others, Lam and Greenblatt treated the ion flow as a continuous fluid and obtained a scalar velocity potential which describes the flow in all regions except in the vicinity of the sheath. However, for a body size which is large compared with the Debye length, the sheath is very thin and follows the shape of the body closely. As a result, Lam and Greenblatt assumed that ion flow at the sheath edge approximates the ion flow at the body edge. They presented plots of data which show ion flow velocity vs. position on the body edge and ion current density at the sheath edge vs. body size. It sould be emphasized that these plots cover only the front of very large satellites. The technique of Lam and Greenblatt cannot be extended into the wake because the (collisionless) ion flow there is not adequately described by their system of equations.

In 1964 Maslennikov and Sigov[21-23] attacked the problem in much the same manner as Davis and Harris. They made approximately the same assumptions concerning the problem; however, they chose a body size comparable to a Debye length--this important computational difference permitted them to

obtain numerical solutions which were much more accurate than those of previous investigators. It should also be noted that Maslennikov and Sigov determined the ion charge density by means of the "super-particle" technique--many ion trajectories are followed simultaneously, and the ion charge density at any given point is assumed proportional both to the number of ions passing through a small volume cell surrounding the given point and to the length of time during which each ion remains in the particular cell. This method is similar to the "particle-in-cell" technique used by some investigators (e.g., Refs. 24 and 25) to determine charge densities for time-dependent plasma problems with one or more space dimensions.

Maslennikov and Sigov succeeded in obtaining reasonable flow fields and potential distributions around small ionospheric satellites. Their work confirms the conclusions of Davis and Harris that the net charge density is positive in front of the satellite and generally negative in the wake. In certain regions of the wake, high positive charge densities occur as a result of ion focusing by the electric field. These local maxima in the charge density occur in some cases not only directly downstream of the satellite but also above and below the axis of the wake. Maslennikov and Sigov also showed that the size of the region perturbed by the electric field, at least in the wake, is limited less by the Debye length than by the Mach number of the ions and by the cross-sectional area of the satellite. In addition, for the first time it was predicted that a series of spatial oscillations

of the electric potential occurs in the wake. These potential variations arise from the inertia of the streaming, collisionless ions under the action of the electric field. Moreover, it will be shown later in the present work that an axially symmetric satellite (Maslennikov and Sigov's sole choice of satellite shape) apparently is required for the formation of such spatial oscillations. It should also be mentioned that Maslennikov and Sigov extended their work to the difficult parameter region where body size is considerably less than Debye length and ion Mach number is slightly larger than unity.

In 1966 Parker[26,27] solved numerically the problem of a planar probe designed to determine ionospheric density and energy when mounted flush with the surface of a satellite. The satellite was assumed to be an infinite half-plane. The electron density of the surrounding plasma was not restricted to that given by the Boltzmann factor nor were the ions assumed to have zero temperature. As a result, the model used by Parker describes the motion of the ions and electrons much more accurately than previous calculations. In order to obtain the charge density, Parker evaluated the integral over velocity space of the distribution function for each species at each point of interest. The limits of velocity space which are a function of the point of interest were obtained by sampling the whole of velocity space with a number of particle trajectories. Those particles which reach the source of plasma far away from the satellite surface contribute to the charge density integral; those particles which return to the probe or satellite surface or are trapped into quasi-infinite orbits do not contribute. (Quasi-infinite orbits

are those trajectoreis which remain in the neighborhood of the satellite for an arbitrarily long time.) Therefore, determination of the limits of velocity space at each spatial point in the region of interest requires the evaluation of a very large number of trajectories. Moreover, the failure to assume the Boltzmann factor for electron density introduces an additional computational difficulty into the problem for the following reason: Since the satellite velocity is much greater than the ion thermal velocity but much less than the electron thermal velocity, ions possess--in addition to their thermal energy--a kinetic energy relative to the satellite which electrons do not possess. As a result, ion trajectories are much less sensitive than electron trajectories to errors in the electric field; therefore, the evaluation of electron trajectories is much more difficult.

Parker succeeded in obtaining a current-voltage characteristic for the planar probe and the net charge distribution near the surface of the satellite. Even more important, he contributed to the understanding of the computational problems which arise when the assumptions of zero ion temperature and of the Boltzmann factor for electron density are relaxed.

In 1967 Taylor[28,29] in a manner similar to Parker, solved the problem of an infinitely long satellite with a rectangular cross section. He assumed the electron density to be given by the Boltzmann factor and the ions to have a finite temperature and to fill in the wake as if they were neutral particles which would not interact with the electric field. Using this assumption for the ion density, Taylor then calculated the resulting potential around the satellite by a

finite-difference method. At a few points in the wake, the ion density was recomputed allowing for the attractive effect of electric field. In spite of the fact that these new ion density values did not arise from a self-consistent electric field, the results not only appeared to agree with much of the previous work done by Davis and Harris[18] and by Maslennikov and Sigov[22] but also contributed to the understanding of the wake-filling mechanism. Specifically, Taylor showed that the electric field attracts ions into the wake at a much faster rate than would be expected if the transverse thermal motion of the ions alone were considered. Moreover, the ion density is greater on the axis of the wake than in the adjacent region. This "hump" in the density splits into two distinct wings which move away from the axis as the wake is extended downstream. This behavior was also found in the solutions of both Maslennikov and Sigov[22] and Alpert et al.[2] Taylor suggests that such a region occurs because two thin streams of ions are attracted into the wake (one from the top edge and one from the bottom edge of the satellite); they meet on the axis of symmetry and pass through each other enhancing the ion density at that point. After crossing, they diverge and diffuse into the ambient plasma again.

C. Outline of Thesis

The works of Parker and of Taylor discussed previously show that although it is possible to include the effect of both ion temperature and electric field in the numerical calculations, this consideration is very costly in terms of computer time. Furthermore, Al'pert et al. showed that when the ion temperature only is considered (the electric field is neglected), the results, obviously, are insufficient to explain and predict the interesting phenomena which are due to the electric interaction. On the other hand, the work of Maslennikov and Sigov indicates that consideration of the influence of the electric field on the ions (the ion temperature is neglected) allows the prediction of a variety of phenomena both near to the satellite and in its wake.

Neglect of the ion temperature is valid as shown in the sixth row of Table II giving the ratio of the ion kinetic energy to the electron thermal energy. Since the ions and electrons have the same thermal energy, this ratio also indicates the magnitude of the ion kinetic energy with respect to its thermal energy. At all altitudes of the ionosphere, this ratio is greater than unity; below 1500 km it is an order of magnitude greater than unity. Therefore, neglect of the ion temperature is not expected to introduce serious error into the results.

Chapter II contains a detailed discussion of the method of solution of the Poisson-Vlasov system of equations with emphasis on the determination of the charge density of the zero-temperature ion-flow field. The method is based upon a concept of streamlines "borrowed" from continuum mechanics.

Since the method is both fast and accurate, the interaction problem may be solved more easily than by other methods. The speed of this method permits the investigation of much larger regions of disturbance and a much greater variety of conditions than was previously possible; the accuracy permits the calculation of quantities such as ion current and satellite drag and permits the detailed investigation of the wake structure.

Chapter II also contains a thorough discussion of an efficient solution of Poisson's equation. The method employed here is a variant of the "alternating direction implicit" scheme for solving five-diagonal matrix equations.[30] The "fast Fourier transform" method described by Cooley and Tukey[31] and used with success by investigators such as Hockney[24] is not applicable since in our case the boundary conditions are not purely rectangular and the mesh spacing is not constant. In summary, the goal of Chap. II is the development of a fast, yet general solution for the equations of the problem.

It should be noted that a multiple ion composition is not considered in Chap. II. Generally, the ionosphere contains at least two and sometimes four species of ions (O^+, N^+, He^+, and H^+). In principle, the inclusion into the solution of multiple ion species at different densities is not difficult. However, in the interest of simplification (which is consistent with the objective of rapid computation), a single species of ion (usually either He^+ or O^+) is assumed.

In Chap. III, the method of solution derived in Chap. II is applied to satellites of various shapes and sizes in a

variety of ionospheric conditions. The parameter space over which the solution is valid is explored, and results are compared with those of a previous work.[21] The total ion current to the satellite and its angular distribution over a cylindrical surface are shown. The drag of the satellite is obtained including that portion caused by ions which are not intercepted by the satellite but are deflected by the surrounding electric field. In the final section of the chapter, the wake behavior is discussed; here different regions of the wake are defined and their properties investigated. The conditions under which spatial variations occur in the potential and charge density are investigated. Furthermore, special attention is devoted to the appearance of an anomalous concentration of ions in two distinct wings in the wake of the satellite; an effort has been made to determine the cause of their appearance.

In Chap. IV, the ion trajectory equation is rederived to include the effect of the geomagnetic field on the problem. Certain results which are similar to those obtained in the previous chapter but are influenced by the magnetic field (such as wake behavior) are calculated and shown. In addition, the magnetic field is permitted to attain values which are higher than those occurring in the ionosphere in order to demonstrate the effect of a magnetic field on a plasma flow in a laboratory simulation experiment.

Chapter V presents the conclusions of the research. Three appendices follow this last chapter. Appendix A contains a detailed derivation of the equation used in Chap. II to

determine the ion density from a pair of adjacent ion trajectories. Appendix B is a discussion of the numerical errors of the solution; this appendix also describes the numerical details of the techniques used to obtain convergent iterates and to approximate the boundary conditions. Appendix C is a description of the computer program and contains a listing of that program.

It should be noted that no attempt has been made to investigate time-dependent phenomena. A steady-state solution is assumed in the satellite reference frame; as discussed in the last section of Chap. III, some experimental evidence exists that this assumption is valid.[32-34] In addition, Alpert et al.[2] discusses the possible occurence of a variety of wave phenomena (electron and ion plasma waves, electromagnetic waves, and Alfvén waves) and suggests that these waves are not dominant in the region near to the satellite.

The method of solution to be described in this thesis is not necessarily limited to ionospheric satellites and Langmuir probes moving in an ionospheric environment. For example, the flow of plasma over a stationary Langmuir probe in the laboratory may be solved by this method. However, the plasma must be collisionless in the region of interest, and the electron component of the plasma must have a thermal speed much greater than the flow velocity. Furthermore, since the ion thermal motion is neglected, the ion kinetic energy should be several times greater than the ion thermal energy.

CHAPTER II: EQUATIONS AND METHOD OF SOLUTION

A. Summary of Equations and Boundary Conditions

In order to solve the problem of the interaction of a satellite with the ionosphere, the following system of equations is employed.

First, the ion and electron number densities are given by the zero-moments of their respective distribution functions:

$$n_{i,e} = \int f_{i,e} d\vec{v}. \tag{2.1}$$

Second, the electric field is given by Poisson's equation:

$$\nabla \cdot \vec{E} = -\nabla^2 V = (e/\epsilon_o)(n_i - n_e). \tag{2.2}$$

Third, the ion and electron distribution functions are given by Vlasov's equation in a coordinate system relative to the satellite when no magnetic field is present:

$$\vec{v} \cdot \frac{\partial f_{i,e}}{\partial \vec{x}} + \frac{e_{i,e}}{m_{i,e}} \vec{E} \cdot \frac{\partial f_{i,e}}{\partial \vec{v}} = 0. \tag{2.3}$$

Physically, the boundary conditions are specified on the satellite surface and at infinity. For the potential,

$$V = V_{sat} \text{ on } \vec{x}_{sat},$$

$$V \to 0 \text{ as } \vec{x} \to \infty.$$

Since the satellite surface is metallic, it is assumed that all incident charged particles are neutralized. Hence, for

the distribution functions, the boundary conditions are

$$f_{i,e}(\vec{x}_{sat}, \vec{v}_{out}) = 0,$$

where $\vec{v}_{out}$ represents the outward-going half space. In the undisturbed region at infinity,

$$f_{i,e}(\vec{x}_{\infty}, \vec{v}_{i,e}) = n_o (m_{i,e}/2\pi kT_{i,e})^{3/2} \exp\left[-m_{i,e}(\vec{v}_{i,e} - \vec{v}_{sat})^2/2kT_{i,e}\right],$$

where $f_{i,e}(\vec{x}_{\infty}, \vec{v}_{i,e})$ is a drifting Maxwellian function.

In the shift to the coordinate system relative to the satellite, the time dependence is removed from Vlasov's equation at the cost of making the distribution function anisotropic at infinity. Because of this anisotropy, nontrivial problems must be at least two-dimensional, both in real space and in velocity space. Two classes of real satellite bodies may be treated in two-dimensional form. The first class is generated by rotating a two-dimensional shape which is mirror symmetric about the line of symmetry. For example, a disk rotated about its diameter becomes a sphere; a finite line becomes a disk. This class of body will be called "axially symmetric." The second class is generated by translating a two-dimensional shape along the third axis. For example, a disk translated in such a manner becomes an infinitely long flat plate. This class of body will be called "planar."

In order to obtain the solution of the interaction problem, the Poisson-Vlasov system of equations [Eqs.(2.1), (2.2),

and (2.3)] is solved by iteration until a self-consistent electric field is found. The zero-order iteration is arbitrarily chosen.

B. Solution of the Charge-Density Equations

1. Electron Density

It is possible to make a simplification which will reduce the difficulty of the problem sufficiently to permit accurate computer solutions. Since the speed of satellites in the ionosphere is at least an order of magnetude less than the average thermal speed of ionospheric electrons, the drift component in the Maxwellian distribution function for electrons may be neglected. As a result, the electron distribution at infinity is isotropic; in the disturbed region however, it is anisotropic because the ion anisotropy influences the electron distrubution through the electric field. If there is no electron current and if the force field can be described by a potential (i.e., if the force is conservative), then the electron number density is given immediately by the Boltzmann factor: [12]

$$n_e = n_o \exp(eV/kT_e) = n_o \exp \Phi.$$

When the satellite potential is strongly negative, the electron current to the satellite is small, and the Boltzmann factor is applicable over most of the disturbed region. Only in the region directly behind and near the satellite where the electrons dominate the net charge density does the use

of the Boltzmann factor for the electron density lead to any significant error in the net charge density. Moreover, in certain cases, the potential does not vary monotonically in the wake, and, therefore, the Boltzmann factor does not give the correct value for the electron density of a collisionless plasma. However, these errors in the electron density influence the development of the potential field only when their effect is allowed to accumulate over distances which are two or more orders of magnitude of the Debye length.[8] Hence, the results are not extended to those cases where the region of possible error is observed to be of this size. Practically speaking, other limitations, such as computer memory size, appear first.

2. Ion Density

General solution. Contrary to electron thermal speed, the ion thermal speed is less than the satellite speed (by an order of magnitude). In the satellite coordinate system, the incoming ions appear to be traveling as a beam, and their thermal velocities may be neglected except far downstream in the wake. Of course, when the random thermal variations in the ion motion are neglected, an unwanted degree of coherence may be introduced into the ion motion, and precautions are necessary in certain cases to avoid unwanted and artificially induced singularities in the ion density. The number density is

$$n(x,y,z) = \int f(x,y,z,u,v,w)\,dudvdw, \qquad (2.4)$$

where $\vec{v} = (u,v,w)$ gives the velocity coordinates for the particle at the point of interest $\vec{x} = (x,y,z)$ and the integration is performed over that region in velocity space where f exists. Since the distribution function is constant along a particle trajectory in a collisionless plasma, it is simple to relate f at the point of interest (x,y,z) to f at infinity.

$$f(\vec{x},\vec{v}) = f\left(\vec{x},\vec{v}(\vec{x},\vec{v}_\infty)\right) = f_\infty(\vec{v}_\infty), \tag{2.5}$$

where $\vec{v} = (u_\infty, v_\infty, w_\infty)$ gives the velocity coordinates at infinity. Equation (2.5) states that the value of f at the point $(\vec{x},\vec{v})$ in phase space is equal to the value of the distribution function f_∞ on the boundary evaluated at the velocity $\vec{v}_\infty$ (f_∞ is assumed to be independent of $\vec{x}_\infty$). This value on the boundary is the sought value at the point $(\vec{x},\vec{v})$ in phase space by virtue of the fact that f remains constant along a trajectory in a collisionless plasma.[35] Of course, determination of the trajectories of all particles in phase space is a nontrivial task which requires the solution of Newton's equations. Hence, it has been demonstrated that the solution of Vlasov's equation can be replaced by the solution of Newton's equations. Equivalently, if the trajectory equations $\vec{v}(\vec{x},\vec{v}_\infty)$ are known, then the characteristics of Vlasov's equation are also known.[36]

Now, by substitution of (2.5) into (2.4)

$$\begin{aligned} n(x,y,z) &= \int f_\infty(u_\infty,v_\infty,w_\infty)\,dudvdw \\ &= \int f_\infty(u_\infty,v_\infty,w_\infty)\left|\frac{\partial(u,v,w)}{\partial(u_\infty,v_\infty,w_\infty)}\right| du_\infty dv_\infty dw_\infty. \end{aligned}$$

Thus, it has been demonstrated that the general problem of finding the number density in a collisionless plasma is equivalent to that of finding both the Jacobian of the trajectory equations and the region of existence for the distribution function at the point of interest. If, for example, the distribution function at infinity is a monoenergetic beam moving with a velocity $\vec{v}_o = (u_o, v_o, w_o)$, then the density is no longer an integral. Since

$$f_\infty = n_o \delta(u-u_o)\ \delta(v-v_o)\ \delta(w-w_o)\ ,$$

then

$$n(x,y,z) = n_o \left.\frac{\partial(u,v,w)}{\partial(u_\infty, v_\infty, w_\infty)}\right|_{\substack{u_\infty = u_o \\ v_\infty = v_o \\ w_\infty = w_o}} .$$

Since an analytical solution for the two-dimensional trajectory equations is difficult to find, the partial derivatives which comprise the Jacobian must be obtained by numerical means. These derivatives of the trajectory equations vary in real space; their variations are governed by ordinary differential equations. The method for finding the Jacobian, however, has not been programmed since more direct methods exist for obtaining the number density when the distribution function of the ions is a monoenergetic beam.

Flow-field method. One such method makes use of a concept analogous to streamtubes in fluid mechanics, where a tube of flux is defined by a set of test particle trajectories which traces the wall of the flux tube in space. It is assumed that no trajectories from either inside or outside the

tube can cross the wall of the tube. Then, whatever material is inside the tube of flux initially remains there for the entire length of the tube. This conservation law is expressed by the equation of continuity in continuum mechanics for a steady state problem:

$$\nabla \cdot \vec{J} = 0,$$

where $\vec{J} = ne\vec{v}$ is the ion particle flux. Integrating this equation over the volume of a flux tube and using the divergence theorem,

$$\int_{\upsilon} \nabla \cdot \vec{J} \, d\upsilon = \int_{S} \vec{J} \cdot d\vec{S} = 0.$$

If the surface of integration is a flux tube, then the only non-zero contribution to the surface integral comes from the two ends of the tube. The particle flux normal to the wall of the tube is zero since the wall has been defined to be in the direction of the particle flux. Thus,

$$I - I_{\infty} = 0 , \tag{2.6}$$

where I_{∞} and I are the total currents ($I=\vec{J}\cdot\vec{A}$) entering and leaving the flux tube, respectively. (The symbol ∞ for infinity designates the undisturbed region.) If the radius of the tube is small compared to distance over which the variables of the problem change, then the particle fluxes at the tube ends can be estimated. It is assumed that the particle density and the velocity remain constant over the tube end and that the velocity vector is parallel to the normal vector of the area at the ends. Then,

$$I_{\infty} = n_{\infty} e\vec{v}_{\infty} \cdot \vec{A}_{\infty} \text{ and } I = ne\vec{v} \cdot \vec{A}, \tag{2.7}$$

where n_∞ and n are the number densities, $\vec{v}_\infty$ and $\vec{v}$ are the particle velocities, and $\vec{A}_\infty$ and $\vec{A}$ are the areas of the two ends of the tube.

In Fig. 2.1 a flux tube defined by two computed trajectories is drawn. The ion density at the point of interest P is obtained by substituting computationally convenient quantities for the velocity $\vec{v}$ and area $\vec{A}$ into Eqs. (2.6) and (2.7). In the planar case, the density is,

$$n = n_\infty \frac{v_\infty \ell_\infty}{v_x \ell'} \quad . \tag{2.8}$$

In this equation v_∞ and v_x are the ion velocities in the x direction at infinity and at the point of interest, respectively; ℓ_∞ and ℓ' are the tube widths in the y direction at infinity and at the point of interest, respectively. [See Appendix A for derivation of Eqs. (2.8) and (2.9).] In the axially symmetric case, there is an additional geometric factor which accounts for the radial compression or expansion of the flux tube (which, in this case, is a ring). Thus, the density is

$$n = n_\infty \frac{v_\infty \ell_\infty y_\infty}{v_x \ell' y} \quad , \tag{2.9}$$

where y is the radial distance from the axis of symmetry to the point of interest, and y_∞ is defined as follows: In order to determine the geometric compression factor, the radial distance of the source of flux at infinity must be calculated. An "imaginary" trajectory is assumed to pass through the point of interest, and its locus is estimated from the two calculated trajectories defining the flux tube. y_∞ is the

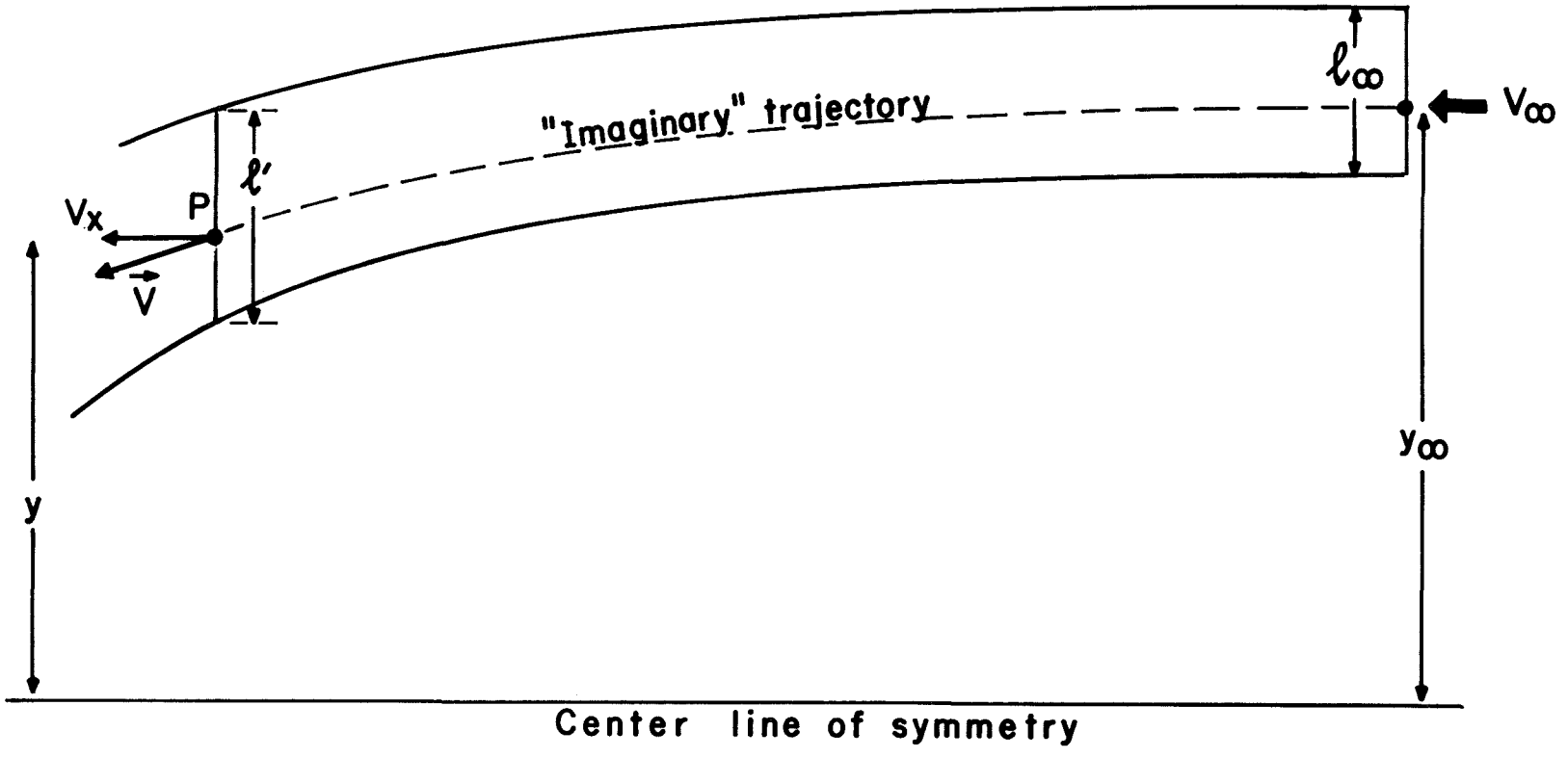

FIG. 2.1. GEOMETRY OF FLOW-FIELD METHOD. FLUX TUBE IS BOUNDED BY TWO CALCULATED TRAJECTORIES. "IMAGINARY" TRAJECTORY PASSES THROUGH POINT OF INTEREST P.

radial distance from the axis of symmetry to the point at which the "imaginary" trajectory is estimated to begin.

If the two adjacent trajectories intersect, at the point of intersection the tube width ℓ' is zero, and the charge density is infinite. Hence, at grid points in the vicinity of the intersection, abnormally high values of the ion density occur. However, in succeeding iterates of the Poisson-Vlasov system where the electric field is obtained more accurately, the trajectory crossing is expected to disappear. (See Appendix B for a discussion concerning the influence of crossing trajectories on the accuracy of the solution.)

"Super-particle" method. In order to verify the accuracy of the assumptions made in the flow-field method described above, the method used by Maslennikov and Sigov[21,22] and Kirstein et al.[37] (henceforth called the "super-particle" method) is presented. In this method a beam of ions incident on the region around the satellite is divided into discrete packets of density. The particle at the center of the density packet is assumed to be representative of all particles in the packet. The trajectory of this representative particle is followed over the region of interest. The region itself is divided into volume cells; whenever such a representative trajectory passes through a cell, the packet of density carried by the representative particle is smeared out over the entire cell and is weighted by the amount of time which the particle has spent in the cell. By tracing the paths of all

the density packets in this manner, a complete picture of the number density can be constructed to an accuracy of a volume cell.

The flux of particles in a density packet entering the region is

$$I_\infty = n_\infty v_\infty A_\infty = n_\infty v_\infty \Delta\ell_\infty L_\infty,$$

where L is a unit length in the "invariant" direction (Fig. 2.2). In the volume cell, the flux is

$$I = nvA = n\mathcal{T}/t = n\Delta x\Delta y L/t,$$

where $\mathcal{T}$ is the volume of the cell and t is the time spent in the cell by the representative particle. Since the flux remains constant along the trajectory, the density is

$$n = n_\infty v_\infty \sum \frac{\Delta\ell_\infty t}{\Delta x\Delta y}\frac{L_\infty}{L},$$

where the sum is taken over all particles. For particles which do not pass through the cell, the time spent in the cell, of course, is zero; hence, these particles do not contribute to the charge density of the cell.

A serious disadvantage of the "super-particle" method is that a vast number of trajectories must be computed in order to determine the charge density to a minimal accuracy (which allows only a very coarse solution). In order to estimate that accuracy, suppose that k representative particles (each carrying a unit of charge) pass through a volume cell. Let the k + 1 particle graze one of the walls of the cell. Now let a small perturbation in the field force that particle into the cell. Then the unit charge carried by that particle

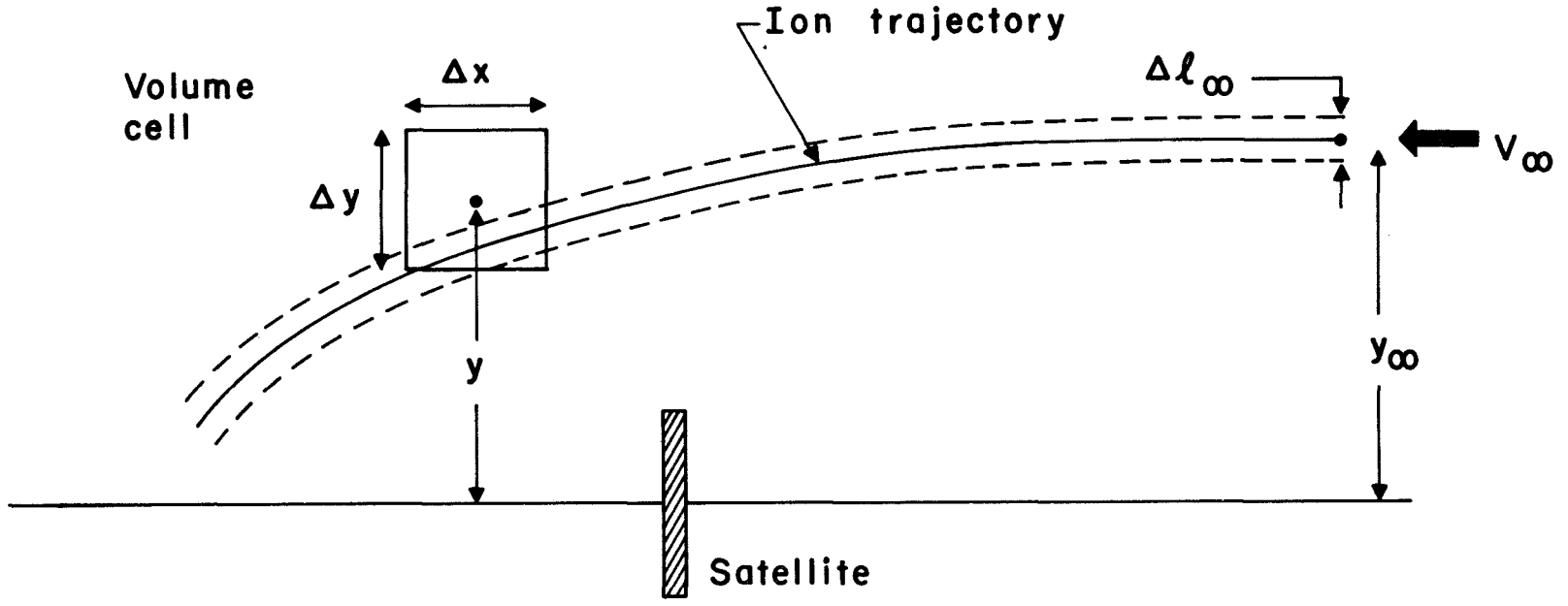

FIG. 2.2. GEOMETRY OF "SUPER-PARTICLE" METHOD.

is assigned to the grid point at the center of the cell, and the charge density of the grid point will increase from k units to k + 1 units. Since this increase is due to an infinitesimally small perturbation in the force field, it can be assumed that the finite change in density is a result of the error of the model. Therefore, the relative error of the charge density when computed by the "super-particle" method is approximately $[(k + 1) - k]/k = 1/k$, where k is the number of particles in a cell. If, for example, 20 trajectories pass through a cell, then the computed charge density is accurate to ±5%. In order to estimate the total number of trajectories needed for a density accuracy of $\pm 1/k$ per cell, it is not necessary to multiply the number of trajectories per cell by the total number of cells. Fortunately, one ion trajectory passes through a large number of cells, a number not less than the number of cells lying in the horizontal direction since the ion beam moves in a nearly horizontal direction. Then the total number of trajectories necessary to provide a charge density accurate to $\pm 1/k$ is found by multiplying the number of trajectories k per cell by the number of cells n lying in the vertical direction, i.e., nk. Typical satellite problems have at least 20 cells in the vertical direction. Therefore, a minimum of 400 trajectories is necessary to obtain a charge density accurate to ±5%.

The major reason why the "super-particle" method requires a large number of trajectories is that very limited use is made of the calculated parameters of the trajectories. Suppose two neighboring particles are traced. As they pass near

a particular cell, their parameters are examined to determine whether both, one, or neither have passed through the cell. The "super-particle" method requires no further data on the particle location. Essentially, the method requires calculation of a smoothly varying trajectory in order to determine whether a particle passes through a particular cell. The actual location of the particle is irrelevant in the "super-particle" method.

Comparison of flow-field and "super-particle" methods. The flow-field method is a considerable improvement over the "super-particle" method. For a given number of trajectories, the accuracy of the former is approximately an order of magnitude greater than that of the latter.

In the flow-field method, the error in the number density arises primarily from the small but discontinuous changes in density value between flux tubes. Although each flux tube is assumed to carry a density which is constant over its cross section, this density varies continuously along the length of the tube as the walls of the tube (represented by two trajectories) compress and expand under the influence of the electric field. In the "super-particle" method, however, each density packet remains constant irrespective of its location in the disturbed region. Although identical information is known about the trajectories (namely, their loci and velocities) in both methods, in the flow-field method that information is used more effectively to obtain the charge density. As a result, only a few (2-5) trajectories per vertical cell are needed to obtain charge density records accurate

to ±5%. Since the ion density computation consumes a considerable portion of the total computation time, the flow-field method provides a more accurate solution in a given span of computer time. It also makes possible the introduction of such complicating factors as an extended region of disturbance, complex satellite shapes, a magnetic field, and accurate estimates of ionospheric satellite properties such as current and drag.

C. Solution of the Trajectory Equations

In order to obtain the ion number density by either the flow-field method or the "super-particle" method, it is necessary to calculate the trajectories for a number of representative ion particles. The trajectories of the representative particles can be computed rapidly if it is assumed that the electric forces acting on the particles are constant over a cell. The potential field from which the electric field is calculated is given only at a finite number of points (as a consequence of the finite-difference method used in Sect. D to solve Poisson's equation). These points, by design, lie at the corners of the volume cells. As a first approximation, it can be assumed that if the potential is known only at the grid points, then the force field is also known only at the grid points and, therefore, is constant over the cell.

The advantage of assuming constancy over a cell is that Newton's equations can be integrated exactly using no further finite-difference schemes. These equations are

$$dx/dt = u, \qquad du/dt = F,$$
$$dy/dt = v, \qquad dv/dt = G,$$

where F and G are the forces per unit mass in the x and y directions, respectively, i.e.,

$$F = -\frac{e}{m_i}\frac{\partial V}{\partial x} \qquad \text{and} \qquad G = -\frac{e}{m_i}\frac{\partial V}{\partial y} \ .$$

Dimensionless variables. These equations can be made dimensionless by introducing the following dimensionless variables.

Let

$$t' = \omega_p t,$$

$$x' = x/\lambda_D,$$

$$v' = v/v_T,$$

where

$\omega_p = (n_o e^2/\varepsilon_o m_e)^{1/2}$ = the electron plasma frequency,

$\lambda_D = (\varepsilon_o kT_e/n_o e^2)^{1/2}$ = the Debye length, and

$v_T = \lambda_D \omega_p = (kT_e/m_e)^{1/2}$ = the electron thermal velocity.

The scale length is chosen to be the Debye length since the electric forces act over distances which are of the order of magnitude of the Debye length. Since the electric potential is of the order of the electron thermal energy, the scale velocity is chosen to be the electron thermal velocity. As a result, the scale time becomes the inverse of the plasma frequency, which is a familiar quantity and is the ratio of the electron thermal velocity to the Debye length. These scaling variables have been introduced primarily to simplify the governing equations and to set the magnitude of the numerical values of length, velocity, and time within one or two orders of unity. The introduction of these scaling variables does not imply any particular assumption about the method of solution. Any length and velocity could have been used in the computer solution; however, this particular choice simplifies the expression of both the trajectory equations discussed here and Poisson's equation to be discussed later.

Also, introduce the following dimensionless variables:

$$\varphi = eV/kT_e \qquad \text{and} \qquad \beta = m_i/m_e .$$

Then set

$$F' = -\frac{1}{\beta}\frac{\partial \varphi}{\partial x'} \qquad \text{and} \qquad G' = -\frac{1}{\beta}\frac{\partial \varphi}{\partial y'} \quad ; \tag{2.10}$$

now, Newton's equations in dimensionless form are

$$dx'/dt' = u' \qquad du'/dt' = F'$$
$$dy'/dt' = v' \qquad dv'/dt' = G'$$

For the remainder of this discussion the primes have been omitted, and all variables are to be considered as dimensionless.

Time of flight through cell. As mentioned previously, these equations may be solved easily if the force remains constant over a cell. Suppose the entrance parameters to a cell are x_o, y_o, u_o, v_o. The exit parameters y_1, u_1, v_1 at the far wall of the cell where $x = x_1$ must be determined by the integration of the first two of Newton's equations,

$$u = Ft + u_o \qquad \text{and} \qquad x = Ft^2/2 + u_o t + x_o .$$

Then the time of flight through the cell is

$$t_1 = \left(- u_o \pm \left[u_o^2 + 2F(x_1 - x_o)\right]^{\frac{1}{2}}\right)/F \tag{2.11}$$

It follows that

$$y_1 = Gt_1^2/2 + v_o t_1 + y_o, \quad u_1 = Ft_1 + u_o, \quad v_1 = Gt_1 + v_o .$$

y_1 is compared with the dimensions of the cell in order to determine whether the particle has left the cell via the far wall. If it has not, the time of flight is recomputed by making the assumption that the particle has left the cell via one of the side walls; this possibility is now checked. In fact, the program makes provision for the case where the particle turns around in the cell and exits at the same wall by which it entered.

Generally, the forces on the particles are very weak compared to the particle inertia. In this case, Eq. (2.11) for t_1, the time of flight, is not accurate numerically, and an expansion of this formula must be used:

$$t_1 = \frac{u_o}{F}\left\{-1 + \left[1 + \frac{2F}{u_o^2}(x_1 - x_o)\right]^{\frac{1}{2}}\right\}$$

$$\approx \frac{u_o}{F}\left(-1 + \left\{1 + \frac{1}{2}\left[\frac{2F}{u_o^2}(x_1 - x_o)\right] - \frac{1}{8}\left[\frac{2F}{u_o^2}(x_1 - x_o)\right]^2 + \right.\right.$$

$$\left.\left. + \frac{1}{16}\left[\frac{2F}{u_o^2}(x_1 - x_o)\right]^3\right\}\right)$$

$$\approx \frac{x_1 - x_o}{u_o}\left\{1 - \frac{1}{2}\left[\frac{F}{u_o^2}(x_1 - x_o)\right] + \frac{1}{2}\left[\frac{F}{u_o^2}(x_1 - x_o)\right]^2\right\}$$

This formula is used for rapid computation of the time of flight in most of the cells of the region of interest. The formula is inaccurate only in cases where F is large, u_o is small, or $x_1 = x_o$; in these cases the originally derived equation must be used.

Electric field. It is appropriate at this point to describe the technique employed to obtain from the potential field the force field necessary for the trajectory calculation. The method of solution for the potential field will be described later in Sec. D. It should be noted that the force field obtained here is one of the sequence of iterates approaching the self-consistent electric field. In order to keep the derivation simple, equal spacing between grid points is assumed; in the computer progrem, variable mesh size is employed in all formulas. The variation in potential is assumed to be quadratic, passing exactly through the potential values of the point of interest and of the two neighboring points (in Fig. 2.3, u_{ij} is the value of the potential ϕ at the grid point (i,j); h is the mesh size).

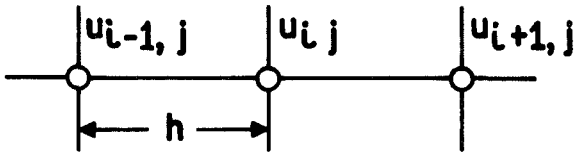

FIG. 2.3. GRID POINTS FOR COMPUTATION OF $\partial\phi/\partial x$ AT $(i,j)^{th}$ POINT.

The equation of such a quadratic is

$$\varphi = \frac{u_{i+1,j}-2u_{ij}+u_{i-1,j}}{2h^2}(x-x_i)^2 + \frac{u_{i+1,j}-u_{i-1,j}}{2h}(x-x_i)+ u_{ij}.$$

Thus the derivative of the potential in the x direction is

$$\frac{\partial\varphi}{\partial x} = \frac{u_{i+1,j}-2u_{ij}+u_{i-1,j}}{h^2}(x-x_i) + \frac{u_{i+1,j}-u_{i-1,j}}{2h} .$$

At the point of interest where $x=x_i$, $\partial\varphi/\partial x = (u_{i+1,j}-u_{i-1,j})/2h$. Apparently this formula is the same as that derived on the basis of a linear approximation. In the case of unequal mesh sizes, however, the two derivations do not yield the same values. In the quadratic case, the point closer to the center point is given more weight than the point farther away; in the linear case, the weights are equal. (For points on the boundary, no neighboring points beyond the boundary exist. As a result, in order to compute derivatives for a boundary point, two inner points on the same side of the point of interest are used instead of one point on one side and one on the other, as in the case of interior points.) Employing the method of computing the derivatives, a complete record of the force field can be constructed in both the x and y directions.

Total trajectory. The representative-particle trajectories which define the flux tubes of the ion flow field can now be calculated. Each particle has an initial position sufficiently far upstream from the satellite that the disturbing effect of the satellite does not influence the motion of particles at that point. The particle enters the first cell

with an initial velocity equal to and opposite that of the satellite. The forces $\vec{F} = (F,G)$ acting on the particle are estimated from the values of the previously calculated force record at points on the two ends of the cell wall. A linear approximation is used to account for the starting location of the particle relative to the wall ends. This estimated force is assumed to be constant over the cell, and the location and velocity of the particle as it exits the cell is calculated by the method described above. These exit parameters become the entrance parameters for the next cell through which the particle passes. A new set of forces is obtained from the force record, and a new set of exit parameters is calculated. As a result, the particle trajectory is a series of small quadratic arcs joined together to form the continuous trajectory. When the particle intercepts a vertical cell wall, its location and x velocity is retained for use in calculating the particle number density; the coordinates of the interceptions with horizontal walls are not needed for the density calculation.

In this collisionless case, particle trajectories may cross each other. For example, a trajectory which grazes the satellite is pulled into the wake and may cross the center line of symmetry. There is a corresponding trajectory which lies below the center line and is the mirror image of the first trajectory. It crosses the center line of the wake region at exactly the same point as the first trajectory. Although its velocity in the horizontal direction (x velocity) is the same as that of the first trajectory, the vertical

velocity (y velocity) is equal to and opposite that of the first. As a result, whenever a particle crosses the center line of symmetry, its y velocity is reversed and the trajectory computation is continued. In this manner, all the trajectories are kept in the upper half of the region, and thus the complete charge densities are obtained even when flux tubes which contribute to the density come from the lower half plane.

It should be noted that the equations of motion remain the same whether the problem geometry is planar or axially symmetric. This apparent independence of the coordinate system arises from the fact that the mathematical form of the gradient of the potential (electric field) does not depend upon the coordinate system used. However, the divergence operator does depend on the coordinate system and, as will be shown below, the equation for the potential which is obtained by means of Poisson's equation is different for each system. In addition, the equation for the charge density which contains a geometric factor is different for each system.

D. Solution of Poisson's Equation

In order to determine the potential in the disturbed region around the satellite, Poisson's equation is used:

$$-\nabla^2 V = \frac{\rho}{\epsilon_o} = \frac{e}{\epsilon_o}(n_i - n_e).$$

Using dimensionless variables where $n' = n/n_\infty$ and n_∞ is the charged particle density at infinity,

$$-\nabla^2 \varphi = n_i' - n_e'.$$

The primes will now be omitted, and these variables are henceforth assumed to be dimensionless. For the axially symmetric and planar cases, the divergence operator may be written as

$$-\left(\frac{\partial^2 \varphi}{\partial z^2} + \frac{1}{r}\frac{\partial}{\partial r} r \frac{\partial \varphi}{\partial r}\right) = n_i - n_e \qquad \text{and}$$

$$-\left(\frac{\partial^2 \varphi}{\partial x^2} + \frac{\partial^2 \varphi}{\partial y^2}\right) = n_i - n_e, \qquad \text{respectively.} \tag{2.12}$$

In discussing the solution of Poisson's equation, the planar case generally will be used. However, when the two cases differ significantly, both of them will be demonstrated.

Poisson's equation is converted into a system of finite-difference equations by dividing the region of interest into a set of rectangular grid points. Although it is numerically convenient to make the distance between the grid points (mesh size) a constant throughout the region, it is more important to make this mesh size much finer both near and directly

behind the satellite (see Appendix B). As a result of the variable mesh size, the algebraic equations are more complicated.

Boundary condition. The boundary condition for Poisson's equation is as follows: the potential is assumed constant and known on the satellite, and it falls off toward zero as the distance from the satellite approaches infinity. Since the region of interest must be finite in order to insure a finite number of grid points, it is impossible to locate the outer boundary at infinity in this model problem. As an alternative, the potential or its gradient, the electric field, is assumed to have a known functional dependence on the distance from the satellite. Generally, a dependence on an inverse power of the distance is assumed. This choice of boundary condition has the advantage that if the boundary were allowed to tend to infinity, both the potential and its gradient, and, in fact, all higher order derivatives of the potential would tend to zero. Studies have been made to estimate the relative merits of the various possibilities; nevertheless, for the satellite-interaction problem, setting of the potential to zero has been shown to be no less accurate than any other approximation of the boundary condition when the overall computation time is considered.[38] Since the zero-potential boundary condition is simple to apply, it is employed here for the solution of this problem.

In order that the number of grid points may be reduced by a factor of two, the problem is made symmetric about the

center line. Therefore, along this center line the normal electric field is zero. In the axially symmetric case, this boundary condition is inherent in the algebraic equations; in the planar case, it must be applied.

Solution of finite-difference equations. The conversion of the partial differential equation into a system of finite-difference equations is rather simple. The axially symmetric case is as follows [in Fig. 2.4, u_{ij} is the value of the potential ϕ at the grid point (i,j); h is the mesh size]:

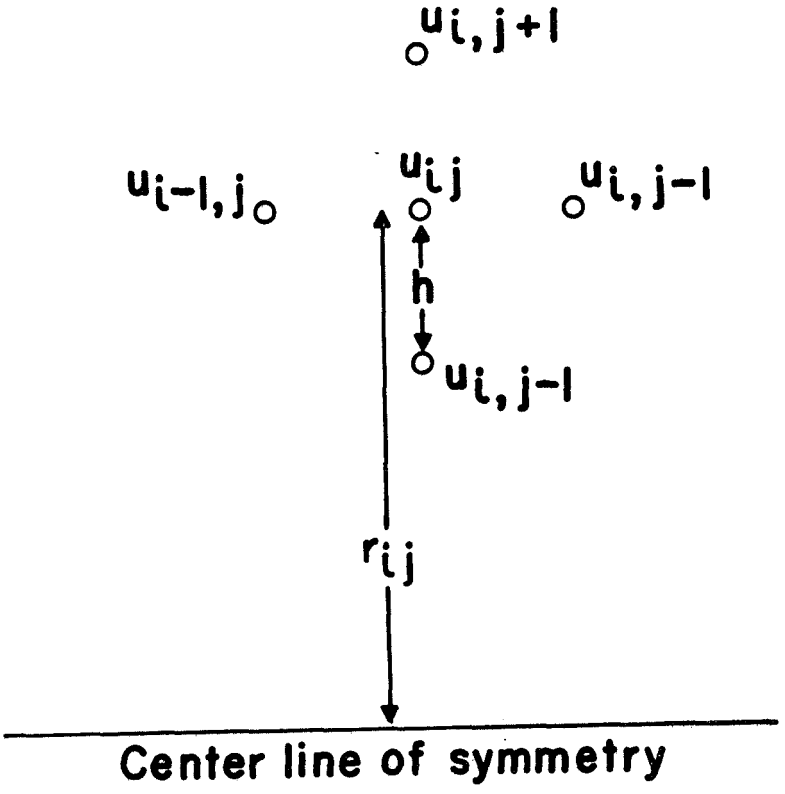

FIG. 2.4. GRID POINTS FOR COMPUTATION OF $-\nabla^2\phi$ AT $(i,j)^{th}$ POINT.

$$-\frac{\partial^2 \varphi}{\partial z^2} \approx -\frac{1}{h}\left(\frac{u_{i+1} - u_{ij}}{h} - \frac{u_{ij} - u_{i-1,j}}{h}\right),$$

$$-\frac{1}{r}\frac{\partial}{\partial r}\, r\,\frac{\partial \varphi}{\partial r} \approx -\frac{1}{hr_{ij}}\left\{(r_{ij}+\frac{h}{2})\,\frac{u_{i,j+1} - u_{ij}}{h} - (r_{ij}-\frac{h}{2})\frac{u_{ij}-u_{i,j-1}}{h}\right\}.$$

The Laplacian is:

$$-\left(\frac{\partial^2 \varphi}{\partial z^2} + \frac{1}{r}\frac{\partial}{\partial r}\, r\,\frac{\partial \varphi}{\partial r}\right) \approx \frac{4}{h^2}\, u_{ij} - \frac{1}{h^2}\, u_{i+1,j} - \frac{1}{h^2}\, u_{i-1,j}$$

$$- \frac{1}{h^2}\left(1+\frac{h}{2r_{ij}}\right)u_{i,j+1} - \frac{1}{h^2}\left(1 - \frac{h}{2r_{ij}}\right) u_{i,j-1}.$$

The planar case can be recovered from the axially symmetric case, if r_{ij} is allowed to tend to infinity, as follows:

$$-\left(\frac{\partial^2 \varphi}{\partial x^2} + \frac{\partial^2 \varphi}{\partial y^2}\right) \approx \frac{4}{h^2}\, u_{ij} - \frac{1}{h^2}\, u_{i+1,j} - \frac{1}{h^2}\, u_{i-1,j} - \frac{1}{h^2}\, u_{i,j+1} - \frac{1}{h^2} u_{i,j-1}. \tag{2.13}$$

Each grid point where the potential is unknown has a similar equation relating the value of the potential at the point (i,j) to the values of the potential at the four neighboring points. These equations may be cast into matrix form--if N grid points exist in the region of interest, the dimensions of the matrix are N x N. Of course, the matrix is sparse and, in fact, has only five non-zero diagonals since the $(i,j)^{th}$ equation always relates the $(i,j)^{th}$ value to only four neighboring values.

This diagonal feature of the matrix suggests an iterative method of solution. In matrix form, the system of algebraic equations is:

$$\underset{\sim}{A}\,\underset{\sim}{u} = \underset{\sim}{\rho} = (\underset{\sim}{n}_i - \underset{\sim}{n}_e),$$

where $\underset{\sim}{u} = \begin{bmatrix} u_{11} \\ \vdots \\ u_{mi} \\ \vdots \\ u_{mn} \end{bmatrix}$, $\underset{\sim}{n}_i = \begin{bmatrix} n^i_{11} \\ \vdots \\ n^i_{ml} \\ \vdots \\ n^i_{mn} \end{bmatrix}$, $\underset{\sim}{n}_e = \begin{bmatrix} n^e_{11} \\ \vdots \\ n^e_{ml} \\ \vdots \\ n^e_{mn} \end{bmatrix} = \begin{bmatrix} \exp(u_{11}) \\ \vdots \\ \exp(u_{ml}) \\ \vdots \\ \exp(u_{mn}) \end{bmatrix}$

and $\underset{\sim}{A} = \frac{1}{h^2}$ $\begin{bmatrix} 4 & -1 & & & & -1 & & & & \\ -1 & 4 & -1 & & & & \ddots & & \mathbf{O} & \\ & -1 & 4 & -1 & & & & \ddots & & \\ & & \ddots & \ddots & \ddots & & \mathbf{O} & & \ddots & \\ & & & \ddots & \ddots & \ddots & & & & -1 \\ -1 & & & & \ddots & \ddots & \ddots & & & \\ & \ddots & & & \mathbf{O} & \ddots & \ddots & \ddots & & \\ & & \ddots & & & & -1 & 4 & -1 & \\ & \mathbf{O} & & \ddots & & & & -1 & 4 & -1 \\ & & & & -1 & & & & -1 & 4 \end{bmatrix}$

(N = m × n, where m and n are the number of horizontal and vertical points, respectively.) The system is nonlinear since the electron density n_e depends on the potential φ through the Boltzmann factor. It has been proved that the iterative technique to be used converges only in the linear case.[30] Nevertheless, in this particular nonlinear case, the technique also converges.

If the matrix were merely tridiagonal instead of five-diagonal, the problem could be solved explicitly. An algorithm based on Gauss' method of elimination determines the exact values of the unknown points if they depend on

only two neighboring points.[30] That is, if the values of the points in the two horizontal chains adjacent to the horizontal chain of interest were known, the exact values in that entire chain of interest could be determined easily. Therefore, it is assumed that the values in the chains above and below the chain of interest are known, and using those values the chain of interest can be solved. Then, proceeding to the next chain above and using the previously computed values for the adjacent chains, the values for the new chain can be found. In this manner a sweep is made through all horizontal chains again and again until the maximum absolute value of the difference between any two iterations is less than the prescribed error bound; then the solution is said to have converged.

In matrix form, this method is equivalent to splitting matrix $\underset{\sim}{A}$ into a tridiagonal matrix $\underset{\sim}{B}$ and a two-diagonal matrix $\underset{\sim}{C}$. It has been stated that the matrix equation having as an operator the tridiagonal matrix $\underset{\sim}{B}$ can be solved explicitly; this is equivalent to finding the inverse operator $\underset{\sim}{B}^{-1}$.

$$\underset{\sim}{A}\,\underset{\sim}{u} = \underset{\sim}{B}\,\underset{\sim}{u} - \underset{\sim}{C}\,\underset{\sim}{u} = \underset{\sim}{\rho}\,(\underset{\sim}{u}).$$

$$\underset{\sim}{B}\,\underset{\sim}{u} = \underset{\sim}{C}\,\underset{\sim}{u} + \underset{\sim}{\rho}\,(\underset{\sim}{u}).$$

$$\underset{\sim}{u} = \underset{\sim}{B}^{-1}\,[\underset{\sim}{C}\,\underset{\sim}{u} + \underset{\sim}{\rho}\,(\underset{\sim}{u})].$$

A solution $\underset{\sim}{u}^{(o)}$ is guessed. Using that solution, a sweep is made over all horizontal lines, and a solution $\underset{\sim}{u}^{(1)}$ is found. Using $\underset{\sim}{u}^{(1)}$, $\underset{\sim}{u}^{(2)}$ can be found. Formally,

$$\underset{\sim}{u}^{(n+1)} = \underset{\sim}{B}^{-1}\left[\underset{\sim}{C}\,\underset{\sim}{u}^{(n)} + \underset{\sim}{\rho}\left(\underset{\sim}{u}^{(n)}\right)\right]$$

When max $|\underset{\sim}{u}^{(n+1)} - \underset{\sim}{u}^{(n)}|$ is less than the error bound, then the iterative procedure is halted.

"Alternating direction implicit" method. Two improvements can be made in this scheme. The first examines the difference between two successive iterates and assumes that a more accurate iterate than either of these two iterates is one which is a linear mixture of these two iterates. That is,

$$\underset{\sim}{u}'^{(n+1)} = \omega \left(\underset{\sim}{u}^{(n+1)} - \underset{\sim}{u}^{(n)} \right) + \underset{\sim}{u}^{(n)}.$$

If $\omega = 0.5$, then $\underset{\sim}{u}'^{(n+1)} = \frac{1}{2} \left(\underset{\sim}{u}^{(n+1)} + \underset{\sim}{u}^{(n)} \right)$, a simple average. If $\omega = 1.0$, then $\underset{\sim}{u}'^{(n+1)} = \underset{\sim}{u}^{(n+1)}$. Therefore, if $\omega > 1.0$, the new solution goes "beyond" either of the two iterates. This method of mixing iterates is called overrelaxation. Naturally, if ω is too large, the iterates will become unstable; in fact, in the linear case ω must be less than 2.0 in order to insure convergence.[30] The best value for the relaxation parameter ω is one which reduces the number of iterates to a minimum for a fixed error bound. In practice, the best value of ω lies between 1.2 and 1.8. This value is difficult to estimate in advance and, therefore, is generally determined empirically even for the linear case.

A second improvement can be made by sweeping not only across horizontal chains of grid points but also across vertical chains. The algorithm is identical in both cases, and, by alternating the direction of the sweep, the fast implicit tridiagonal solution can be applied in both directions.

Coupled with overrelaxation, this "alternating direction implicit" method (ADI) is one of the fastest methods for a computer solution to Poisson's equation with general boundary conditions.[30]

Formally, the ADI method of solution can be expressed as two matrix equations. For the horizontal sweep, $\underset{\sim}{A}$ is split into two matrices $\underset{\sim}{B}_H$ and $\underset{\sim}{C}_H$, where $\underset{\sim}{A} = \underset{\sim}{B}_H - \underset{\sim}{C}_H$, and $\underset{\sim}{B}_H$ is the single upper diagonal matrix relating the values of the horizontal chain of interest with those of the next chain above. Similarly for the vertical sweep, $\underset{\sim}{A}$ is split into two matrices $\underset{\sim}{B}_V$ and $\underset{\sim}{C}_V$, where $\underset{\sim}{A} = \underset{\sim}{B}_V - \underset{\sim}{C}_V$ and $\underset{\sim}{C}_V$ is the single upper diagonal matrix relating the values of the vertical chain of interest with those of the next vertical chain. Then the horizontal sweep is

$$\underset{\sim}{u}^{(n+1)} = \omega \underset{\sim}{B}_H^{-1} \left[\underset{\sim}{C}_H \underset{\sim}{u}^{(n)} + \underset{\sim}{\rho}\left(\underset{\sim}{u}^{(n)}\right)\right] + (1-\omega)\underset{\sim}{u}^{(n)}.$$

The following vertical sweep is

$$\underset{\sim}{u}^{(n+2)} = \omega \underset{\sim}{B}_V^{-1} \left[\underset{\sim}{C}_V \underset{\sim}{u}^{(n+1)} + \underset{\sim}{\rho}\left(\underset{\sim}{u}^{(n+1)}\right)\right] + (1-\omega)\underset{\sim}{u}^{(n+1)}.$$

This procedure is iterated until a convergent solution is obtained.

Boundary points. If an extra line of grid points is added onto the border of the region of unknown points, then the boundary conditions are automatically satisfied when the values of the border points are set equal to the known values

of the potential on the boundary. If the electric field rather than the potential is known, as is the case along the center line of symmetry, then the values of the potential may be calculated on the outer line of grid points by using the potential values from the previous iterate and interpolating. For example, along the center line, the normal electric field is zero; if the potential values of the grid points of the line immediately below the center line are set equal to the corresponding values of the grid points of the line immediately above the center line, then the potential gradient across the center line will be approximately zero for the next iterate.

On the other hand, the algebraic equations governing the potential of the grid points on the boundary may be altered to include the effect of the boundary conditions. It is usually more convenient, however, to leave all equations in identical form and to set the potential of the boundary points to their known values before each iterate. In either case the equations governing the potential of those points which lie of the satellite and whose values are therefore known must be altered in order for the satellite potential to remain at its fixed value as the potential field around the satellite is being determined.

In addition to setting the potential of the boundary points equal to their known values before each iterate, the number density or right-hand side of Poisson's equation must be determined. As described in the previous section, determination of the number density of the ions is difficult and time consuming. Therefore, that calculation is done

only after the potential field has been calculated rather accurately. The electron density, however, is a simple function of the local potential and may be calculated quickly before each iterate. In fact, it must be calculated before each iterate, or the solution of the Poisson-Vlassov system of equations will not converge. The system is more sensitive to changes in the electron density than in the ion density because the electrons have less kinetic energy than the ions and therefore, are influenced by the electric field to a much greater extent.

E. Summary of the Method of Solution

The solution of the system follows in a natural manner. First, by means of the ADI method, Poisson's equation is solved to a moderate degree of accuracy while the ion charge density remains fixed. As the potential converges toward a steady value, the electron density is allowed to follow it. Then, using these values of the potential field, the ion flow field is computed, and the resulting ion charge density is used to compute a new potential field. A succession of potential solutions called major iterates is constructed. When the major iterates converge, the problem is solved.

In order for the major iterates to converge, they must be "underrelaxed." If the ion charge density which is computed from the potential field is used directly to compute a new potential field, the system will not converge. To assure convergence, the new ion density must be averaged with the ion density of the previous major iterate. The relaxation parameter is found empirically to range between 0.25 and 0.75, depending on the inherent stability of the problem. Not only the ion density but also the potential field can be underrelaxed from major iterate to major iterate. In this case, however, the underrelaxation is a refinement of the technique and is not necessary for obtaining a convergent solution. (See Appendix B for the numerical details of the convergence of the solution.)

CHAPTER III: NUMERICAL RESULTS

A. Introductory Remarks

Important quantities. In the computer solution of the problem, the potential, the electric field, the ion-flow field (as represented by a large number of ion trajectories), the ion density and the electron density are obtained as functions of the spatial coordinates in the horizontal (x) and vertical (y) directions. Both the potential field and the ion-flow field have smaller variations in their values than the remaining quantities and are, therefore, easier to plot. Since the potential is, in a sense, the result of "double integration" of the charge density (the charge density being the result of "double differentiation" of the potential in Poisson's equation) both numerical errors and rapid variations in the charge density are "smoothed out" in the potential. Because of this fact alone, the potential field will be plotted. Moreover, the potential field is of considerable interest since its values can be compared with experimental values measured by satellite instrumentation. The ion-flow field will be plotted also since measurable quantities such as ion current and satellite drag can be obtained from it. Moreover, since the ions are hypersonic, their trajectories are influenced only moderately by the electric field and therefore their slow variations can be plotted smoothly and accurately. On occasion, plots of other variables such as ion number density will be shown in order to emphasize properties of the wake or to compare with experimental data.

Comparison with independent solution. Generally, a computer solution is assumed correct only after it has been compared with an analytic solution for the same problem. In the problem under consideration, however, no analytic solution is possible when the physical parameters of the problem are set equal to values which occur for a satellite in the ionosphere. Analytic solutions do exist for problems where one or more of the parameters are vanishingly small or infinitely large (limiting cases). However, as is usual for this type of problem, the computer program cannot be extended to these limiting cases of parameter space.

Nevertheless, there is a means of testing the accuracy of the computer solution in this case. It can be compared with another numerical solution obtained for identical parameters, where identical assumptions are made, but an independently derived method of solution is used. Such a numerical solution which has identical assumptions and which is derived in an independent manner was obtained by Maslennikov and Sigov.[21,22] Assuming zero ion temperature and the Boltzmann factor, they obtained the potential field around a spherical satellite having a radius of one Debye length. The satellite is moving at 10^6 cm/sec in an ionosphere composed of cold oxygen ions and warm electrons at a temperature of 5000°K. These values for ionospheric conditions correspond to an ion kinetic energy which is a factor 19.4 greater than the electron thermal energy. For their choice of parameters, a computer solution using the method discussed previously in Chap. II was found for the potential field. A contour plot of the potential is shown in Fig. 3.1. The satellite potential is zero relative

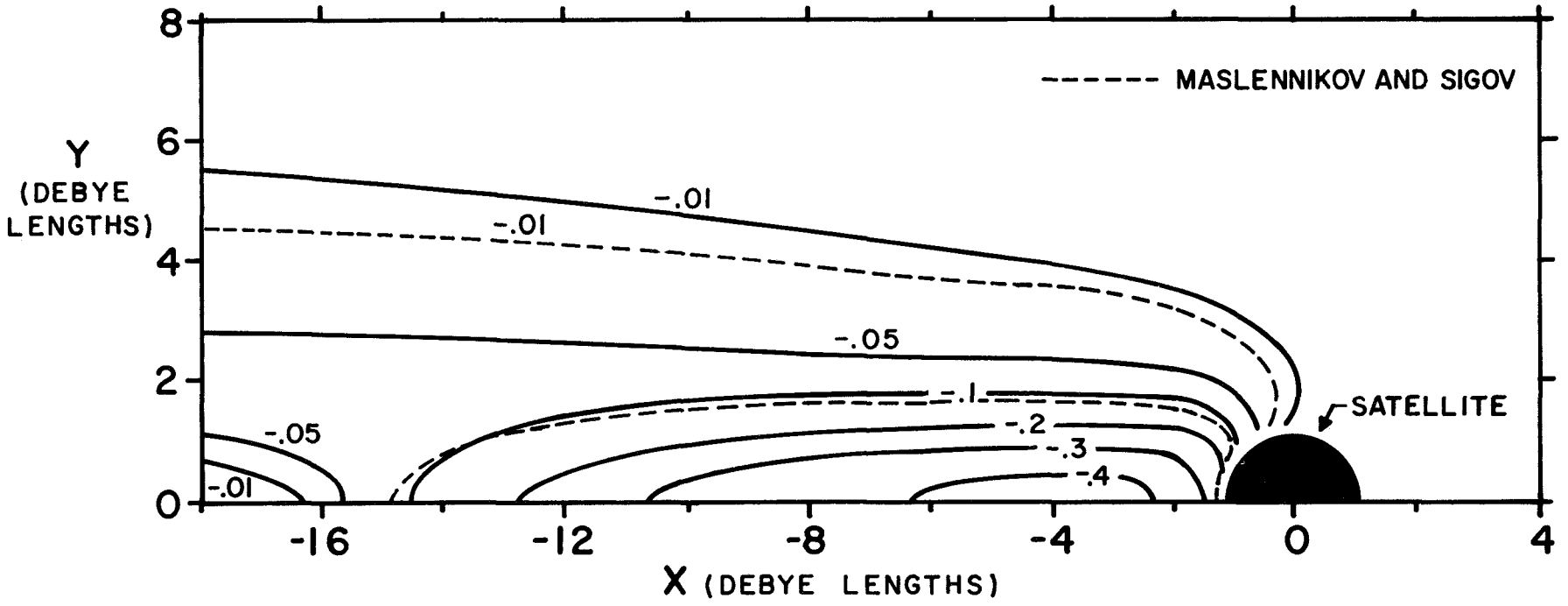

FIG. 3.1. CONTOUR PLOT OF POTENTIAL FOR SPHERICAL SATELLITE. (ION KINETIC ENERGY = $\hat{E}_{KE}$= 19.4, ϕ_{sat}= 0, r_{sat}= 1). DASHED CONTOURS ARE TAKEN FROM SOLUTION OF MASLENNIKOV AND SIGOV (SEE REF. 21).

to the ambient plasma, the horizontal and vertical axes are measured in Debye lengths, and the ions move from right to left. In the contour plot the dotted contour lines are taken from the potential field solution of Maslennikov and Sigov.[21] The agreement is well within the accuracy claimed for the two solutions. (See Appendix B for a discussion of the numerical accuracy of the solution of the present study.) It must be remembered that for the two solutions the exterior boundaries, mesh sizes, number of ion trajectories, number of iterations, and, in fact, the overall methods of solving Poisson's equation and the ion density equation are derived independently. Therefore, it is reasonable to assume that no gross miscalculation has been made in either of the two solutions.

Satellite shapes. Since in the satellite frame of reference the ion kinetic energy is usually much greater than the electron thermal energy (the ratio of the ion kinetic energy to the electron thermal energy, defined as the dimensionless quantity $\hat{E}_{KE}$, is much greater than unity), the forces which alter the ion trajectories are weak, and the attracted ions travel considerable distance downstream before they enter the disturbed region. The shape of the wake, therefore, is generally much longer than it is wide. Hence, it is both efficient and convenient to use rectangular rather than polar grid lines to divide the region of interest into discrete areas. However, it is both inconvenient and inefficient to approximate a spherically shaped satellite by means of a rectangular grid.

A shape which is convenient for a numerical solution is an infinitely thin disk whose normal is parallel to the direction of the flow velocity. The representation of a thin disk

on a rectangular grid is simply a vertical segment, one end of which lies on the axis of rotation. When this line segment is rotated about the symmetry axis, the resulting figure of revolution is a disk. The line segment is easy to represent on a rectangular grid; a number of consecutive grid points on a vertical line is designated as the satellite body, and the values of the potential at these points are set equal to the satellite potential.

The body dimension in the flow direction does not strongly influence the development of the disturbed region; the cross section of the body accounts for the removal of the ions from the disturbed region.[2] Therefore, if the radius of the disk (length of segment) is equal to the radius of the sphere and if all other parameters are equal, then the resulting contour plots of potential are expected to be very similar except in the neighborhood of the satellite body. Adjacent to the body, the lines of equipotential will have to match the equipotential surface of the body; therefore, in this area the lines may differ for the two bodies.

Figure 3.2 is taken directly from Fig. 3.1; in Fig. 3.2 however, as in most later figures of potential and ion flow, the vertical axis has been expanded in order that the disturbed region may be shown more clearly. Figure 3.3 is a contour plot of potential for a disk satellite; all other parameters are identical to that of Fig. 3.2, (i.e., $\hat{E}_{KE} = 19.4$, $\varphi_{sat} = 0$, $r_{sat} = 1$). The vertical axis has also been expanded. As expected, the two figures have a very similar character for the development of the potential field. The regions of

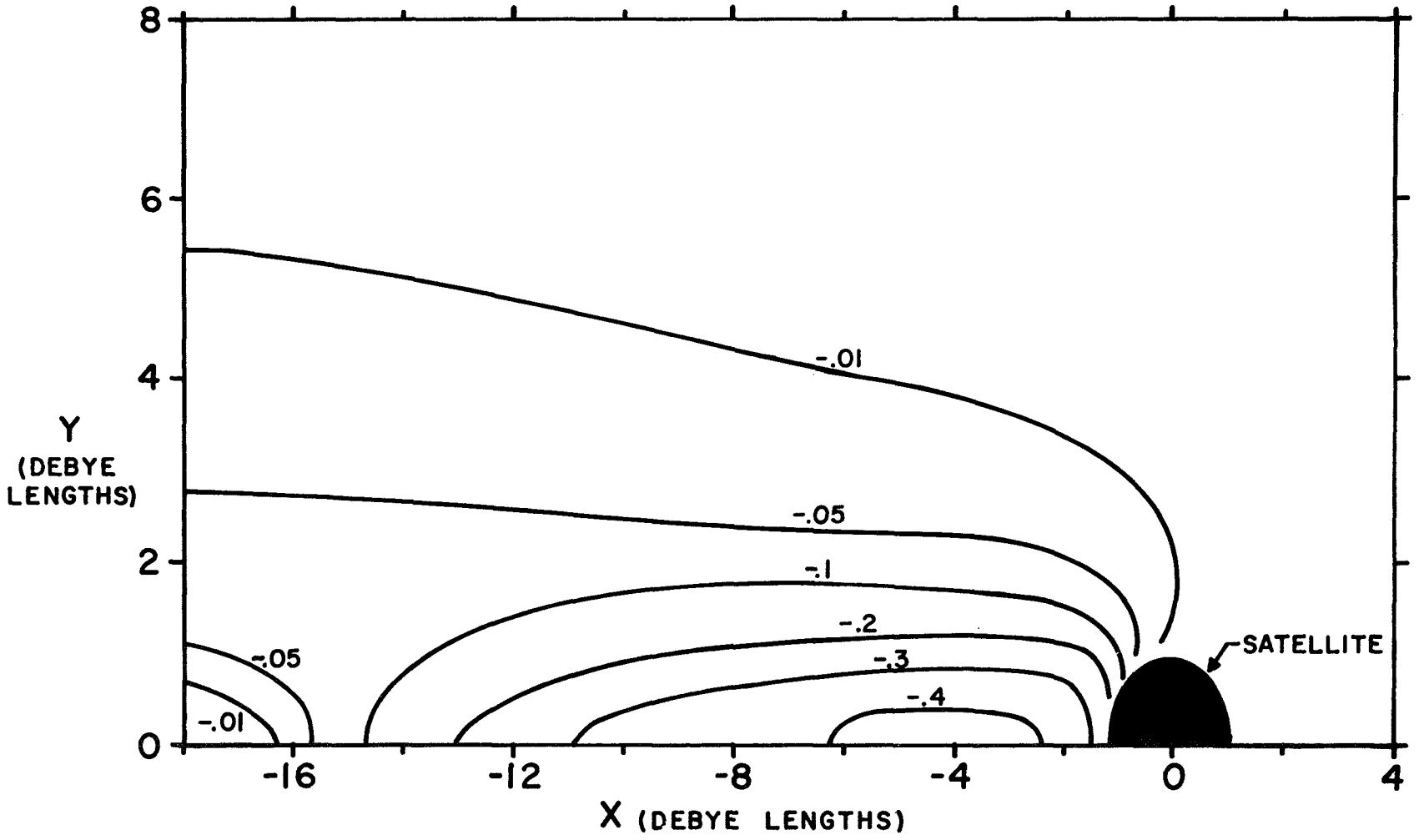

FIG. 3.2. CONTOUR PLOT OF POTENTIAL FOR SPHERICAL SATELLITE ($\hat{E}_{KE}$= 19.4, ϕ_{sat}= 0, r_{sat}= 1). IDENTICAL TO FIG. 3.1 EXCEPT FOR EXPANDED VERTICAL SCALE.

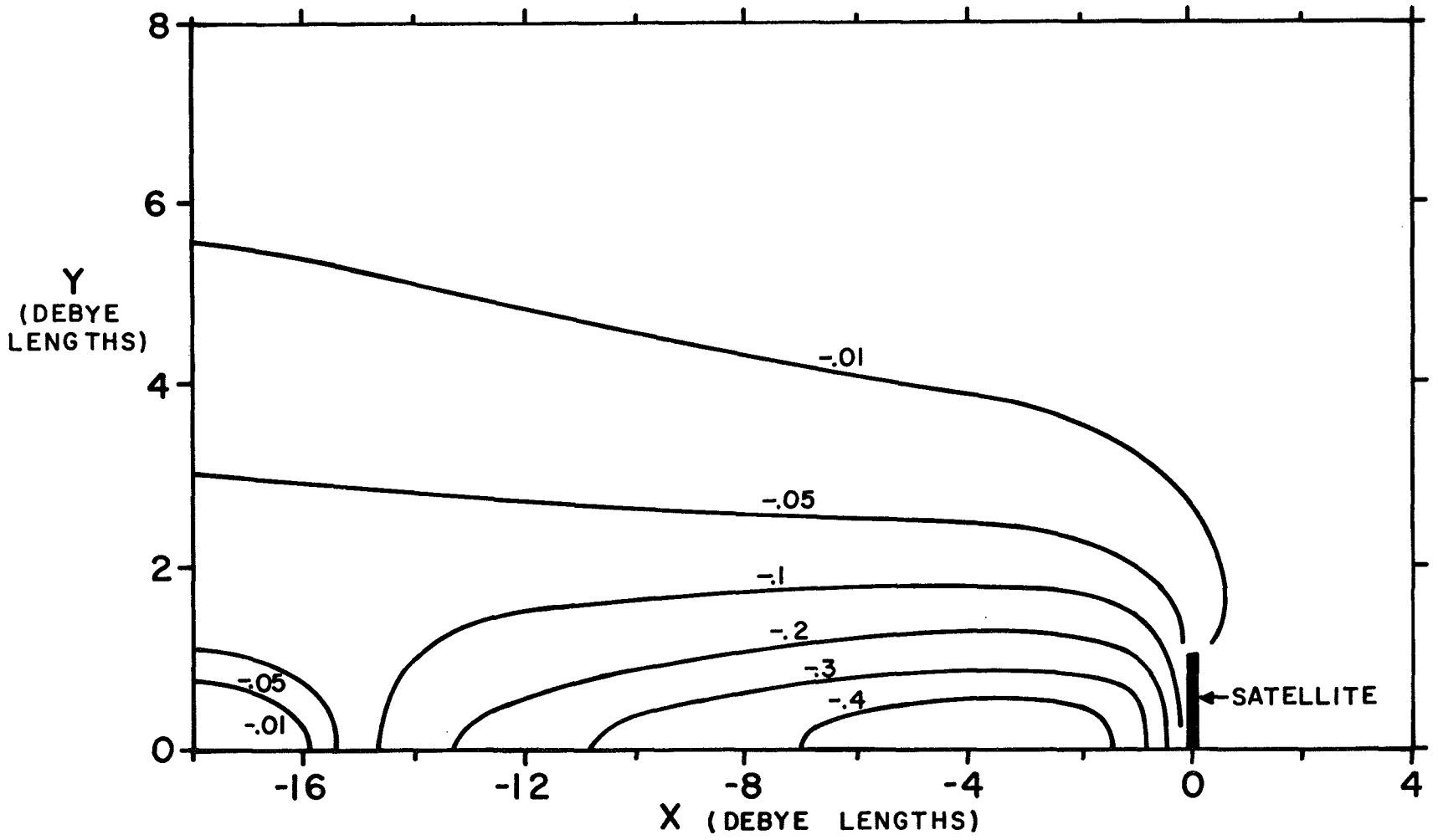

FIG. 3.3. CONTOUR PLOT OF POTENTIAL FOR DISK SATELLITE ($\hat{E}_{KE}$= 19.4, ϕ_{sat}= 0, r_{sat}= 1). NOTE SIMILARITY WITH FIG. 3.2.

disturbance are nearly identical; furthermore, the depths of the potential wells directly behind the satellite are identical. Even around the satellite, the two figures show a remarkable similarity in spite of the fact that the body shapes are different. Because of these very similar results and the fact that the numerical solution is considerably simplified for the line segment case (resulting in a 20% decrease in computer time and an unmeasurable increase in programming convenience), further results were obtained mostly for the disk case and its planar analog, the infinitely long flat plate. Nevertheless, certain results (e.g., ion current to satellite) will have a dependence on the horizontal dimension of the satellite; in such cases, results will be provided for the sphere and cylinder as well as for the disk and plate.

Range of parameters. Since the solution to the interaction problem has now been tested by comparison with a previous solution, the satellite and ionospheric parameters are varied to obtain results over the widest possible range. Part of the results obtained constitute a complete set of plots of the equipotential contours and the ion flow field for various values of the parameters. Those parameters describing the satellite and its environment include satellite shape, satellite potential φ_{sat}, satellite radius r_{sat} (or half-width in the case of a plate), and the kinetic energy of the ions $\hat{E}_{KE}$. The electron temperature and the charged-particle number density appear indirectly in these parameters by means of the normalizing quantities of electron thermal velocity, Debye length, and plasma frequency. The satellite shapes chosen

are the two most commonly found in application, a sphere and a long cylinder (end effects neglected), and two others which are the most convenient to study, a disk and a long flat plate (likewise, end effects are neglected). The disk and plate are similar in behavior to the sphere and cylinder, respectively. Both the cylinder and plate are oriented in such a direction that their axes are perpendicular to the flow velocity.

Results were obtained for a half-width as large as 25 Debye lengths. At this half-width a rather large amount of core memory ($\approx 10^7$ bits) and, therefore, an unusual computer were needed for the solution of the problem. A satellite of this size has the properties of a "large" satellite where "large" means, in the literature, $r_{sat} >> 1$. A further increase in the satellite size did not seem warranted when the resulting information was compared with the computer time necessary and the ensuing cost. A lower limit of 0.2 Debye lengths was chosen since few satellites or even satellite probes of this half-width ($\approx$ 0.3 cm at 3000 km altitude, smaller at lower altitudes) are found in practice. This solution can be classified as a solution for "small" body size ($r_{sat} << 1$) and compared with other solutions for "small" bodies. In addition, at this half-width value, the grid spacing must be much smaller than the Debye length, and as a result, the computer time required to achieve a solution for smaller body size increases very rapidly. (For further discussion on grid spacing, see Appendix B.)

In a few cases, the satellite potential is set as high as zero; as a result, the electron number density is not

exactly proportional to the Boltzmann factor. Nevertheless, since the inaccuracy occurs only in the neighborhood of the satellite, the solution is approximate only in the small region surrounding the satellite and is still generally useful. The lower limit to the satellite potential is a function of the other parameters of the problem. At very negative potentials some of the ions, strongly influenced by the satellite potential, reverse their paths (the sign of their x velocity relative to the satellite changes from negative to positive). Since the program is not designed to follow reversed trajectories, it abandons the solution. In all cases, however, the satellite potential is set at least as negative as -15 times the electron thermal energy kT_e and in some cases is as negative as $-40\ kT_e$.

The ions have a mass β relative to the electron mass and a velocity u_s relative to the electron thermal velocity. The solution depends on these two parameters only through the ion kinetic energy relative to the electron thermal energy kT_e, (to be discussed later) where

$$\hat{E}_{KE} = \beta u_s^2/2.$$

This parameter is related to the familiar ion Mach number M by $\hat{E}_{KE} = M^2/2$, where M is the ratio of the satellite speed to the ion acoustic speed $(kT_e/m_i)^{\frac{1}{2}}$. The lower limit of this parameter is 1.2 at which point the ion density calculation is susceptible to numerical error to such an extent that a convergent solution becomes difficult(see Appendix B). This

lower limit is well below the minimum of about 6 occurring in the ionosphere. The upper limit of the ion kinetic energy is 36. Higher values of this parameter do not contribute much insight into the behavior of the interaction and serve only to increase the area of the disturbance and, consequently, the computation time.

In summary, the range of parameters for which solutions have been obtained is: $-40 < \phi_{sat} < 0$, $0.2 < r_{sat} < 25$, and $1.2 < \hat{E}_{KE} < 36$. Solutions have been obtained for the plate, disk, cylinder, and sphere geometries.

B. Current Collection

In this section, the method of solution is applied to determine, for the first time in detail, the properties of current collection by satellites. In particular, the influence of the physical parameters upon the ion current is investigated thoroughly, and plots of ion current vs. satellite potential are shown. These plots may be employed for the analysis of experimental data. As an application, an exact value for the floating potential is calculated at the end of the section.

1. Ion Current

Introduction. The ion current collected has a basic component arising from the current swept up by the moving satellite. Consider a satellite at plasma potential, i.e., with zero potential relative to the plasma. In the satellite frame of reference, it appears that a beam of ions intercepts the satellite. It is assumed that the intercepted ions are either absorbed by the surface or neutralized and reflected as neutral particles. This ion current will be referred to as the "ram" current and in dimensionless units is equal in value to $I_{io} = u_s A_s$, where u_s is the satellite speed and A_s is the cross-sectional area of the satellite. For a disk or a sphere the cross-sectional area is $A_s = \pi r_{sat}^2$; for a cylinder or a plate, $A_s = 2 r_{sat} L$, where L is the length of the cylinder or plate. For these two satellite bodies, therefore, it is convenient to find the ion current per unit length L

(in units of Debye length) rather than the total ion current Henceforth, the "ram" current for ions I_{io} will be considered in the case of spheres and disks as that current incident on the entire surface of the body; for cylinders and plates it will be that current per unit length incident on the body.

As the satellite potential is permitted to become more negative (ion-attracting), its ion current increases. This increase arises from the increase in the number of ions attracted to the satellite body. This increase is, however, slow because the negative potential has a moderate effect on the ion trajectory.

Normalization of ion current. Figure 3.4 shows the normalized ion current I_i collected by a plate satellite as a function of satellite potential. The ion current has been normalized by the value of the "ram" current in order to show clearly the effect of the ion-attracting potential as it is increased negatively. It is interesting to note that the normalized ion current collected by a satellite at plasma potential is not exactly equal to unity. The actual value of the plasma potential current in this case is 0.9994. The reason for this minor discrepancy is that the negative potential occurring in the wake curls slightly over the edge of the satellite and in front of it. (See Fig. 3.3 which is a contour plot of the potential field for a similar case.) Although the field is negative and is therefore ion attracting, it is in such a position that it deflects a minute, yet measurable portion of the ions making up the "ram" current away from the satellite. Nevertheless, the difference between the "ram"

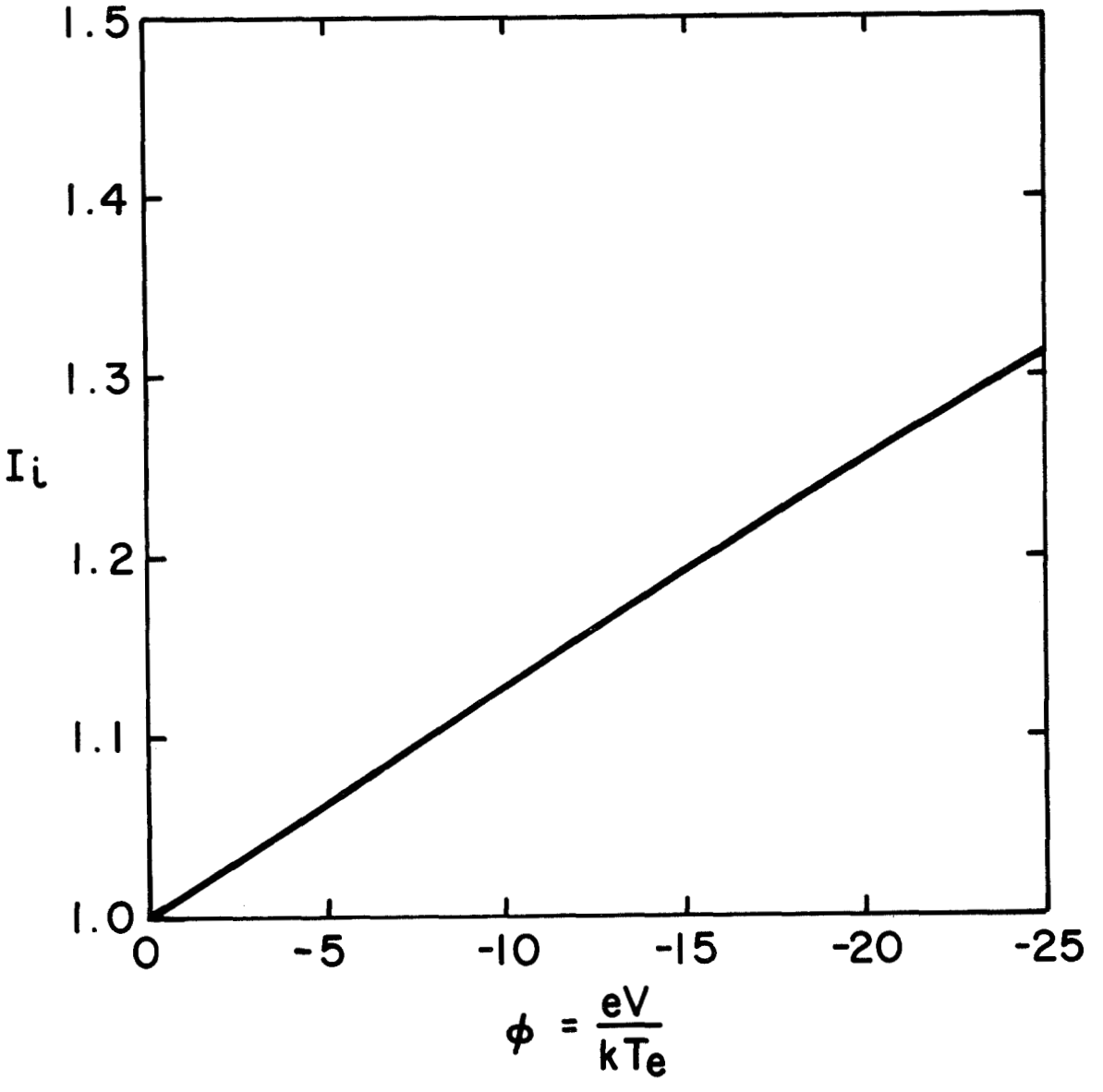

FIG. 3.4. ION CURRENT VS. POTENTIAL FOR PLATE SATELLITE ($\hat{E}_{KE}$= 12, r_{sat}= 1). NOTE NEARLY LINEAR DEPENDENCE.

current and the plasma potential current is very small, and, therefore, the two ion currents shall be considered as one.

For the chosen parameters ($\hat{\mathcal{E}}_{KE}$= 12 and r_{sat}= 1, corresponding to a body radius of 1.5 cm at a 1000-km altitude), the growth rate of the ion current is only 1.3% per unit of satellite potential. As a result, if the ion current is to be significantly larger than the plasma potential value I_{io}, then the satellite must have a potential which is of the same order of magnitude as the ion kinetic energy.

Functional dependence of ion current on potential. Close examination of Fig. 3.4 reveals that the ion current has a near linear dependence upon negative satellite potentials. This dependence is not unexpected since Medicus[39] and Brundin[40] have shown that the ion current to a sphere or cylinder in a central-force field is linearly dependent on the potential. This figure, however, shows that for a plate satellite in a noncentral-force field the ion-current dependence is nearly linear. Other figures to be shown later indicate the same nearly linear behavior of ion current over a variety of satellite shapes and a wide range of parameters. It can be argued that nonlinearity in the ion current is not expected to occur until the satellite potential has become extremely negative, i.e., many times larger than the ion kinetic energy. Unfortunately, this possibility cannot be investigated with the present program. At these strongly negative potentials, some of the ion trajectories reverse their velocity in the x direction, and the program, unable to calculate the correct ion density, becomes invalid and

discontinues the computation. Hence, for these extreme values of potential, the ion current is not determined.

It is possible to use the results of certain experiments to give an indication of the behavior of the ion current for larger ion-attracting potentials. Experiments simulating the satellite-ionospheric interaction have been done with small bodies in ion beams.[32,41] These experiments show that saturation occurs for neither moderately nor, in fact, highly negative potentials. A possible explanation for the lack of saturation in the ion current is that the ion density decreases in the neighborhood of the front of the body when the potential is made more negative. This decrease in ion number density arises from the increase in the ion velocity as the ion is accelerated toward the body. Therefore, the shielding effect on the potential field by the positive charge density is somewhat reduced. As a result, the potential field is not shielded sufficiently to alter the nearly linear dependence of the ion current on the body potential.

Influence of satellite geometry on ion current. In a strict sense, it is not true that the cross section of the satellite is the only body dimension which influences the behavior of the plasma flow. To a certain extent a sensitive variable, such as the ion current, is dependent upon the exact shape and length of the satellite. Consider a disk and plate satellite of equal radius and half-width. At zero potential they collect equal normalized ion currents, namely "ram" current. However, as the satellite potential is made negative, the two satellites collect unequal quantities of normalized ion current. The disk collects current from the surrounding "two-dimensional"

ring area, whereas the plate collects from the "one-dimensional" strip area above and below the plate. The ring increases in area as the collection region is extended radially; the strip undergoes no such geometric increase. As a result, the disk can be expected to attract more ion current than the plate at a given negative potential. Moreover, the sphere and other axially symmetric bodies will attract more ion current than their planar counterparts. Figure 3.5 shows that the ion current collected by the disk and sphere is greater than that collected by the plate and cylinder for equal body radii.

The ion current, to a certain extent, depends on the length of the satellite in the flow direction. At zero satellite potential, the plate and cylinder collect equal amounts of ion current. Since both bodies are planar, differences in their ion current for negative body potentials cannot be attributed to the geometric effect discussed above. However, since the cylinder has a finite thickness, some of the attracted ions which would not intercept a plate would intercept the sides of a cylinder and contribute to the collected ion current. The greater surface area which a cylinder has allows it to intercept more of the attracted ions than a plate having the same cross section. The same argument applies to a sphere as compared to a disk of equal cross section. In general, the bodies with finite thickness in the flow direction can be expected to collect a larger amount of ion current than their infinitesimally thin counterparts. Another examination of Fig. 3.5 shows that the ion current for a sphere and cylinder is, in fact, larger than the ion current for a disk and plate, respectively. Although the currents themselves are not vastly

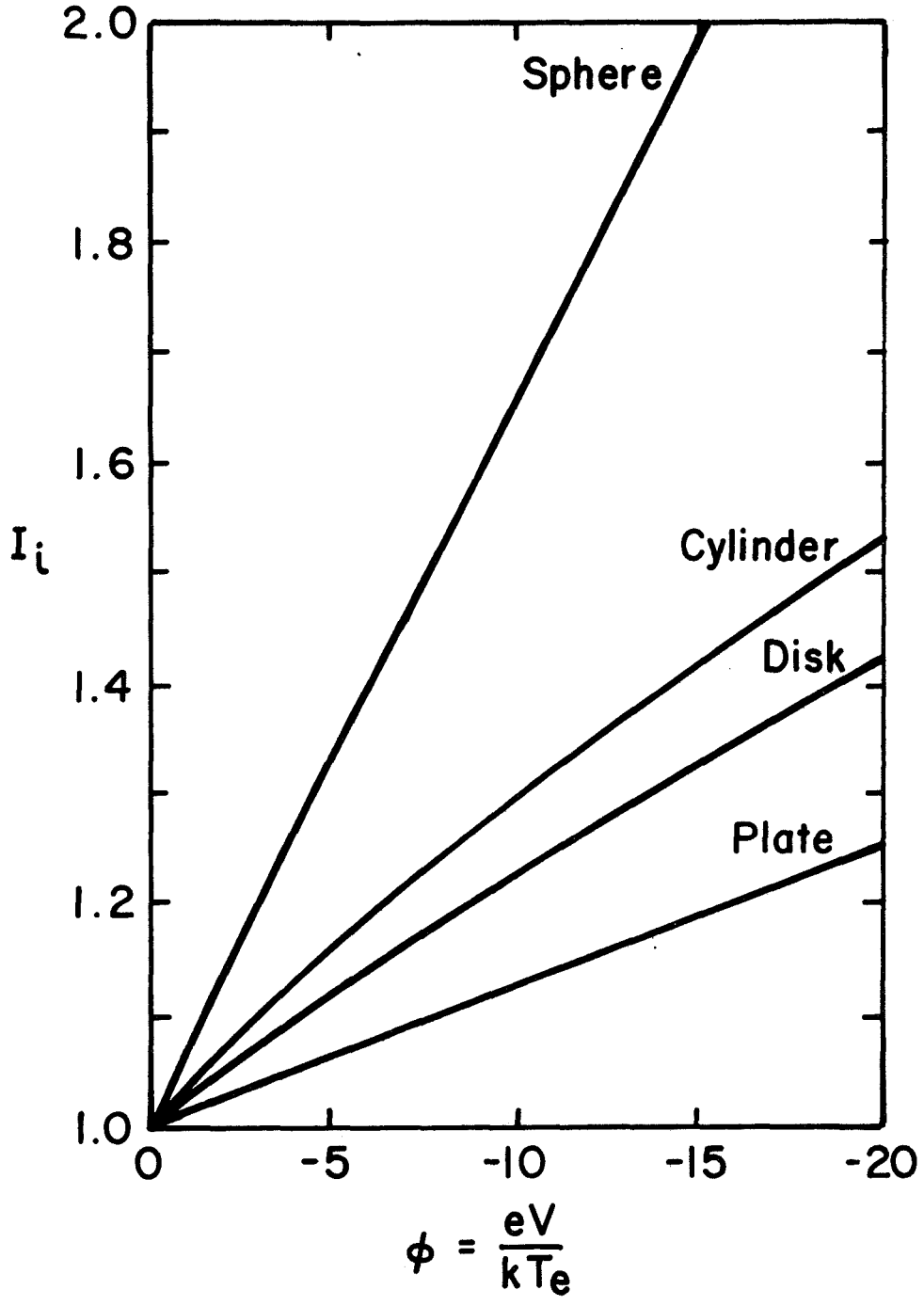

FIG. 3.5. ION CURRENT VS. POTENTIAL FOR DIFFERENT SATELLITE BODIES ($\hat{E}_{KE}$= 12, r_{sat}= 1).

different, their rates of growth as a function of satellite potential differ by as much as factor of two.

Angular dependence of ion flux. The detailed behavior of the ion flux (current per unit area) as a function of the location on the surface of a cylinder satellite is of considerable interest. Since certain satellite instrumentation is sensitive to the incident charged particle flux, it is important to know how the flux varies as a function of the polar angle θ between the direction normal to the surface at the point of interest and the direction of satellite flight. The electron flux can be expected to be independent of the polar angle since the thermal velocity of the electrons is much greater than the satellite velocity and, hence, the electron flux is uniform over the entire surface. The ion flux will depend on the polar angle of the point of interest since the incident ions appear to be moving as a beam. Therefore, if the satellite is rotating or "tumbling" about an axis parallel to the cylinder axis, satellite instrumentation will record an ion flux varying from zero at the rear to a maximum value at the front. When the ion beam intercepts a satellite at plasma potential, the ion flux to the front surface can be expected to be proportional to the cosine of polar angle θ. This dependence means that at the very front of the satellite, the ion flux is at a maximum; the flux decreases until at a right angle to the flow, the flux is zero and remains zero over the entire back surface of the satellite. When the satellite potential is made negative, the ion flux not only increases on the frontal area but also is finite in that part of the rear where the ions intercept the satellite. This additional collection area grows as the satellite is made more negative.

Figure 3.6 shows the ion flux J_i (normalized by the incident flux u_s of the beam) as a function of the polar angle θ. The ion flux at zero satellite potential is a cosine function. The line does not extend to $\pi/2$ (i.e., 1.57) radians because in the computer program the trajectory spacing must be extremely small for accurate determination of the angle where the ion flux becomes zero (the grazing angle). Extrapolation of the obtained results, however, shows that as expected the grazing angle is $\pi/2$ radians. At a satellite potential of -10, the resulting ion flux is similar to a cosine curve displaced by a positive bias. The figure shows that the extrapolated grazing angle is shifted from a right angle to one which lies in the rear region of the satellite. The integrated ion flux is the ion current; hence, in this figure that portion of the increase in the ion current due to the additional ions attracted to the front of the satellite can be distinguished clearly from that portion due to the finite thickness of a cylinder satellite.

Figure 3.7 shows the ion flux to a cylinder satellite for a variety of satellite parameters. In all cases, the ion flux has an approximate functional dependence on polar angle in the form of an incremented cosine function. This general functional form has been observed on a rocket launched in the lower ionosphere (220-500 km).[11] The ion flux, measured by a small probe mounted in the body of the rocket, has a zero value when the probe is in the far back area of the rocket. The polar angle at which the zero ion flux begins is estimated to be $\approx 130^{\circ}$. In addition, the polar angle is zero at the point where the ion flux is a maximum. The shape of the ion-flux curve as a

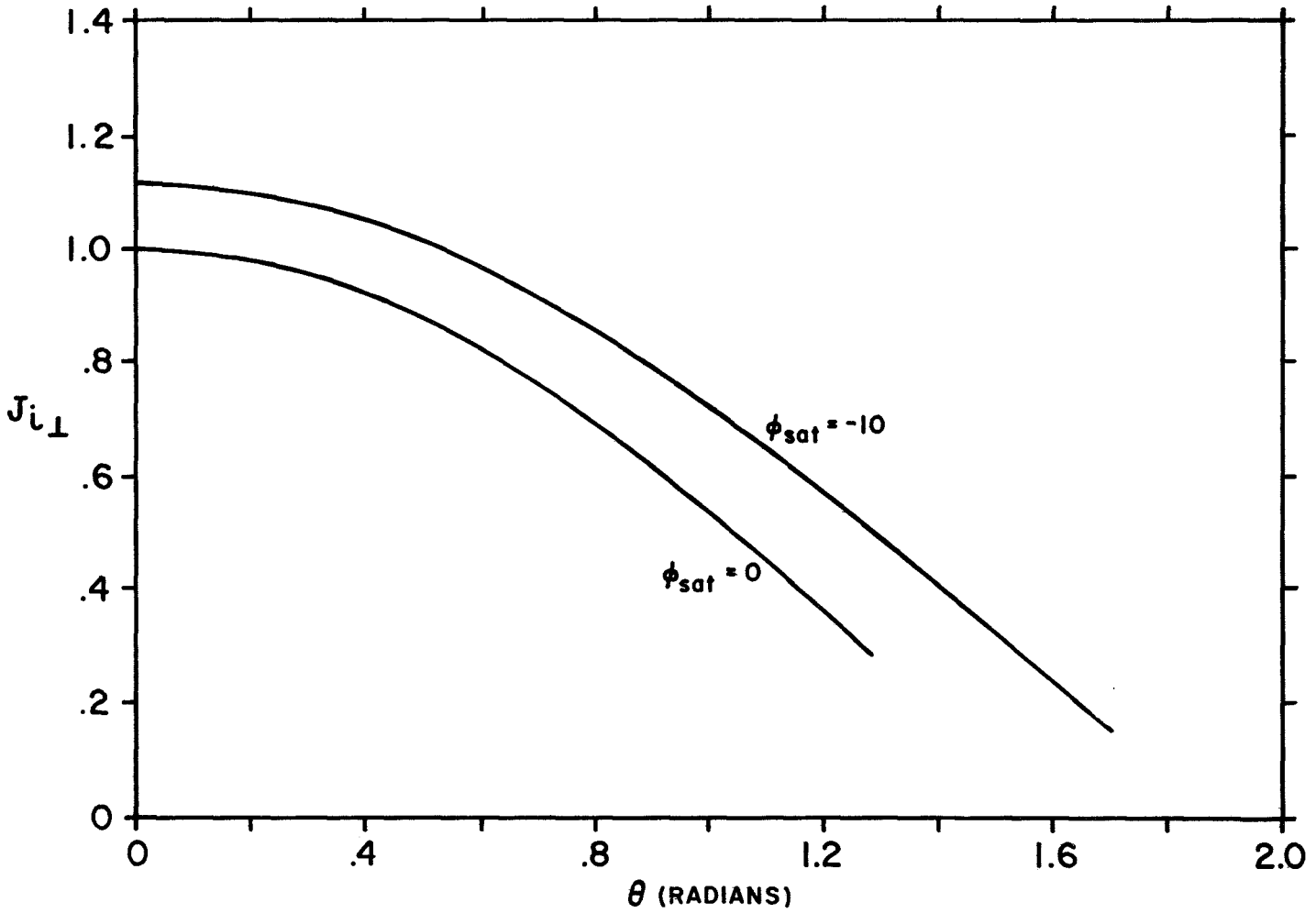

FIG. 3.6. ANGULAR DISTRIBUTION OF NORMAL ION FLUX TO CYLINDRICAL SATELLITE ($\hat{E}_{KE}$= 12, r_{sat}= 1).

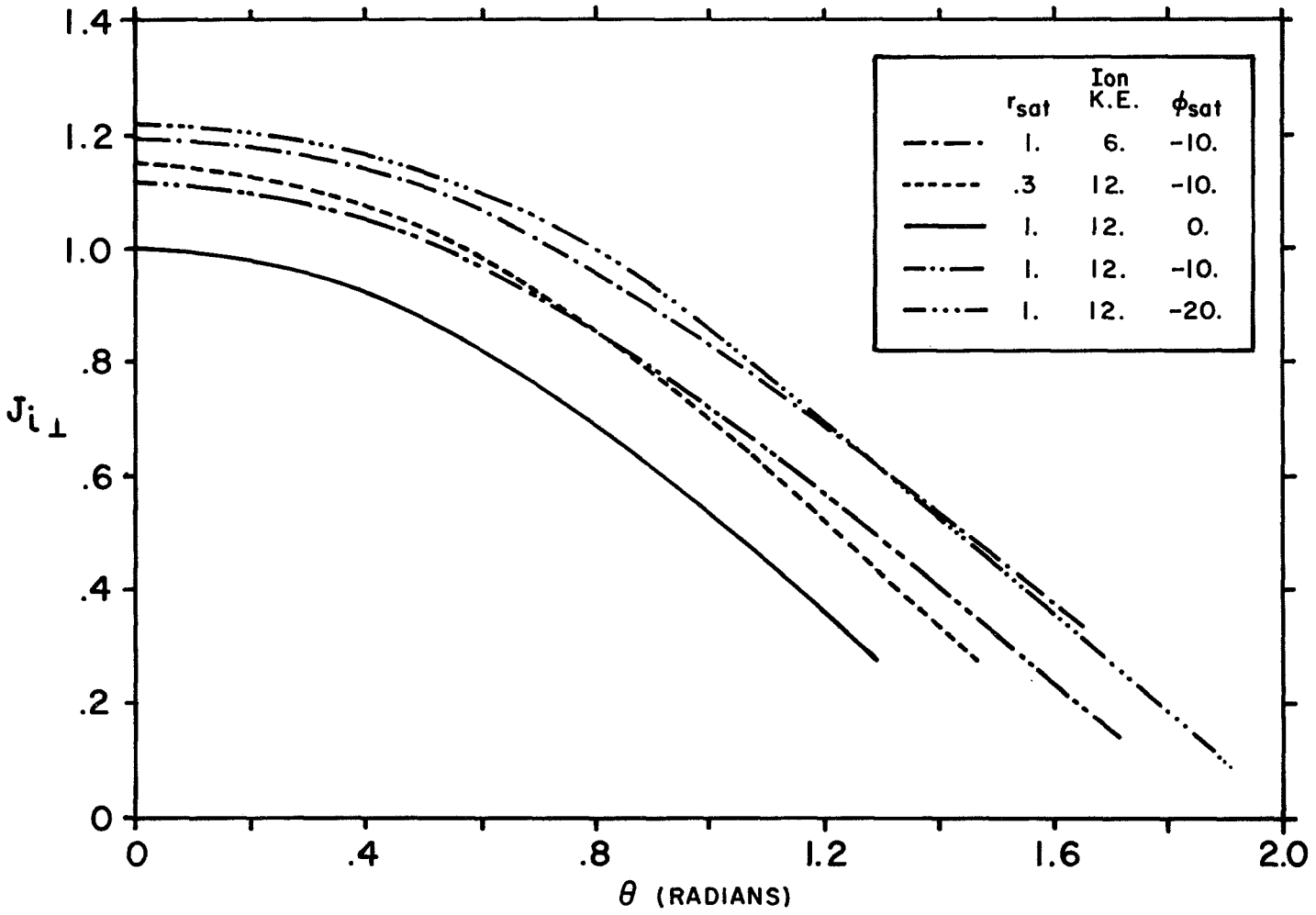

FIG. 3.7. ANGULAR DISTRIBUTION OF NORMAL ION FLUX TO CYLINDRICAL SATELLITE WITH VARIOUS PARAMETERS. NOTE THAT DEPENDENCE IS SIMILAR TO INCREMENTED COSINE FUNCTION.

function of angle is remarkably close to that of an incremented cosine function.

Influence of satellite radius on ion current. The satellite radius has an important effect on ion collection by satellites. Of course, the larger the satellite radius, the larger the ion current it collects. However, the normalized ion current I_i does not depend directly on the variations in radius since the normalizing "ram" current is proportional to the satellite cross-sectional area. Nevertheless, the normalized ion current is dependent indirectly on the radius r_{sat}. Since the attractive electric field of a satellite with negative potential can extend over a distance of the order of a few Debye lengths in the vicinity of the satellite, the ion collection area is also of the order of a Debye length. For satellites whose radius is large compared with the Debye length ($r_{sat} >> 1$), the increase of the normalized ion current with increasing ion attracting potential will be quite small. The overall ion current will be large, but the relative contribution due to the attractive potential will be small. On the other hand, for satellites whose radius is small compared with the Debye length ($r_{sat} << 1$), the attracted ion current will be quite large when compared with "ram" current.

Figure 3.8 shows that the rate of growth increases as the half-width of the plate satellite is made progressively smaller. Note that the curve for the parameter $r_{sat} = 25$ extends to a satellite potential of only -15. At a more negative potential on the "large" satellite, some of the ions, influenced by the electric field in the wake for an unusually long time, reverse their trajectories. In this case, the calculation is terminated.

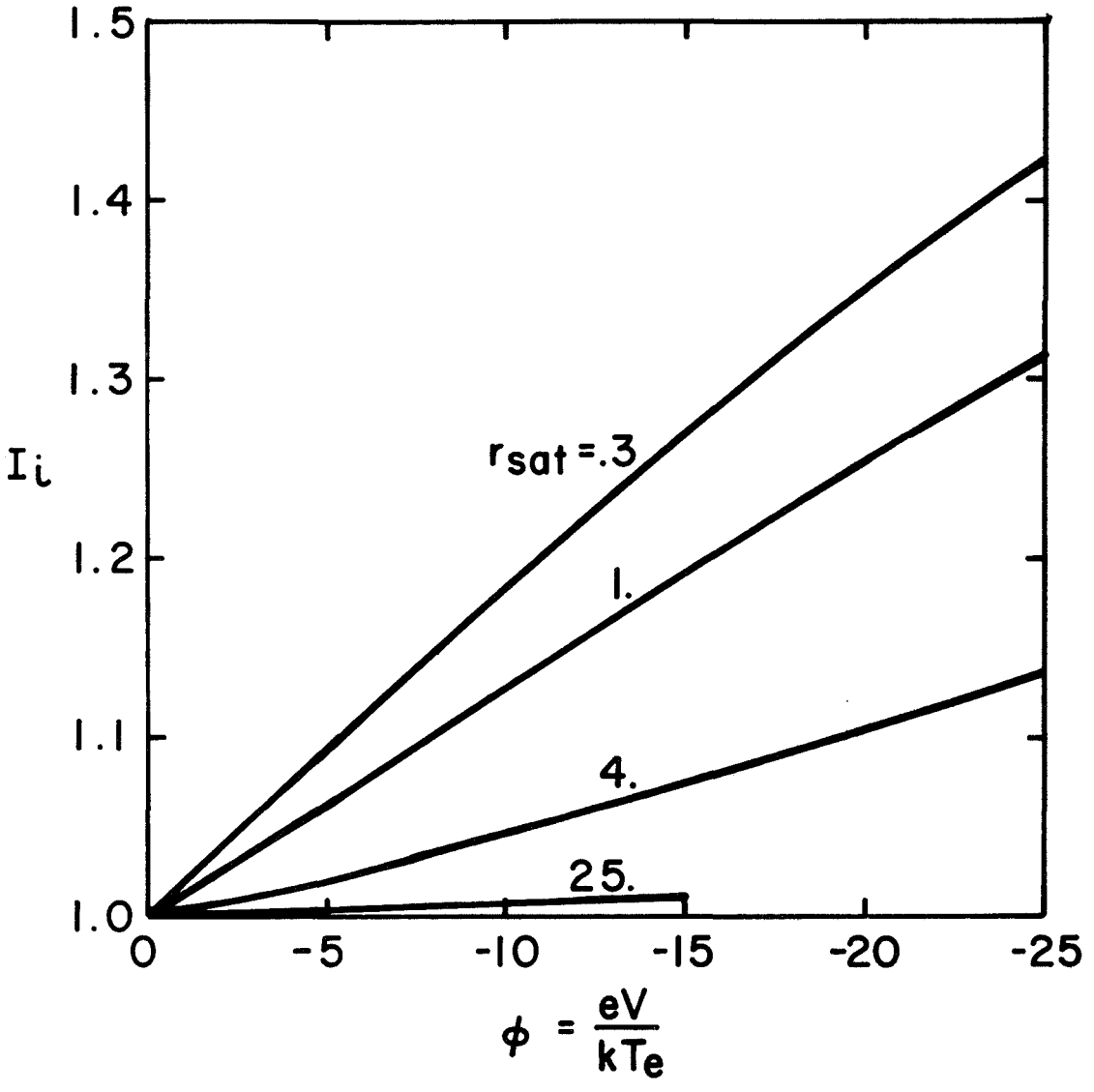

FIG. 3.8. ION CURRENT VS. POTENTIAL FOR PLATE SATELLITES OF VARIOUS SIZE ($\hat{E}_{KE}$= 12).

The results indicate that the ion current collected by a "large" satellite (most real ionospheric satellites are "large") is almost entirely independent of the ion-attracting satellite potential. The ion current is essentially the "ram" current and is dependent only on the cross section and speed of the satellite. (The number density and electron temperature dependence appear indirectly through the Debye length.) For satellites of "moderate" size ($r_{sat} < 10$), however, the ion current has a significant dependence on the potential, as can be seen in Fig. 3.8.

The significance of parameter $\hat{E}_{KE}$. The ion current collected by the satellite is a function not only of the satellite parameters but also of the ion parameters. Both the ion-mass ratio and the initial ion velocity influence the development of the ion-flow field but not in a unique and individual manner. Rather, the flow field is dependent on the ion kinetic energy, and only through this single parameter do the ion mass and velocity influence the trajectories. In fact, the orbit equation (i.e., Newton's equations without the time variable) indicates that the trajectory of a particle in a conservative force field is dependent only on the initial position, direction, and energy of the particle. The velocity along the trajectory, however, does not depend only on these three initial conditions; the velocity of a light ion is, of course, greater than that of a heavy ion if both ions have equal initial energy. Since the problem is assumed to be steady, only the path of the ion and not its velocity along the trajectory determines the ion density. Hence, the ion kinetic energy is the unique ion parameter on which the flow field (and, consequently, the potential field) depends.

The fact that the trajectory is not dependent on the ion mass and initial velocity except by way of the initial energy can be deduced by introducing scaling relations.[33] However, the argument is heuristic in nature, and, as a result, not so satisfactory as a direct proof. A laboratory experiment which was designed to measure ion current to a body in an environment simulating the ionosphere was used to check the validity of the ion kinetic energy assumption.[32] The results indicate that the assumption is correct within the accuracy of the experiment.

As a check on the numerical accuracy of the computer program, a sample case was run to test the ion energy assumption. For this case, the ion mass was increased by a factor of 16, and the satellite velocity was decreased by a factor of 4 in order to insure that $\hat{E}_{KE}$ would remain constant. The ion current, a sensitive variable in the problem, was found to remain independent of the ion mass and velocity when the ion kinetic energy was constant. Hence, it was proved that it is sufficient to present results as a function of the ion kinetic energy $\hat{E}_{KE}$ rather than both the ion-mass ratio β and the satellite velocity u_s.

Influence of ion kinetic energy on ion current. Figure 3.9 shows tha influence of $\hat{E}_{KE}$ on the ion current as a function of potential for a plate satellite. Because of the usual normalization, the ion current at plasma potential is independent of $\hat{E}_{KE}$. However, the ion current at negative potentials is dependent upon the "stiffness" of the ion trajectories. As a result, the rate of growth of the ion current decreases with increasing $\hat{E}_{KE}$.

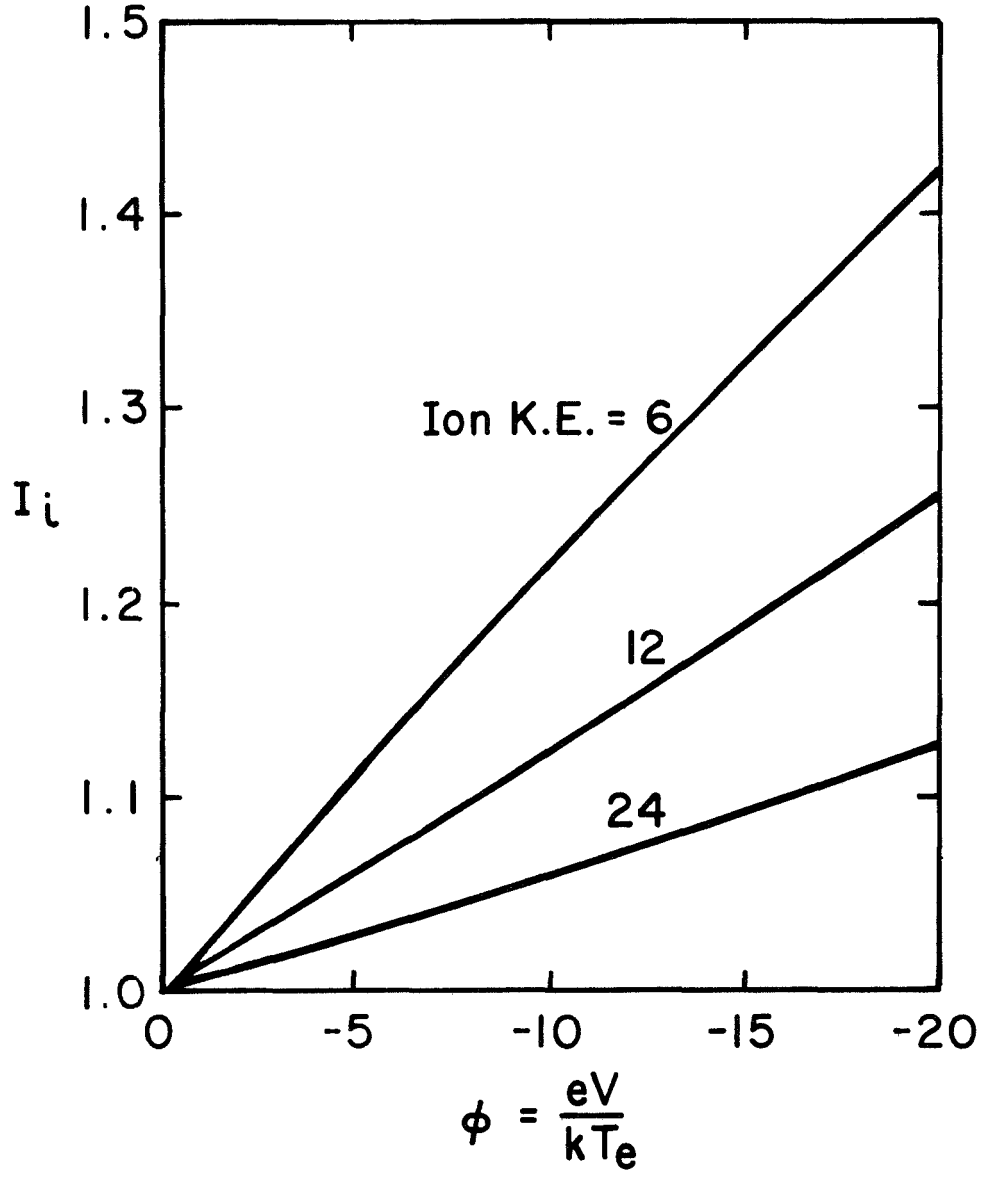

FIG. 3.9. ION CURRENT VS. POTENTIAL FOR PLATE SATELLITE WITH VARIOUS ION KINETIC ENERGIES $\hat{E}_{KE}$ (r_{sat}= 1).

2. Electron Current

The ion current collected by satellites having been discussed thoroughly, it is now appropriate to consider the electron current. Fortunately, the solution for the electron current is considerably simpler because of the inherent assumptions made about the electron distribution function. It has been assumed that since the thermal speed of the electrons is an order of magnitude greater than that of the satellite, the electron distribution function is Maxwellian. Then the normal electron flux per unit area at the satellite surface is $N_e e\bar{c}_e/4$ which in dimensionless units becomes $J_e = (2\pi)^{-\frac{1}{2}} n_e$. If the Boltzmann factor is substituted for n_e, then it follows that the dimensionless electron current I_e collected over the satellite surface area S is

$$I_e = SJ_e = (2\pi)^{-\frac{1}{2}} S \exp(\varphi_{sat}). \tag{3.1}$$

For example, the surface area of a sphere is $4\pi r_{sat}^2$; for a disk, the surface area is twice the cross-sectional area, i.e., $2\pi r_{sat}^2$, since electrons are collected from both the front and back surfaces.

3. Net Current

Approximate value of floating potential. Since the electron current collected by a satellite at plasma potential is much greater than the ion current collected, the satellite acquires a negative charge. The negative potential at which the net current is zero (i.e., the satellite "floats" electrically in the plasma) is called the floating potential. It

is important to determine the floating potential of satellites since any instrumentation which is grounded to the satellite will acquire this negative potential with respect to the surrounding plasma.

A good estimate of the floating potential can be made by assuming that the ion current is approximately equal to the "ram" current I_{io} when the satellite is at the floating potential. In dimensionless units, the "ram" current is

$$I_{io} = u_s A_s, \tag{3.2}$$

where A_s is the cross-sectional area of the satellite. By setting (3.1) equal to (3.2), the potential φ_{sat} may be obtained;[2]

$$\varphi_{sat} = \ln[(2\pi)^{\frac{1}{2}} u_s A_s/S]. \tag{3.3}$$

In the case where the satellite is a plate or a disk, the ratio of the cross-sectional area to the total surface area A_s/S is 2. For example, if the satellite is at an altitude of 1000 km where $\hat{E}_{KE}$= 12 and the dominant ion is helium (β = 7344), then u_s=.0571. At these values of the parameters, the floating potential φ_{sat} obtained from Eq. (3.3) is -2.64.

Exact value of floating potential. The floating potential can be obtained more precisely by including in the calculation the dependence of ion current on the satellite potential. Since the floating potential is negative, the collected ion current is greater than the "ram" current. As a result, the floating potential can be expected to be not quite so negative as -2.64, the originally estimated value.

Figure 3.10 shows both the ion current and the total current collected by plate satellite (which is one Debye length in half-width) as a function of satellite potential. As above, the ions are assumed to be helium and to have a kinetic energy of 12. Both the total current and the ion current have been divided by the ion "ram" current I_{io} in order to maintain consistency with the previous figures showing ion current. The floating potential, obtained by setting the total current equal to zero, is -2.52. This computed value of the floating potential is about 5% less than the estimated value and represents the correction obtained when the ion current is calculated as a function of potential. The logarithmic dependence of the floating potential on such corrections reduces their effect. As a result, further calculations of floating potential for changes in the parameters will not differ significantly from the case shown. In this figure, the current goes off scale when the satellite potential approaches zero. The insert in this figure shows the total current on a reduced scale over a range of satellite potential from zero to -10. Notice the extremely large contribution made by the electrons when the satellite is at plasma potential.

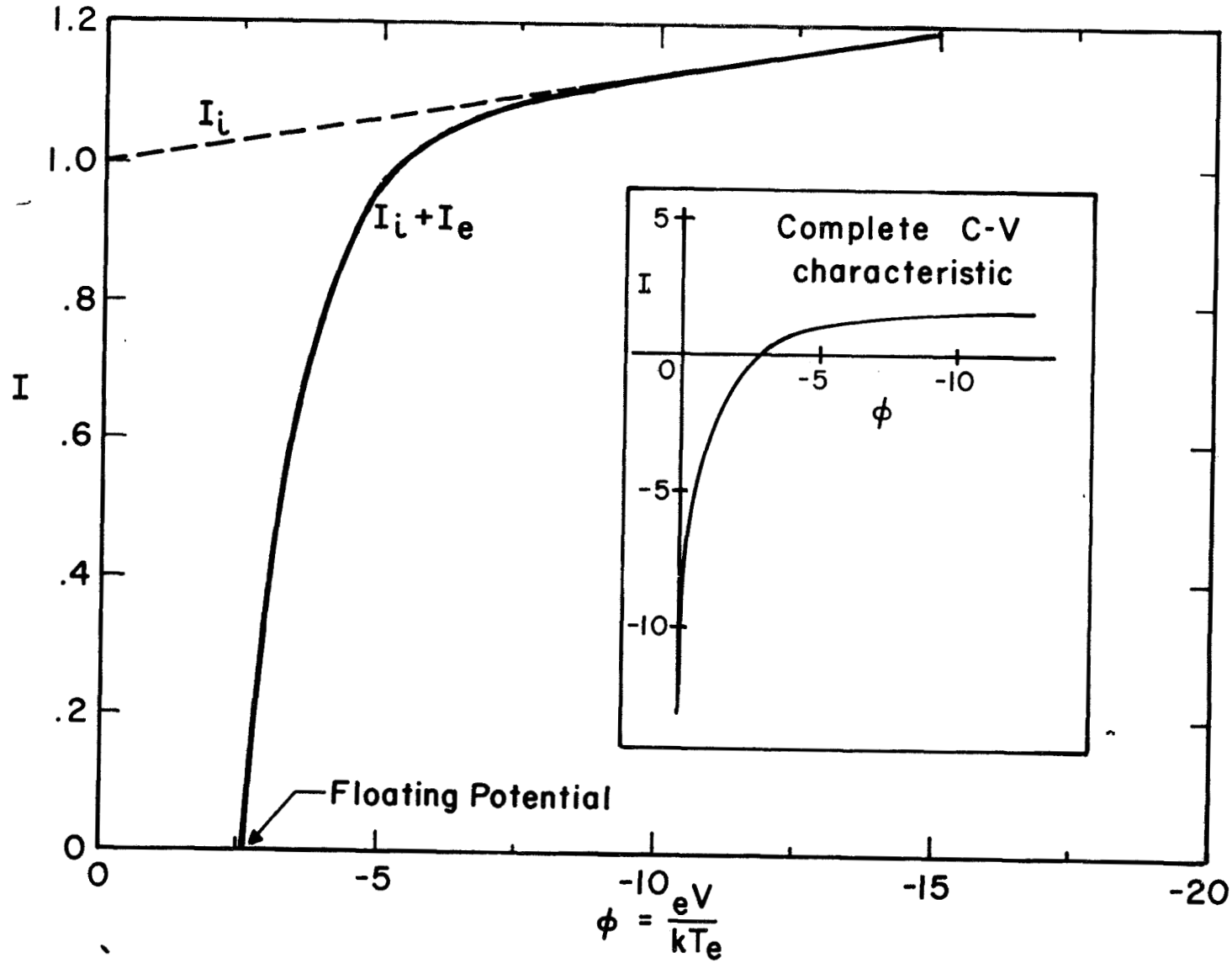

FIG. 3.10. NET CURRENT VS. POTENTIAL FOR PLATE SATELLITE ($\hat{E}_{KE}$=12, r_{sat}= 1). INSERT SHOWS NET CURRENT OVER GREATER RANGE.

C. Satellite Drag Due To Ionospheric Plasma

The dominant component of plasma drag. The ionospheric plasma flowing toward the satellite transfers part of its momentum to the satellite. The direction of the net momentum transfer is opposite to that of the satellite velocity; hence, a net drag acts upon the satellite. In the lower ionosphere, where the plasma density is much less than the neutral-particle density, the plasma drag is much smaller than the neutral-particle drag. However, in the upper ionosphere (above 1500 km), these two are comparable.

The component of the plasma drag due to electrons is negligible since the light electrons have a thermal velocity which is much greater than the satellite velocity. As a result, if the potential field about the satellite is monotonic, the net momentum transfer to the satellite by the electron flux (which is uniform over the surface of the satellite) is zero. Furthermore, if the potential field is not monotonic and the electron flux is greater on one side of the satellite than on the other, the resulting electron momentum transfer will remain extremely small in comparison with the ion momentum transfer because of the large ion mass ratio. Therefore, only the ion component of the plasma drag need be considered.

Lower and upper limits of plasma drag. The basic component of the drag arises from the momentum transfer of those ions which are swept up by the satellite. In keeping with the terminology above, the drag of the swept-up ions is called the "ram" drag. It is assumed that the ions which intercept the satellite surface are neutralized. After neutralization, the

ions are emitted diffusely or they are reflected specularly. The momentum transfer of the diffusely emitted particles is proportional to their thermal velocity which in the case of perfect accommodation is proportional, by definition, to the square root of the satellite temperature. Depending upon its location and its internal heat sources, the satellite can have a temperature of several hundred degrees Kelvin. In fact, the surface itself can be at different temperatures depending upon whether it is facing the sun. As a lower limit for the satellite temperature, absolute zero is assumed. At this temperature, the reemitted particles have no momentum and do not contribute to the drag. Therefore, a satellite which diffusely reflects ions with zero velocity has the lowest possible plasma drag.

In order to obtain an upper limit to the momentum transferred by the neutralized ions, specular reflection must be considered. The surface is assumed to be a perfect mirror of momentum, i.e., the component of particle velocity tangential to the surface after reflection is equal to that before reflection, and the normal component after reflection is equal to and opposite that before reflection. The relative kinetic energy of the specularly reflected ions, equal to that of the incident ions, is equivalent to a temperature of 10^4 ^{o}K, at least. Since this equivalent temperature is much larger than the temperture a satellite could have under any conceivable ionospheric condition, the momentum transfer by specularly reflected particles is much larger than that by diffuse reflection and is, therefore, an upper limit.

The actual surface interaction of the incident ions is not known exactly. Laboratory experiments simulating both satellite surfaces and ionospheric conditions indicate that the

interaction is a mixture of both diffuse and specular reflections, with the diffuse type probably being dominant.[42] The coefficient of the mixture (known as an accommodation coefficient in rarified-gas theory) is defined as[42]

$$\sigma = \frac{p_i - p_r}{p_i - p_s} ,$$

where p denotes the normal momentum flux and the subscripts i and r denote the incident and reflected components. The term p_s is the normal momentum flux of the gas if it were diffusely reflected from the surface at a mean thermal speed corresponding to the surface termperature. The coefficient is strongly dependent on the angle of interception; of course, the momentum transfer from the diffuse component is dependent on the satellite temperature. Since the mixture coefficient cannot be assumed, drag data will be presented for both extremes of the surface interaction, namely, the lower and upper limits corresponding to diffuse reflection with zero velocity and to specular reflection, respectively. Incidentally, the lower-limit case is equivalent to the case of no reflection whatsoever. In this case, the ions would accrete on the satellite surface and eventually coat it.

Normalization of drag results. If ions at the satellite surface are assumed to undergo diffuse reflection with zero velocity (indicated by the subscript "dr"), then the change in ion velocity at the surface is simply u_s when the satellite is at plasma potential. Hence, the "ram" drag in dimensionless units is equal to $\beta u_s^2 A_s$. For clarity of presentation (as discussed previously), the net drag obtained henceforth will

be normalized by the "ram" drag $\beta u_s^2 A_s$. As a result, the normalized drag D_{dr} of a satellite at plasma potential is approximately unity. If the ions undergo specular reflection (indicated by subscript "sr") at the surface of a plate or disk satellite, the velocity change is $2u_s$; the resulting normalized drag D_{sr} is approximately 2. For a real case where ions undergo both diffuse and specular reflection, the normalized plasma drag of a plate or disk satellite at plasma potential will lie somewhere between the lower and upper bounds of 1 and 2.

Approximate drag for diffusely reflective satellite. When the satellite potential is negative, ions are accelerated toward the satellite, and those trajectories which intercept near the satellite edge are bent inward. The resulting drag is a complicated function of the angle of interception, the speed at interception, and the total number of ions which intercept. For the case of diffuse reflection, however, the drag due to intercepted ions can be obtained easily. If the region surrounding and including the satellite is considered to be a "black box," the horizontal momentum transfer to this box is the difference in momentum of the intercepted ions after they intercept the satellite and before they enter the box. The momentum after interception is zero, and the momentum before entrance is $\beta u_s^2 A_i$, where A_i is the area of interception in the free-streaming region outside the "black box." Hence, the normalized drag D'_{dr} (due to intercepted ions which are diffusely reflected) is equal to the normalized ion current collected by that satellite, i.e., $D'_{dr} = I_i$. This equality holds for all satellite bodies and ionospheric conditions.

Additional electric drag. An additional component of drag, however, arises from those ions which are deflected by the electric field surrounding the satellite but do not intercept the satellite. This component is called the electric drag since, in a sense, it is the pressure of the electric field on the satellite. Although the electric drag is generally smaller than the drag of the intercepted ions, it is not insignificant. In order to calculate the electric drag, the momentum of those ions which miss the satellite is determined both before they enter the disturbed region and after they leave it. Since the potential field is conservative, the energy of the deflected ions does not change; however, the vertical velocity of the departing ion is not zero, and the horizontal velocity is less than that of the incoming ion. As a result, a net loss of momentum to the satellite arises. For the case of diffuse reflection, therefore, the total drag is the sum of the drags of the intercepted and deflected ions.

Increase in drag of specularly reflective satellite. For the case of a satellite which reflects ion specularly at the surface, another component of drag arises (in addition to the electric drag). Consider an ion which undergoes acceleration toward a negatively charged satellite and eventually intercepts it. As the ion is being accelerated, it exerts an equal and opposite force on the satellite and therefore, accelerates the satellite (a negative drag). At the point of impact, the ion gives up its additional momentum to the satellite. If the ion is reflected diffusely, the negative drag at the time of ion acceleration is equal to the additional drag at the time of impact; hence, the velocity change along the trajectory need

not be considered. On the other hand, if the ion is reflected specularly, the transfer of momentum at ion impact not only compensates the negative drag but also gives to the satellite an additional positive drag equal in magnitude to the negative drag. Hence, when a specularly reflective satellite is ion attracting, the increase in drag due to intercepted ions arises from both the increase in number and velocity of intercepted ions.

Approximate drag for specularly reflective satellite. In order to calculate the drag for a specularly reflective satellite, the ion velocity at the point of satellite intersection must be known. If the trajectories of the intercepted ions are assumed to be straight, then the approximate drag of those ions on a plate or disk satellite can be calculated. Use of the energy conservation law gives the horizontal ion velocity at the surface after impact as

$$u = (u_s^2 - 2\varphi_{sat}/\beta)^{\frac{1}{2}} = u_s(1 - \varphi_{sat}/\hat{E}_{KE})^{\frac{1}{2}} \quad ,$$

where φ_{sat} is negative. Hence the transfer of momentum to the satellite is $u_s[1 + (1 - \varphi_{sat}/\hat{E}_{KE})^{\frac{1}{2}}]$. If the number of incident particles is assumed proportional to the normalized ion current I_i, the resulting normalized drag is

$$D'_{sr} = I_i[1 + (1 - \varphi_{sat}/\hat{E}_{KE})^{\frac{1}{2}}].$$

The factor contained in the brackets represents the approximate increase in drag of a specularly reflective satellite over that of a diffusely reflective one. Of course, the electric drag, as well as the effect of non-horizontal trajectories, is omitted from the drag estimate D'_{sr}.

Drag for both moderate and large bodies. Figure 3.11 shows the normalized drag of a plate satellite (one Debye length half-width) as a function of satellite potential. The cases of diffuse and specular reflection (D_{dr} and D_{sr}, respectively) are shown. The dashed lines are the estimates for the drag D'_{dr} and D'_{sr}. The difference between the estimated drag D'_{dr} and the actual drag D_{dr} for a diffusely reflecting satellite is equal to the electric drag. Similarly, the difference between D'_{sr} and D_{sr} is equal to the same electric drag plus a small correction for the bending of the ion trajectories at the point of impact.

The drag for a large satellite as a function of potential is shown in Fig. 3.12. For the diffusely reflecting satellite, the drag remains approximately constant as the potential is made more ion attractive. Even the electric drag is very small compared to the "ram" drag. For the specularly reflecting case, however, the increase in drag due to the increase in the ion velocity has a sizable effect. Hence, for large, specularly reflecting satellites, the normalized drag depends strongly on the potential, while normalized ion current collected by large satellites depends weakly on the potential. Maslennikov and Sigov[23] calculated the drag of diffusely reflective spheres, cones, and disks; they did not consider the case of specular reflection. Where their results overlap with those presented in this thesis, the agreement is excellent.

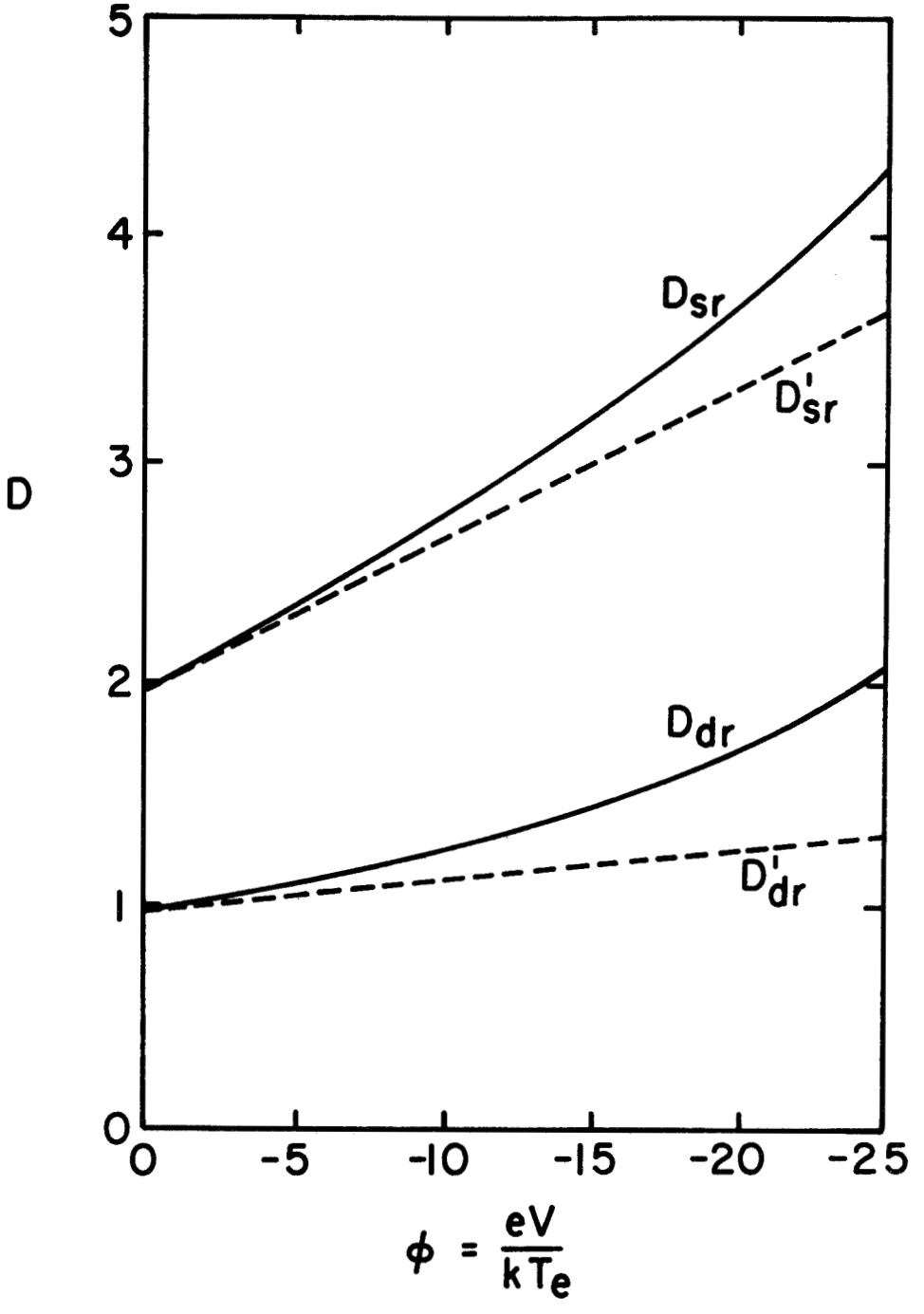

FIG. 3.11. DRAG VS. POTENTIAL FOR PLATE SATELLITE ($\hat{E}_{KE}$= 12, r_{sat}= 1). SPECULAR REFLECTION IS INDICATED BY "sr" AND DIFFUSE REFLECTION BY "dr." DASHED CURVE IS APPROXIMATE SOLUTION.

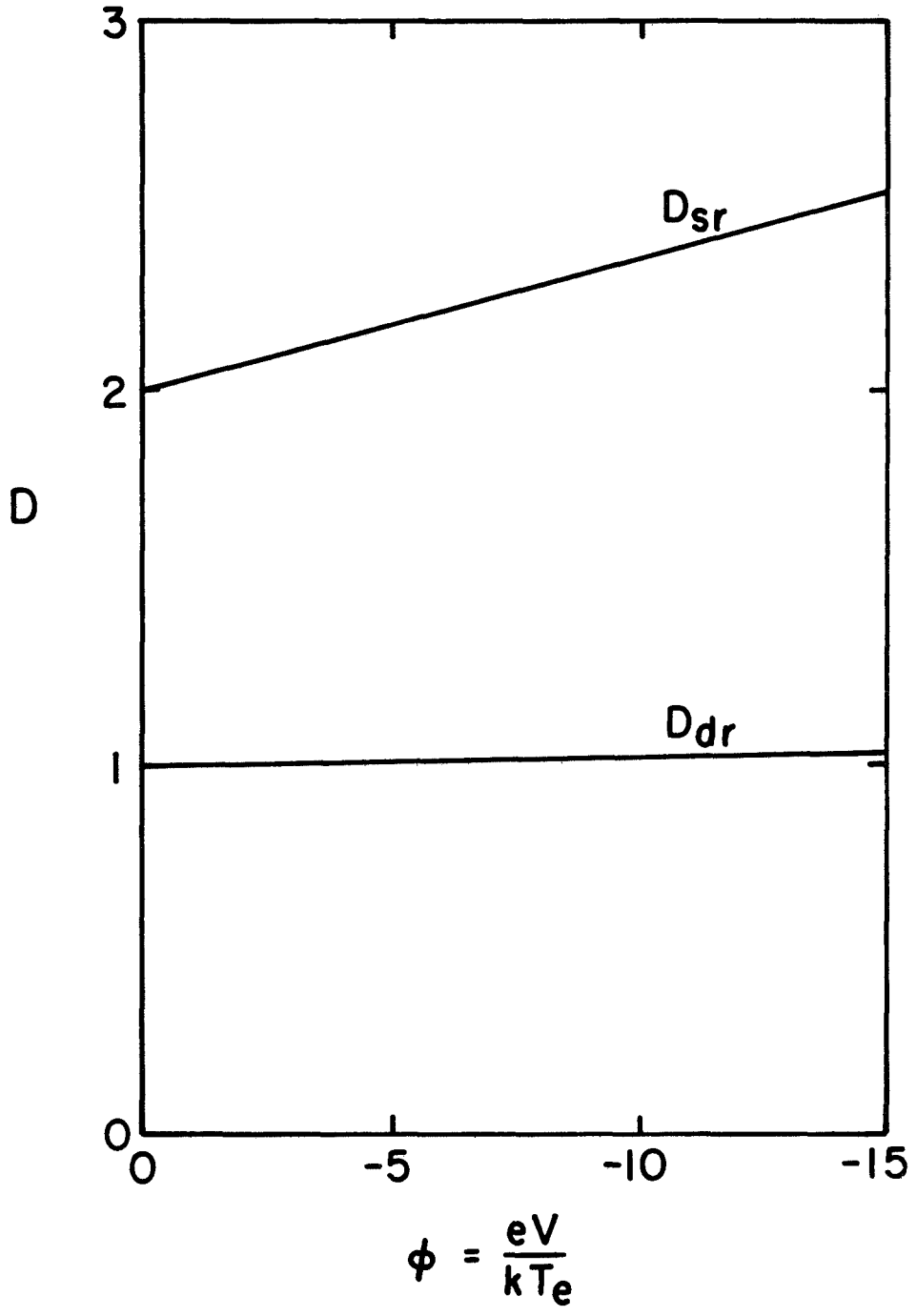

FIG. 3.12. DRAG VS. POTENTIAL FOR PLATE SATELLITE ($\hat{E}_{KE}$= 12, r_{sat}= 25).

D. Structure of the Satellite Wake

1. The Near Wake

Definition of near wake. When the satellite intercepts ions impinging on it from the front, an ion-free region is created in the satellite wake. The ions are assumed to have zero temperature, and if the satellite potential is ignored, then the ions continue their straight trajectories and do not fill in the wake. The electrons, however, having a thermal velocity which is an order of magnitude greater than the satellite speed, abound in the region directly behind the satellite. Hence, the wake region has a net negative charge density, and an electric field arises. The direction of the field is such that it reduces the electron density and attracts the ions streaming past the satellite into the wake. The ions adjacent to the ion-free region respond to the attractive field of the wake, and their trajectories are bent toward the wake. Ions are attracted into the wake from both the top and bottom edges of the ion-free region and meet on the axis of symmetry. In the region extending from the satellite to the point at which the first ion trajectory intercepts the axis, the wake is completely ion free. The ion-free region is shaped roughly like a triangle where the base of the triangle is the rear of the satellite and the two sides are the trajectories of the ions which have grazed the top and bottom edges of the satellite.

Length of near wake. An order-of-magnitude estimate of the length of the triangular ion-free region can be made if it is assumed that the electric field in the wake is a unit of potential (equivalent to the electron thermal energy) acting over a Debye length. In dimensionless units this

electric field corresponds to unity. (Since in actuality the field magnitude is somewhat less, this estimate for the ion-free wake length is a lower bound.) The time necessary for an ion under the influence of a constant force to travel from the edge of the satellite across the wake to the axis of symmetry is

$$t_{wake}=(2\beta r_{sat}/E)^{\frac{1}{2}} \approx (2\beta r_{sat})^{\frac{1}{2}}.$$

During that time, the ion travels downstream with an approximate velocity u_s; the resulting distance in the x direction is

$$d_{wake}= u_s t_{wake}=(2\beta u_s^2 r_{sat})^{\frac{1}{2}} = 2(\hat{E}_{KE} r_{sat})^{\frac{1}{2}}. \qquad (3.4)$$

For example, for a plate satellite with a half-width of a Debye length and an $\hat{E}_{KE}$ of 12, the length of the ion-free portion of the wake is at least 7 Debye lengths.

Figure 3.13 is a plot of the ion-flow field showing representative ion trajectories. In the figure, the plotted trajectory which is drawn first into the wake is not the grazing trajectory. In fact, the grazing trajectory is not shown here, since the trajectories selected for display have approximately equal intervals between them. However, examination of the results indicates that the grazing trajectory crosses the axis of symmetry at about 12 Debye lengths downstream of the satellite, a length which is of the same order of magnitude as the estimated value.

Figure 3.14 is a contour plot of the potential field. In most of the wake, where the potential lines are parallel

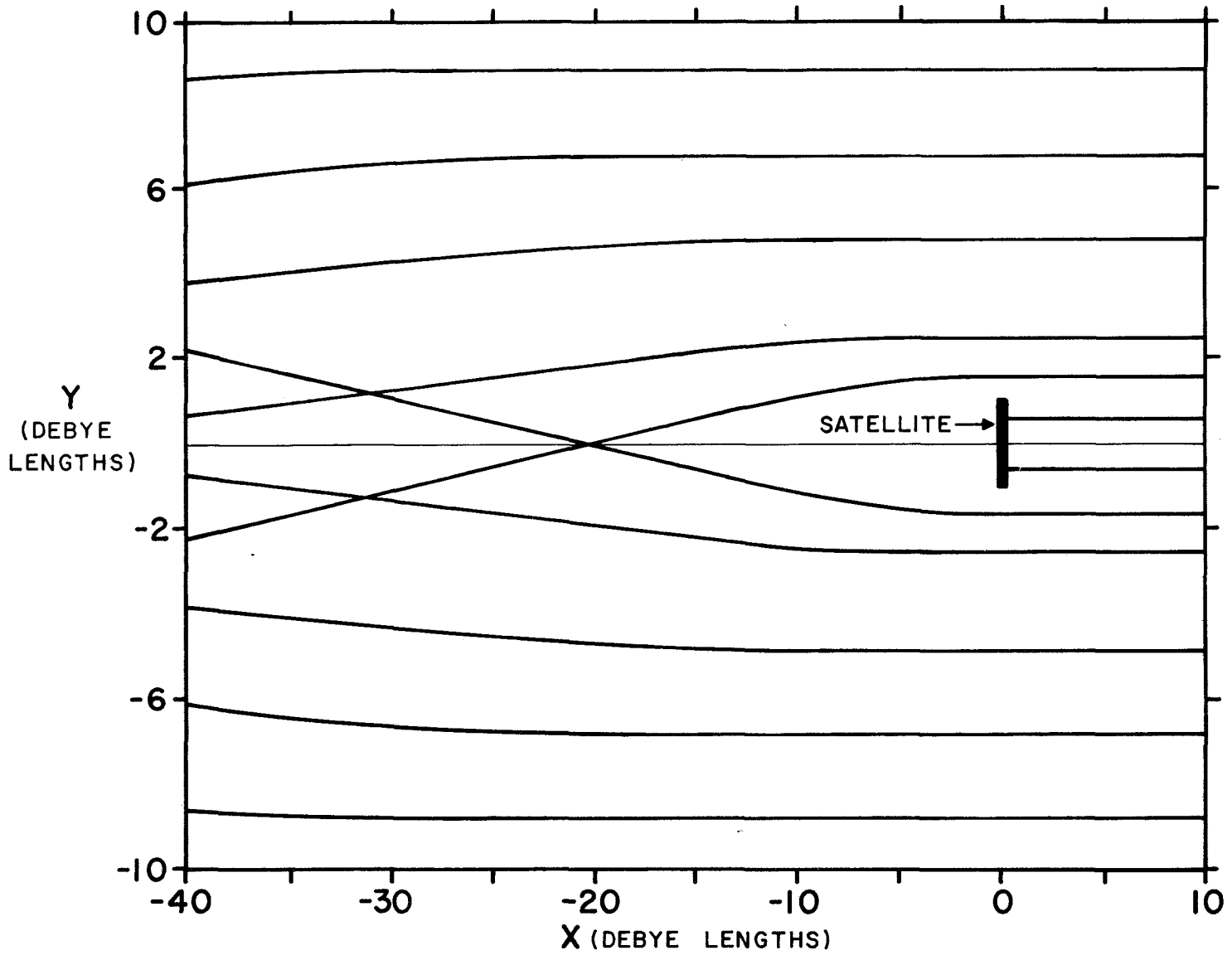

FIG. 3.13. ION TRAJECTORY PLOT FOR PLATE SATELLITE ($\hat{E}_{KE}$= 12, ϕ_{sat}= 0, r_{sat}= 1).

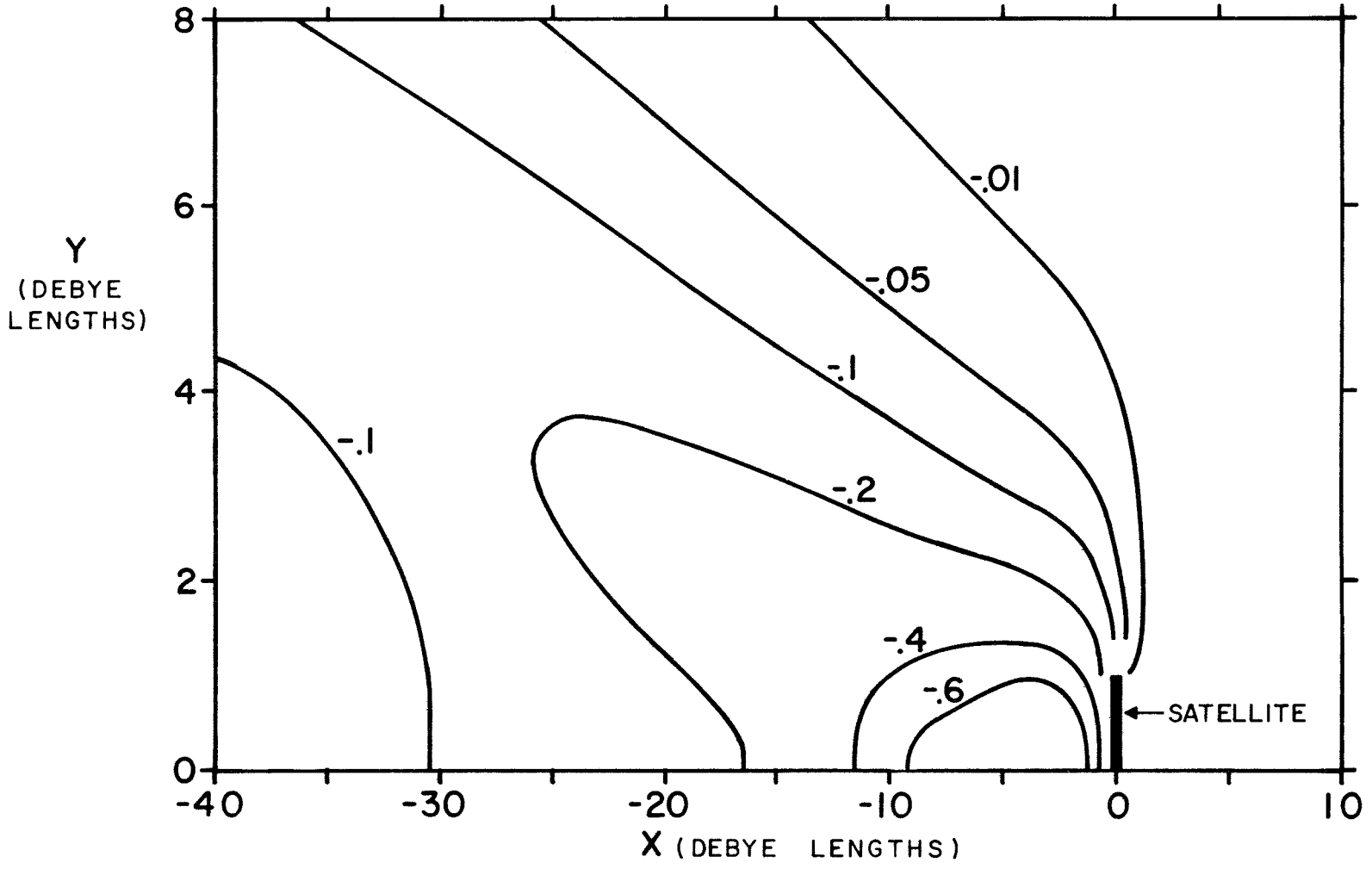

FIG. 3.14. CONTOUR PLOT OF POTENTIAL FOR PLATE SATELLITE ($\hat{E}_{KE}$= 12, ϕ_{sat}= 0, r_{sat}= 1).

to the flow direction, the resulting electric field is perpendicular to the flow direction and attracts the ions into the wake. The magnitude of the electric field is approximately 0.4 unit of potential per Debye length. Since this value is considerably less than unity, the fact that the estimated length of the ion-free region is smaller than the actual length is not unexpected.

Influence of satellite potential on length of near wake. If the satellite has a negative potential, the y velocity of the ions flying past the satellite and into the wake is increased from zero by the ion-attracting field surrounding the satellite. As a result, the grazing and adjacent ions cross the axis of symmetry sooner than they would if the satellite were at plasma potential. Consequently, the ion-free region of the wake is considerably shorter. Figures 3.15 and 3.16 show the ion-flow and potential fields, respectively, of a plate satellite. The parameters are the same as those in the previous pair of figures, except that the satellite potential is -5 in units of electron thermal energy.

Near wake of large satellite. When the satellite radius is made larger, the resulting ion-free region also becomes larger. Since the ions must travel a considerable distance from the edge of the satellite to the axis of symmetry, they go a considerable distance downstream before crossing. The estimate of the ion-free wake length given by Eq. (3.4) predicts that the length is proportional to the square root of the satellite radius. Hence, when the satellite radius is large compared to a Debye length, the near wake region is also large. The region is filled solely by electrons and, if the

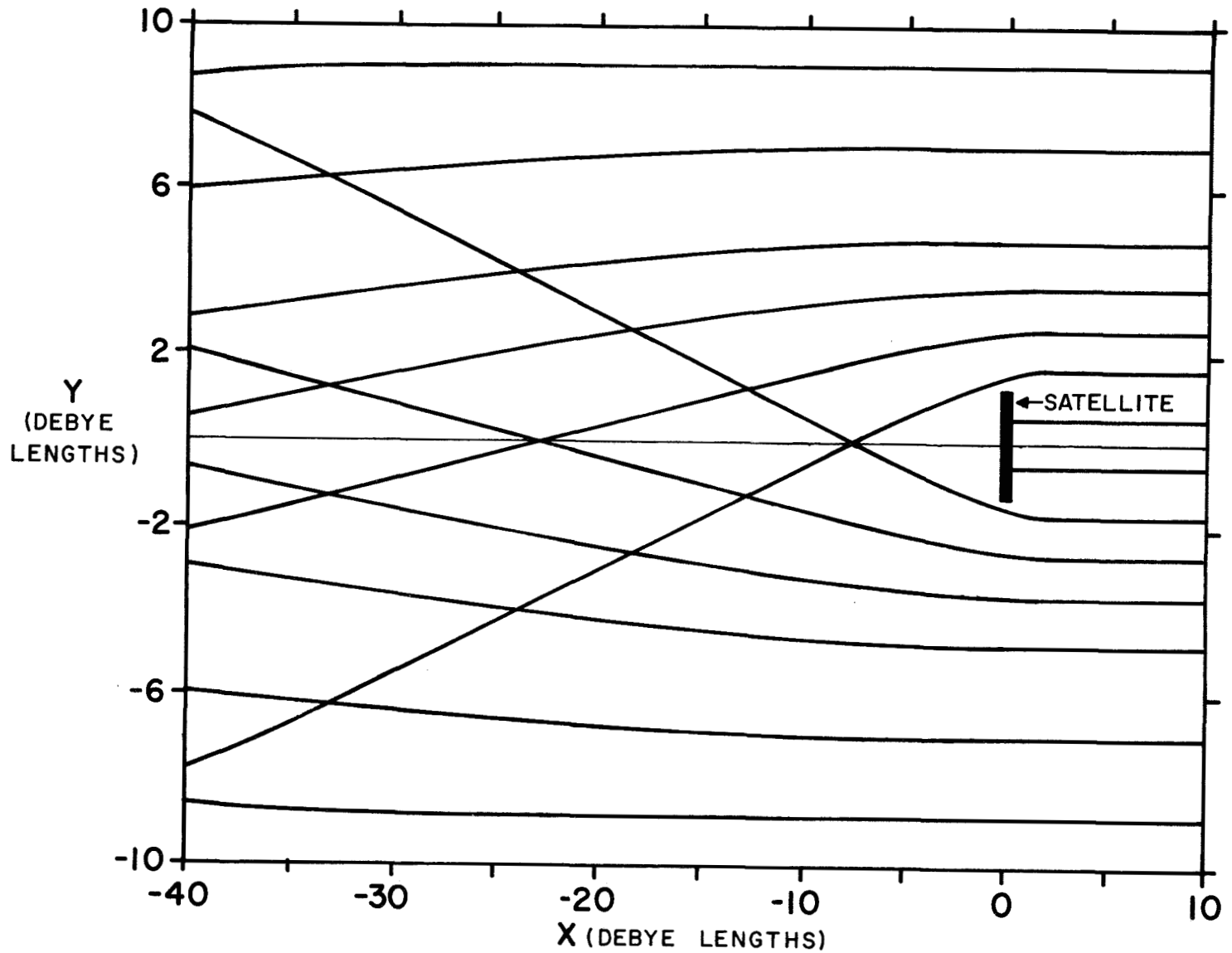

FIG. 3.15. ION TRAJECTORY PLOT FOR PLATE SATELLITE ($\hat{E}_{KE}$= 12, ϕ_{sat}= -5, r_{sat}= 1).

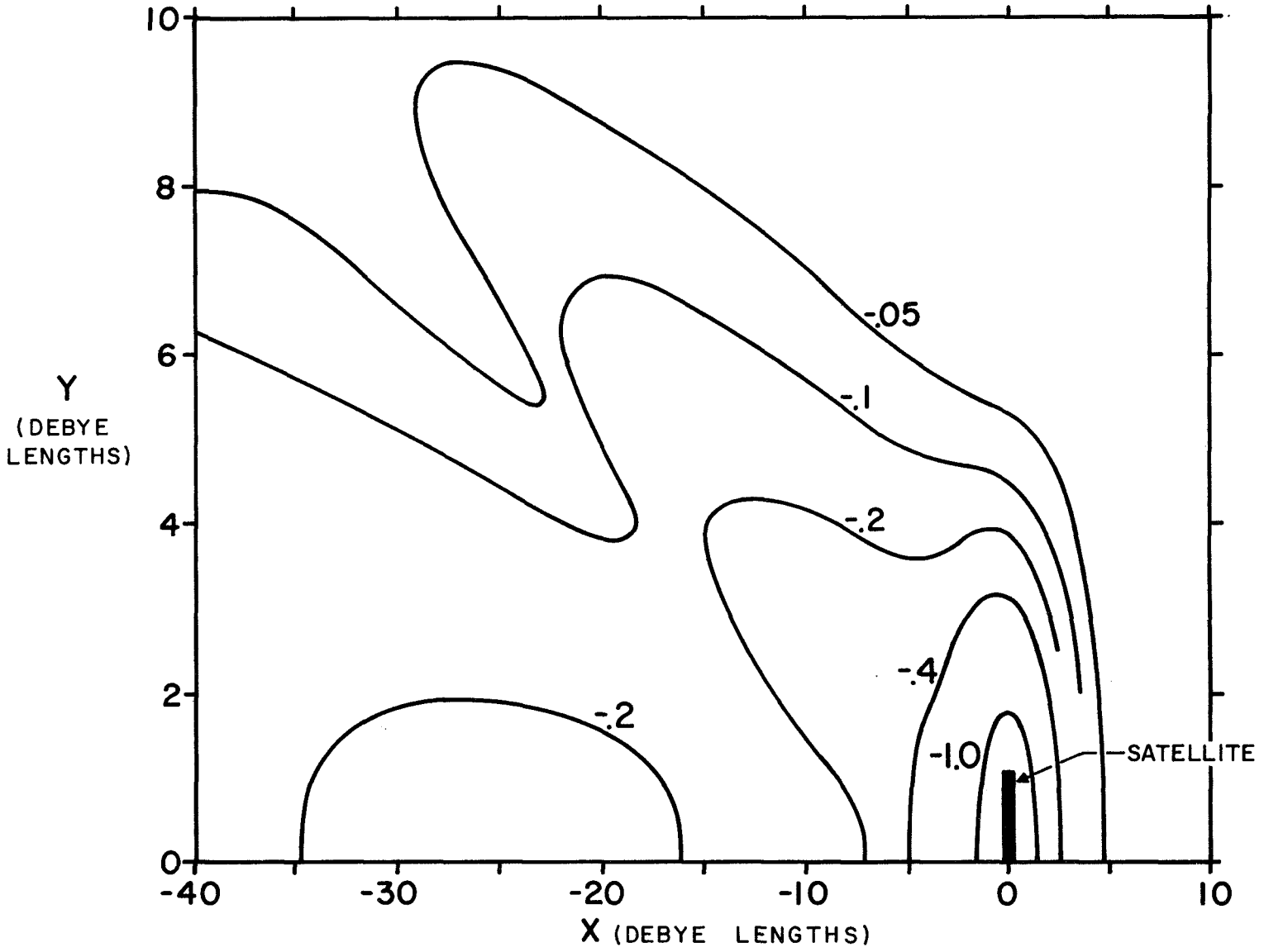

FIG. 3.16. CONTOUR PLOT OF POTENTIAL FOR PLATE SATELLITE
($\hat{E}_{KE}$= 12, ϕ_{sat}= -5, r_{sat}= 1).

electron density in this region were comparable to the ambient value, the resulting electric field would be enormous. Therefore, inside the large ion-free region the dimensionless potential has a negative value which is a few times greater than unity. The resulting electron density is then only a small fraction of the ambient value. The large region which is ion free can be considered to be nearly electron free as well. The net charge density is approximately zero, and in this case, Poisson's equation which governs the potential degenerates to Laplace's equation.

One consequence of the zero charge density in the region directly behind the satellite is that the electric field can extend for many Debye lengths downstream. For example, if the satellite is not at plasma potential, the extent and decay of its potential into the plasma-free region is dependent more on the size of the satellite than on the Debye length. Another way to understand this phenomenon is to consider the Debye length a function of the <u>local</u> electron density. In the region where the electron density is very small, the "local" Debye length is large; hence, the electric field extends over a region which although large is only of the order of a few "local" Debye lengths.

Figures 3.17 and 3.18 are plots of the ion-flow and potential fields for a plate satellite having a half-width of 25 Debye lengths. In order to shorten the plasma-free region of the wake and, consequently, to decrease the required computer memory, the value of the ion kinetic energy is set at 6 (occurring at an altitude of 1500 km). For the same reason, the satellite potential is set equal to -5. The contour plot of potential in Fig. 3.18 shows quite clearly the difference

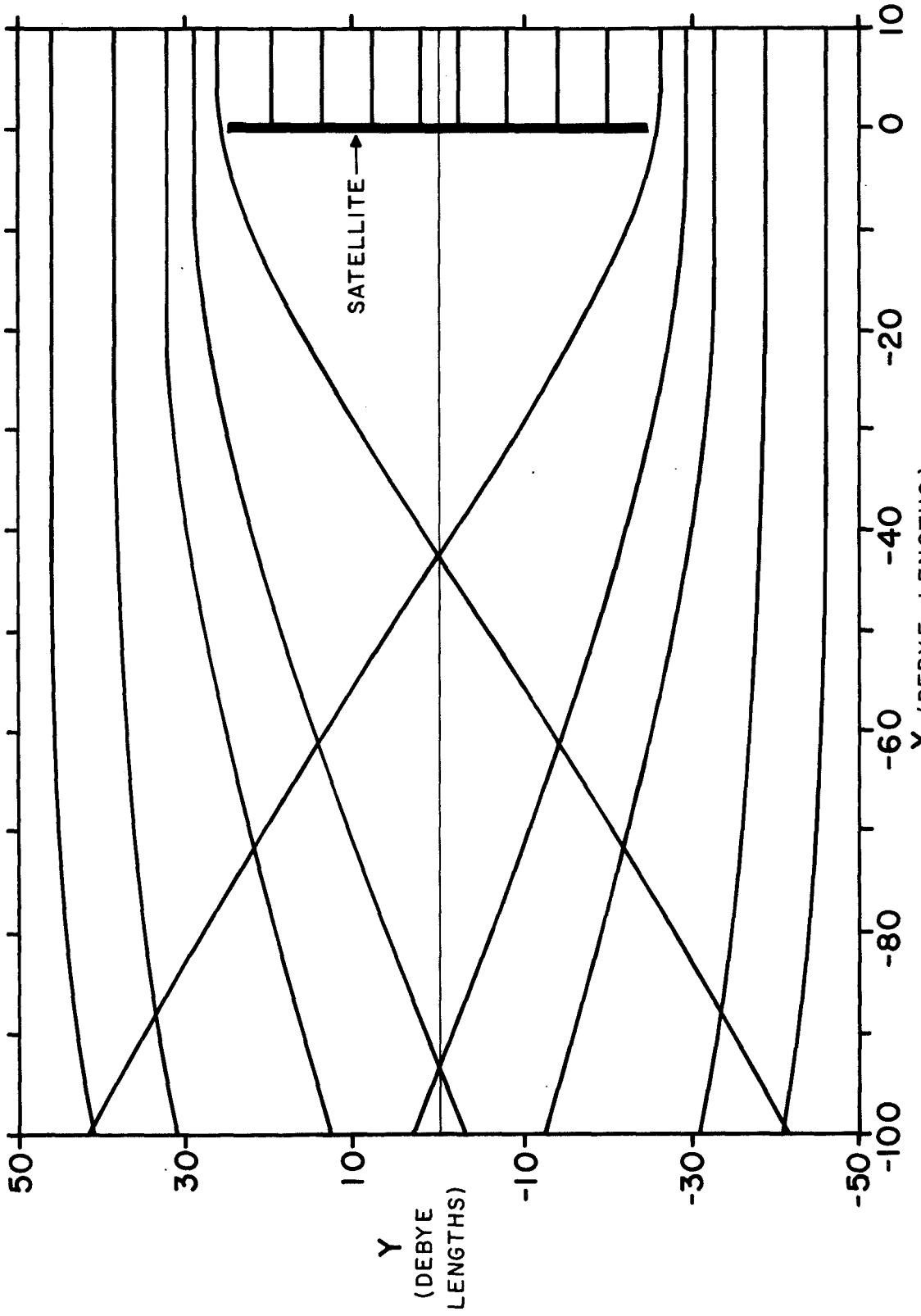

FIG. 3.17. ION TRAJECTORY PLOT FOR PLATE SATELLITE ($\hat{E}_{KE}$= 6, ϕ_{sat}= -5, r_{sat}= 25).

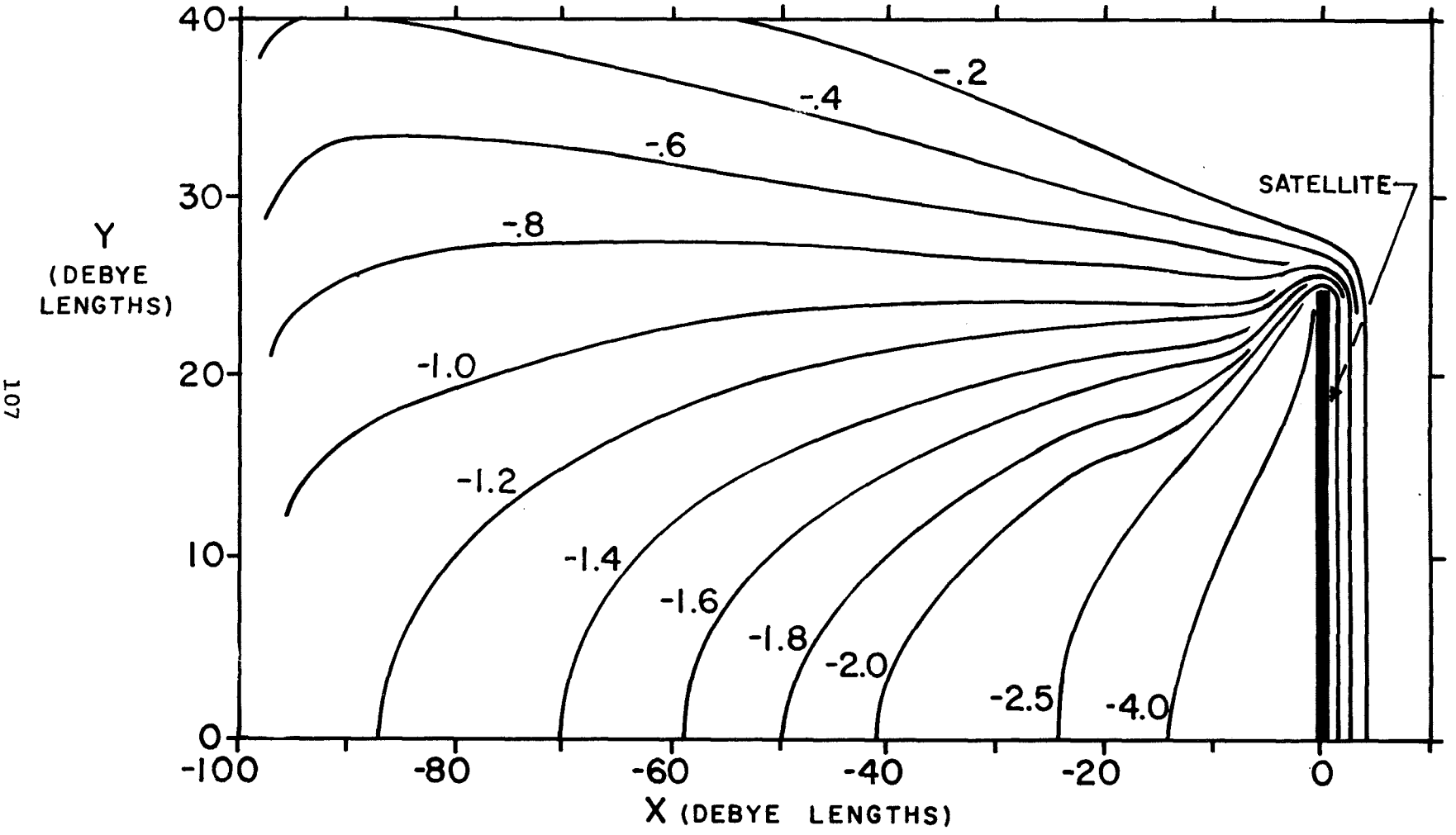

FIG. 3.18. CONTOUR PLOT OF POTENTIAL FOR PLATE SATELLITE
($\hat{E}_{KE}$= 6, ϕ_{sat}= -5, r_{sat}= 25).

between the plasma behavior in the front of the satellite and that in the back. Within a few Debye lengths of the front surface, the value of the ion density is nearly the ambient value; the electron density is much smaller. Hence, a net positive charge density occurs which shields the negative potential of the satellite. In the theory of electrostatic plasma probes, this shielding region is called a sheath. As is characteristic of sheaths, the lines of constant potential are dense and are parallel to the body surface.

In the wake, however, a recognizable sheath does not exist. The net charge density is nearly zero in the region directly behind the satellite, and the potential field of the satellite is not shielded by a sheath. As a result, the lines of constant potential extend into the wake over distances which are comparable to the body radius rather than to the Debye length of the problem. The satellite wake has a behavior which is fundamentally different from that at the satellite front. Therefore, only those theories which take into account the sizable variations of the ion and electron densities in the wake are adequate to describe the potential and ion-flow fields there.

2. The Midwake (Planar Geometry)

Definition of midwake. It has been established that the self-consistent electric field attracts the free-streaming ions into the wake from both the top and bottom edges of the wake. These two streams of ions meet on the axis of symmetry. Since the problem is assumed to be collisionless, the two streams interact with each other only by means of the electric field.

The ion density in the area where the streams intersect is simply the sum of the ion density of each stream. If the satellite has axially symmetric geometry, the geometric factor makes the ion density of each stream infinite on the axis. For that reason, the discussion of the axially symmetric case is deferred until later.

Consider the wake of a satellite which is of the planar class and whose half-width is not large compared to a Debye length. In the wake region where the two ion streams cross each other, the ion density increases but does not reach the ambient value. Consequently, a weak electric field exists here. This partially neutralized region, called the midwake, borders the ion-free near wake. Across the border a sharp gradient occurs in the ion density. Hence, the potential field of the midwake is significantly different from that of the near wake, and the regular shape of the potential lines is perturbed.

Formation of ion beams. The perturbation in the field of the midwake influences most strongly the ions which first cross the center line of symmetry (the border ions). As the two groups of border ions (from the top and bottom edges of the satellite) pass through each other, they undergo focusing by the perturbed potential field. When the groups reappear on the other side of the line of symmetry, their densities are above the ambient, and they behave as two narrow beams of ions. Since the two beams are coherent for a remarkably long distance, they are quite distinct from the two broad streams of ions which cover the remainder of the midwake. The ion beams are at equal angles with respect to the line of symmetry and form a V-shaped region of enhanced ion density in the midwake.

In Fig. 3.14, the distortion of the potential field which forms the ion beams can be seen as a perturbation of the lines of constant potential; see for example the line corresponding to -0.05. In the corresponding trajectory plot (Fig. 3.13), the beam cannot be shown because it is extremely thin and difficult to plot. However, in a corresponding contour plot of the ion density (Fig. 3.19), the outline of the beam can be seen clearly as a line of constant ion density which has a value greater than the ambient density.

When the beams reach into the free-streaming ions, their density is superimposed on the nearly neutral plasma background and disturbs the region. Since the two beams have an excess of ion charge, an electric field arises. The effect of the field on the beams increases their widths and decreases their density as they move into the free-streaming ions. Finally the beams diffuse until they are only a small perturbation superimposed on the background plasma, and the electric field vanishes.

Enhancement of ion beams by a satellite potential. The process which creates the beams can be enhanced by application of a negative satellite potential. Since the electric field is strongest in the region adjacent to the satellite, those border ions grazing the satellite are given an initial y velocity before they enter the wake field. As a result, at the point of beam formation, the vertical velocities are higher, and the angle between the beam and the flow direction is larger. Furthermore, the beams are broader and have a higher density; therefore, they penetrate farther into the free-streaming plasma and disturb a larger region. Figure 3.20

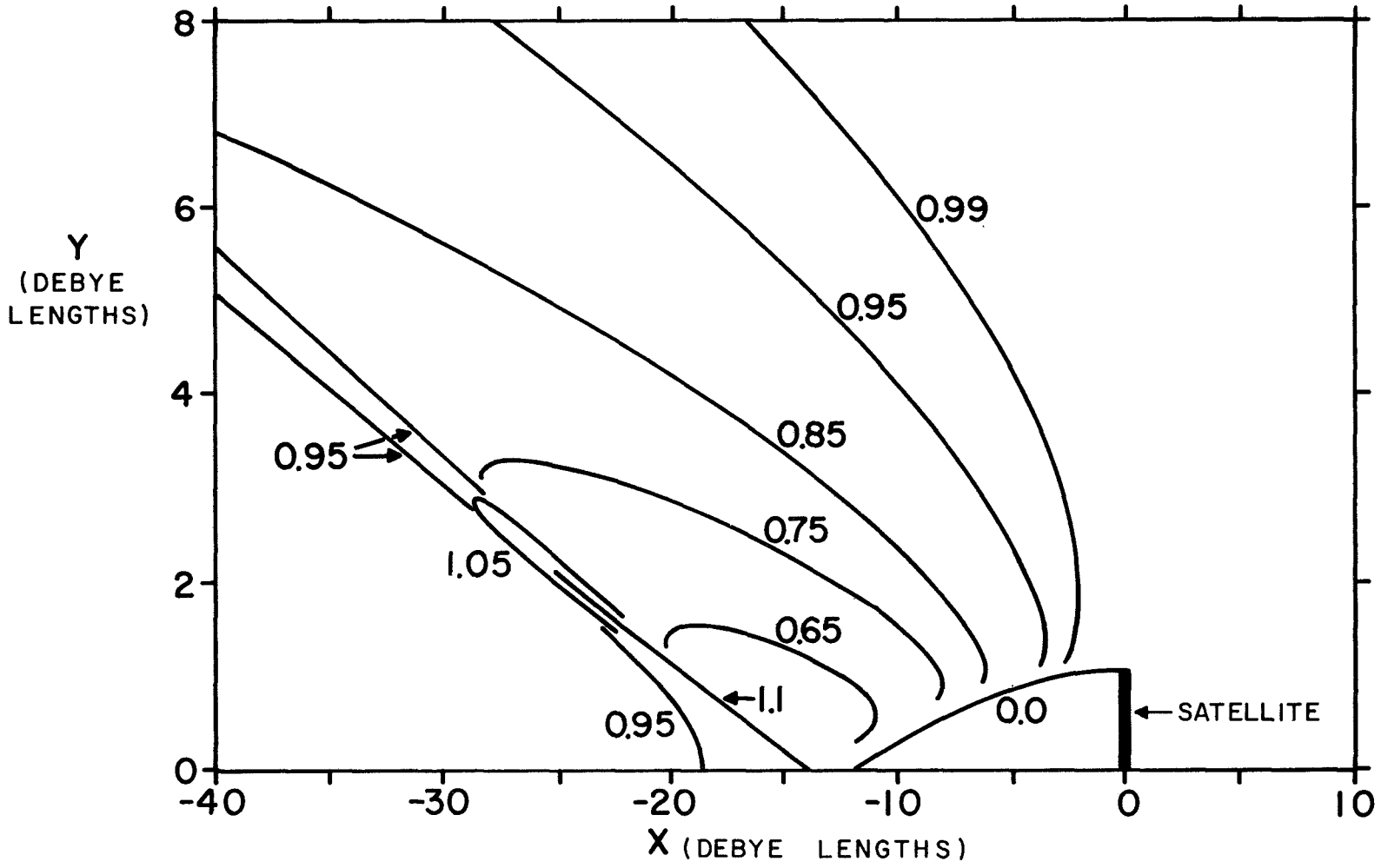

FIG. 3.19. CONTOUR PLOT OF ION DENSITY FOR PLATE SATELLITE ($\hat{E}_{KE}$= 12, ϕ_{sat}= 0, r_{sat}= 1).

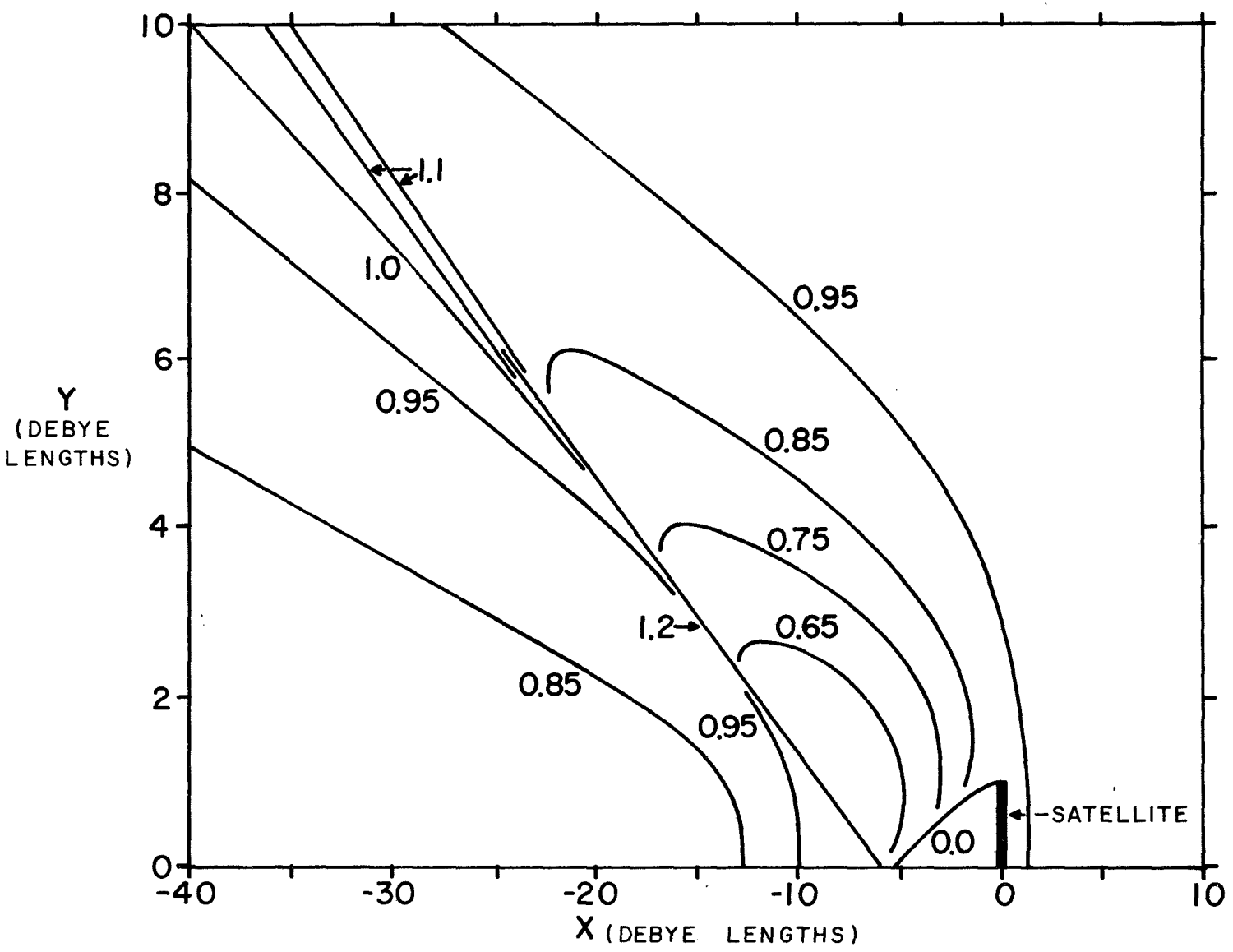

FIG. 3.20. CONTOUR PLOT OF ION DENSITY FOR PLATE SATELLITE ($\hat{E}_{KE}$= 12, ϕ_{sat}= -5, r_{sat}= 1).

shows the ion density for the case where the satellite potential is -5. For this case, a contour plot of potential and an ion-flow field have been shown already in Figs. 3.15 and 3.16.

Absence of ion beams in case of large satellite. Now consider the case of a large satellite where the wake is very wide. In this case, the attracted ions undergo an acceleration which is toward the axis of symmetry and which extends over a long distance. As a result, the ion density in the midwake is small when compared with the ambient. (In the far wake, of course, the ion density slowly rises to the ambient density.) In the region where the ion streams intersect, the density, as usual, doubles. However, since the density gradient across the border is small, the potential field is not perturbed, no focusing of ions occurs, and no beams are created. In Fig. 3.18, the contour plot of potential for a large satellite (r_{sat} = 25) is shown. Strong perturbations in the potential lines are not present. The sudden increase in ion density and the formation of two beams, characteristic of satellites of moderate size, are entirely absent in this case. Otherwise, the behavior of the wake is similar to the previously discussed case.

Comparison of prior work with respect to ion beams. Al'pert et al.[2] predicted a V-shaped region of enhanced ion density in the wake. In their solution, the electric field was treated as a perturbation to the motion of thermal ions. Taylor[28] also predicted the occurrence of the V-shaped region and attributed its formation to the border ions which pass near the top and bottom edges of the satellite. Taylor's solution was obtained under the

assumption of thermal ions and a first-order approximation of the electric field. The solution of Maslennikov and Sigov [21-23], for the potential and ion density contain a distortion which can be attributed to regions of enhanced ion density off the axis of symmetry. By making use of the method of solution described in the present study, the V-shaped region of enhanced ion density was investigated to determine the influence of satellite parameters on it. Since the beams were found in all solutions (except in the case of large satellites) and since ion thermal motion was ignored, the electric field is clearly responsible for the formation of the beams. Furthermore, the work of the previous investigators indicates that consideration of the ion thermal motion in the problem does not destroy the coherence of the beam trajectories and, hence, the formation of the beams.

In spite of the large body of evidence for the existence of the beams which numerical investigations have produced, the possibility exists that the solutions do not accurately describe the flow of ions around satellites. Observations of ion density in the vicinity of satellites have not confirmed the existence of off-axis regions of enhanced ion density.[11] However, in a laboratory experiment simulating the ionospheric flow around a body, Hester and Sonin[34] obtained results which strongly indicate that two ion beams exist in the wake of moderately sized bodies. In order to determine the ion-flow field, these investigators used a cylindrical ion probe which can resolve the flow direction of an ion beam to within a few degrees. The probe, when placed on the axis of symmetry in the wake of a plate,

revealed the presence of two ion beams crossing the axis. Furthermore, plots of ion density show the projection of the beams into the far wake for a remarkably long distance. Since the ions in the experiment of Hester and Sonin have almost no thermal motion, the results from their work can be compared with the numerical solution in the present study. For a small plate in the present case and a small cylinder in their case (with all other parameters identical--$\hat{E}_{KE} = 10$, $r_{sat} = 0.21$, $\varphi_{sat} = -9$), the half-angle of expansion of the V-shaped region is 0.35 and 0.34 radians, respectively. This close agreement between a laboratory experiment and these computer calculations gives added confidence to the actual existence of ion beams behind a satellite.

The numerical results from the present study suggest that ion beams behind a satellite have not been observed because the satellites previously examined had radii much larger than a Debye length. Moreover, the results of Hester and Sonin indicate that for a body of radius 19.5, the ion beams are not created and only a slight enhancement of ion density exists along the edge of the wake. A small or moderate body size is apparently necessary to insure the existence of the ion beams.

Extension and expansion of midwake. The beams themselves make only a minor contribution toward the neutralization of the electron-rich midwake. In order for the wake to be even partially neutralized, a large number of ions must be attracted into it. However, as these ions are drawn into the wake, the ion density decreases to a value less than the ambient. Hence,

the excess electron density in the wake is only partially neutralized, and the wake remains slightly disturbed. Furthermore, as the ions are removed from the surrounding region to neutralize the wake, that region itself becomes electron-rich. The disturbed region, therefore, grows outward as it proceeds downstream.

It must be remembered that the problem is collisionless, and, therefore, the disturbance is not damped by collisions. Once the collisionless plasma is disturbed, the disturbance persists until the variations in the electron and ion densities and the resulting electric field are distributed over a large volume of plasma. In fact, the present investigation has shown that the variations persist as far downstream as the solution has been extended. (See Appendix B for a discussion of the influence of the boundary location on the solution.) The disturbance moves in the vertical direction as well as the horizontal, and, as a result, the region of disturbance grows with the extension of the wake. However, the magnitude of the electric field becomes smaller further downstream, and likewise the ion and electron densities approach their ambient values. The energy associated with the disturbance remains roughly constant along any vertical line, but it is spread over an increasingly larger distance. Thus, the two-dimensional character of the problem provides a mechanism for damping the disturbance. The damping is fundamentally unlike collisional damping, but, nevertheless, it is an effective means of restoring the disturbed plasma to ambient conditions.

It should be emphasized that the disturbance is a steady-state phenomenon with respect to the satellite. Such possible time-dependent phenomena as electromagnetic and Alfven waves, the "two-stream" instability, or Landau damping have not been investigated as possible sources of damping. Laboratory experiments designed to measure the ion density in body wakes have shown that the wake is steady-state.[32-34] Hence, the consideration of the time-dependent processes is not expected to contribute additional insight into the understanding of that portion of the wake which is strongly disturbed.

3. The Midwake (Axially Symmetric Geometry)

High ion density on wake axis. The planar geometry having been thoroughly discussed, it is now appropriate to consider the axially symmetric geometry. As discussed in Chap. II, the ion density as a function of the flux tube width [Eq. (2.9)] contains a factor which is inversely proportional to the radial distance of the point of interest. This geometric factor takes into account the compression of the flux ring as the representative trajectory approaches the axis of symmetry. On the axis itself the ion density is singular. Of course, the singularity is not expected in reality; even a slight thermal motion in the ions destroys the coherence of the flux ring near the axis. Nevertheless, high ion densities are expected in the vicinity of the axis since the shape of a satellite of the axially symmetric class is an efficient means of focusing ions onto the axis.

The singularity in the ion density which occurs on the axis has been avoided in the solution by choosing grid points which do not lie on the axis. If the ion temperature is neglected, the grid points can be no nearer to the axis than 0.1 Debye lengths. At this radial distance the ion density arising from those trajectories which cross the axis may be as large as ten times the ambient density. The result of keeping the grid points off the axis is achievement of high ion densities while avoiding singularities and neglecting ion temperature. Under these assumptions, the solution is expected to approximate the behavior of axially symmetric satellites.

Spatial oscillations. The near wake of an axially symmetric body is ion-free as it is in the case of a planar body. Similarly, in the region bordering the ion-free region, two ion streams begin to neutralize the electron-rich wake. Furthermore, near the axis where the streams intersect, the ion density increases rapidly. Since the geometry of the problem is axially symmetric, the wake in the neighborhood of the intersection becomes extremely ion-rich. The resulting electric field is in such a direction that it opposes the arrival of more ions. The potential becomes positive, and further down the wake an ion-free region is created. The field in that region is ion-attracting and the potential is negative. The regions of negative and positive charge density alternate down the wake, and their magnitude diminishes slowly. Consequently, regions of positive and negative potential are formed in the vicinity of the axis of symmetry.

Since the magnitudes of the ion concentrations near the axis can be very large, the electric field is much larger than in the planar case. Hence, the wake ions are influenced strongly by the field which is alternately attractive and repulsive. Each wake trajectory undergoes a series of reversed deflections until it crosses the axis and is deflected permanently out of the wake.

Since the axially symmetric satellite focuses the ions to high values of density, spatial oscillations in both the net charge density and the potential are characteristic of this class of satellite. The clear distinction between the ion-free near wake and the partially neutralized midwake in the case of a planar body is not possible in this case. In addition to the ion-free regions which occur many times on the wake axis, ion-rich regions now appear. Hence, the structure behind a planar satellite is fundamentally different from the structure behind an axially symmetric satellite, and the two cases must be considered separately.

Comparison of wake for two geometries. Figures 3.21 and 3.22 show the potential and ion-flow fields of a disk satellite. The ion kinetic energy has been set equal to the low value of 1.2 in order to enhance the formation of the wake. The low value of $\hat{E}_{KE}$ allows the ion to react more quickly to the electric field; as a result, the interesting behavior is contained in a relatively short distance. In order to compare this case with a planar case, the potential field of a plate satellite is shown in Fig. 3.23. The remaining satellite parameters are identical to the case shown in Fig. 3.21. Note the series of alternating potential regions in the former figure; note the complete absence of a complex structure in the latter.

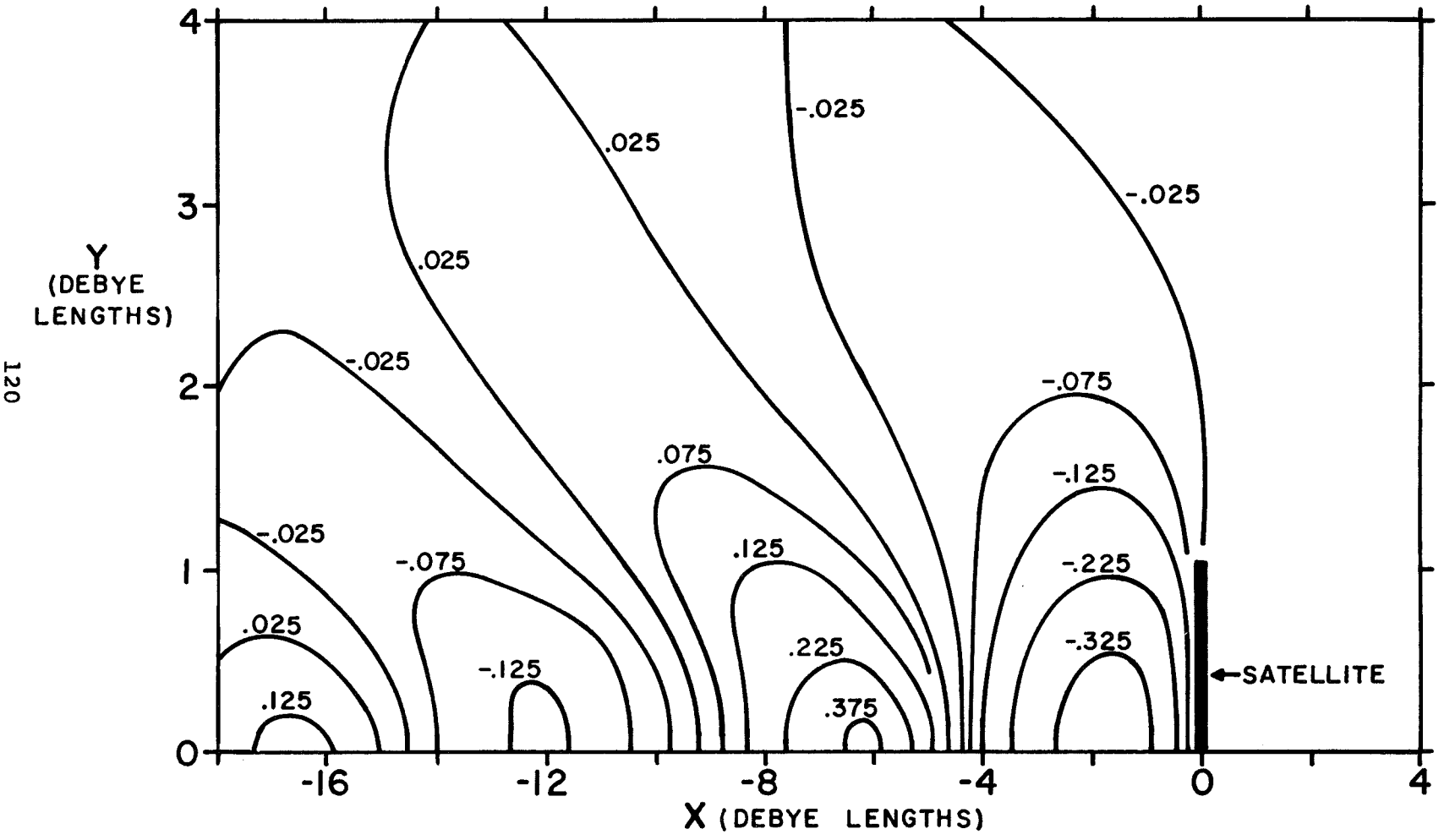

FIG. 3.21. CONTOUR PLOT OF POTENTIAL FOR DISK SATELLITE ($\hat{E}_{KE}$= 1.2, ϕ_{sat}= 0, r_{sat}= 1).

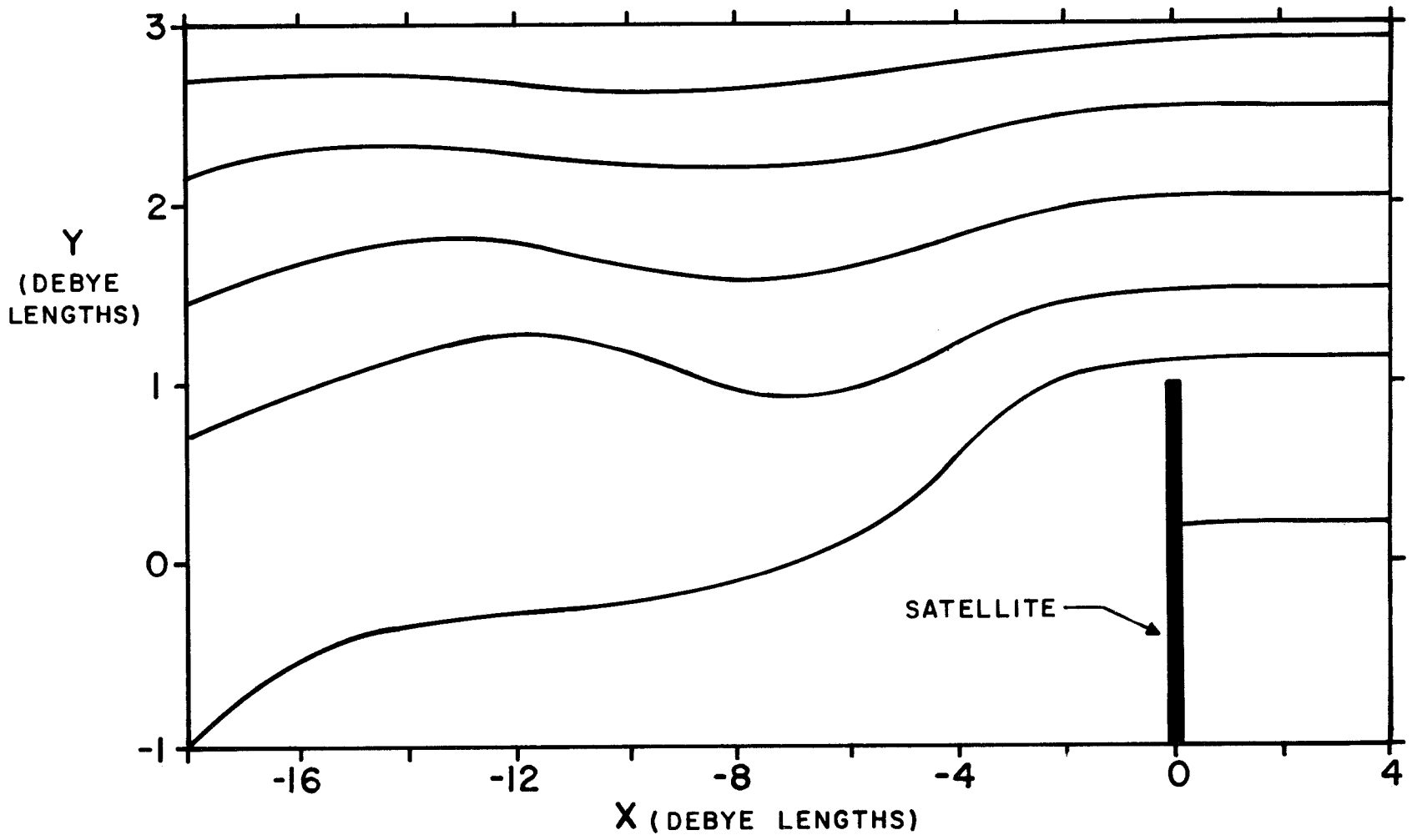

FIG. 3.22. ION TRAJECTORY PLOT FOR DISK SATELLITE ($\hat{E}_{KE}$= 1.2, ϕ_{sat}= 0, r_{sat}= 1).

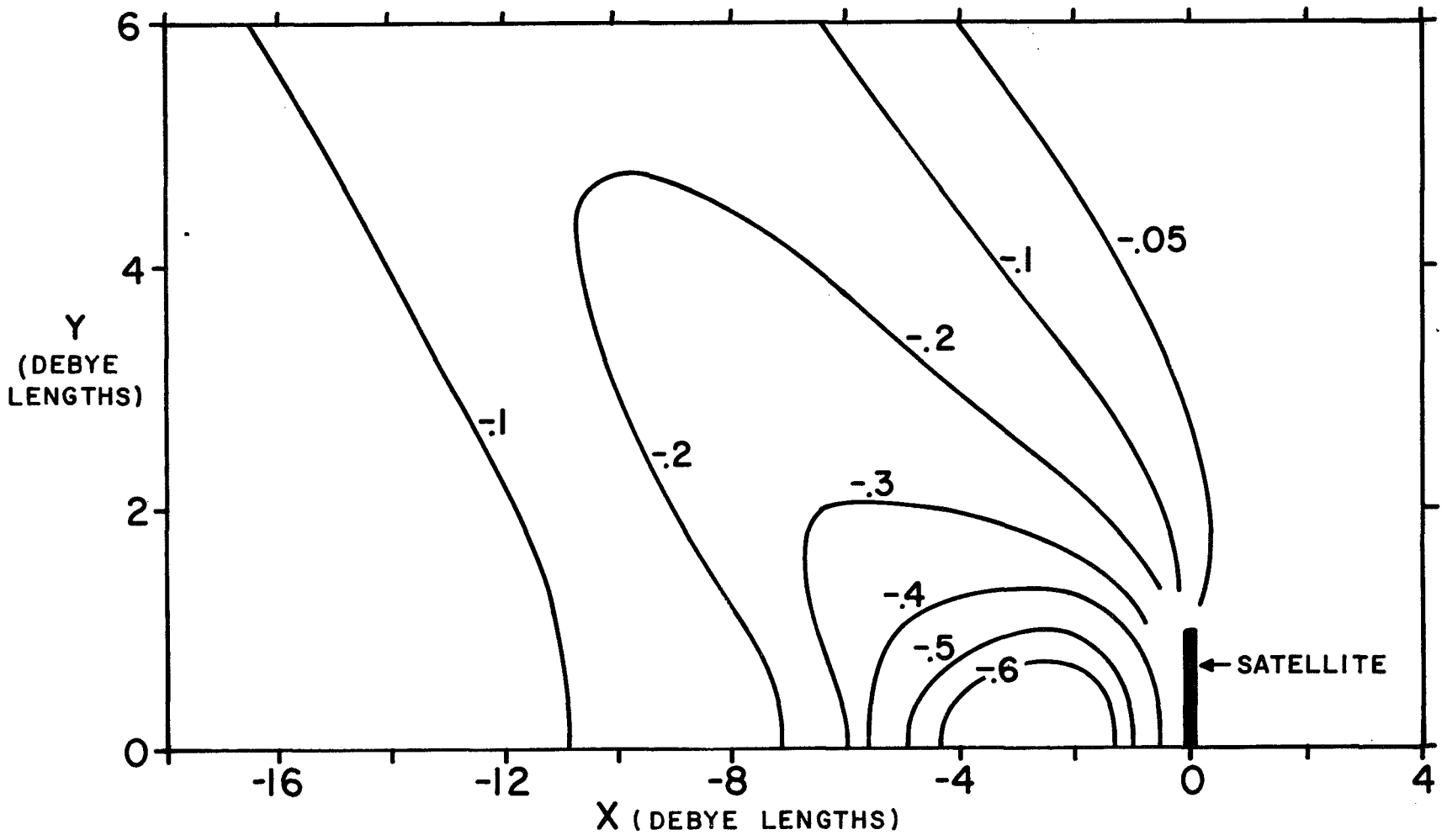

FIG. 3.23. CONTOUR PLOT OF POTENTIAL FOR PLATE SATELLITE ($\hat{E}_{KE}$= 1.2, ϕ_{sat}= 0, r_{sat}= 1).

CHAPTER IV: INFLUENCE OF A UNIFORM MAGNETIC FIELD

A. Equations and Methods of Solution

Planar geometry. If a uniform magnetic field is introduced into the problem, the field will influence the motion of the charged particles and, hence, the development of the disturbed region around the satellite. Since the field is uniform, the problem remains spatially two-dimensional when the planar class of body shapes is considered. For the axially symmetric class, the magnetic field, although uniform, would appear to have a changing direction with rotation of the body. Even if the magnetic field were parallel to the axis of rotation, the problem would not remain spatially two-dimensional. The magnetic field would force the ions to move in a direction perpendicular to both the field and the velocity vector, and the resulting motion would not be independent of the angle about the axis of rotation of the body. In this case the third spatial dimension, angle, would have to be considered. Hence, in order to keep the problem spatially two-dimensional in a uniform magnetic field, only the planar class of body can be solved.

Modification of computer program. Since most of the equations describing the physical behavior of the problem remain valid in the magnetic field case, only a small portion of the program must be changed. Poisson's equation is applicable in the case of a steady and uniform magnetic field as well as in the electrostatic case. Since the electron density is proportional to the Boltzmann factor,[12] that portion of the program which employs Poisson's equation to solve for the potential when the ion density is known can be used

without modification in the magnetic field case. However, that portion of the program which is used to calculate the ion trajectories must be modified to take into account the influence of the magnetic as well as the electric field on the motion of the ions.

In the derivation of the pure electric interaction, the force term of Newton's equation was set equal only to the electric field. In dimensionless variables, from Eq. (2.10),

$$F = -\frac{1}{\beta}\frac{\partial \varphi}{\partial x} \text{ and } G = -\frac{1}{\beta}\frac{\partial \varphi}{\partial y} \quad ,$$

where the vector $\vec{F} = (F,G,H)$ is the dimensionless force per unit mass on the ion, and $\beta = m_i/m_e$ is the ion mass ratio. H is the force per unit mass in the z direction and is zero in the purely electric case.

If a uniform magnetic field is to be introduced into the problem, the force term in Newton's law must be appropriately modified. With the Lorentz force included, the force term becomes (in the dimensionless units of Chap. II)

$$\vec{F} = \frac{1}{\beta}\,(\vec{E} + \vec{v} \times \vec{B}), \tag{4.1}$$

where vector $\vec{v} = (u,v,w)$ is the ion velocity and $\vec{B}$ is the dimensionless magnetic field. The unit magnetic field which allows the Lorentz force to be written in its simplest form has a value $B_o = (n_o m_e/\epsilon_o)^{\frac{1}{2}}$. At this value of the magnetic field, the <u>electron</u> gyrofrequency $\omega_{ge} = (eB_o/m_e)$ is equal to the plasma frequency ω_p.

The "cold" ions acquire a velocity component in the z direction due to the magnetic field. These velocities in turn affect the ion velocity components in the x and y directions by interacting with the magnetic field. The magnetic force, being considerably weaker than the electric force, is taken in account through a correction to the ion trajectories. Thus, the entire program for solving the electrostatic interaction of a satellite with the ionosphere can be used to solve the case of the joint electrostatic and magnetostatic interaction.

In this thesis, two cases will be considered: a magnetic field $\vec{B} = (B,0,0)$ parallel to the flow velocity and a magnetic field $\vec{B} = (0,B,0)$ perpendicular to both the flow velocity and the invariant z direction.

Parallel magnetic field. In component form Eq. (4.1) is for a parallel magnetic field,

$$F = \frac{1}{\beta} E_x \; ; \qquad G = \frac{1}{\beta}(E_y + Bv); \qquad H = \frac{1}{\beta}(E_z - Bw).$$

Let $\vec{E}$ and $\vec{B}$ be constant over a small volume cell in the region of interest. At $t = 0$, let $u = u_o$, $v = v_o$, and $w = w_o$. Then the velocity vector at time t is obtained by direct integration of Newton's equation:

$$u = (E_x/\beta)t + u_o,$$

$$v = (w_o + E_y/B) \sin \omega_{gi} t + (v_o - E_z/B) \cos \omega_{gi} t + E_z/B,$$

$$w = (w_o + E_y/B) \cos \omega_{gi} t + (v_o - E_z/B) \sin \omega_{gi} t - E_y/B,$$

where $\omega_{gi} = B/\beta$ and is the ion gyrofrequency in units of plasma frequency.

Since all gradients are zero in the z direction, the equations for x and y are obtained by integrating only the equations for u and v and by setting $x = x_o$ and $y = y_o$ at $t = 0$. Thus:

$$x = x_o + u_o t + E_x t^2/2\beta,$$

$$y = y_o - (1/\omega_{gi})(w_o + E_y/B)(\cos \omega_{gi} t - 1) + (1/\omega_{gi}) \sin \omega_{gi} t.$$

The equation for w is retained in order to determine the z velocity at each point.

Over a small volume cell, the parameter $\omega_{gi} t$ remains small compared to unity. (Recall that ω_{gi} is the dimensionless ion gyrofrequency and is less than the electron gyrofrequency by a factor β). Hence, the trigonometric functions can be expanded about the parameter $\omega_{gi} t$ and can be replaced by polynomials in powers of $\omega_{gi} t$. If terms up to the fourth order of $\omega_{gi} t$ [i.e., $(\omega_{gi} t)^4$] are retained, then the trajectory equations are:

$$x = x_o + u_o t + E_x t^2/2\beta,$$

$$y = y_o + v_o t \left(1 - \frac{\omega_{gi}^2 t^2}{6}\right) + \left(\frac{E_y}{\beta} + \omega_{gi} w_o\right) \frac{t^2}{2} \left(1 - \frac{\omega_{gi}^2 t^2}{12}\right). \tag{4.2}$$

In addition,

$$w = w_o \left(1 - \frac{\omega_{gi}^2 t^2}{2}\right) - v_o \omega_{gi} t \left(1 - \frac{\omega_{gi}^2 t^2}{6}\right) - \frac{E_y}{\beta} t \left(\frac{\omega_{gi} t}{2}\right).$$

In order to determine the exit parameters for a cell, these equations must be inverted and the time t_1 of the flight of an ion through the cell must be obtained. If the exit wall of the cell is defined by a vertical line $x = x_1$, no difficulty

exists. The expansion (2.11) used in the pure electric field case to determine t_1 as a function of x_o, u_o, E_x, and $x = x_1$ can be used in the same manner to determine t_1 in this case. However, if the cell boundary is given by a horizontal line $y = y_o$, then the equation is a fourth order polynomial in t and cannot be solved by the original technique.

Rather than to attempt to invert Eq. (4.2) for y, and obtain the exact time of flight across the cell, that time can be approximated by neglecting the magnetic field. Then the magnetic field effects can be estimated by using the approximate value for t_1, and the value for t_1 again can be determined by inverting a quadratic equation. The first approximation for t_1 is given by

$$y = y_o + v_o t + (E_y/\beta)(t_1^2/2).$$

Let this value of t_1 be t_1^*. Now v_o is replaced by a slightly different value

$$v_o^* = v_o [1 - (\omega_{gi} t_1^*)^2/6],$$

and E_y/β is replaced by

$$E_y^*/\beta = (E_y/\beta + \omega_{gi} w_o)[1 - (\omega_{gi} t_1^*)^2/12].$$

Now the equation for y_1 can be written as,

$$y_1 = y_o + v_o^* t_1 + (E_y^*/\beta)(t_1^2/2).$$

This equation is a quadratic in t_1 and can be solved for t_1 in the same manner as in the pure electric field case. When

the value of $\omega_{gi} t_1$ is much less than unity, then this value of t_1 is nearly identical to that value of t_1 which would have been obtained if the fourth-order polynomial in t_1 had been solved directly.

By tracing the ion trajectory from volume cell to cell, the entire trajectory is constructed from the small parabolic segments spanning each cell. Since the ion velocity w in the z direction is now being considered, the complicated helical motion which charged particles in an electric field undergo is incorporated into the program. Regardless of the fact that the ion velocity is being calculated for all three dimensions, the problem remains spatially two-dimensional. As long as no spatial gradients are present in the z direction, the problem is invariant in that direction.

Perpendicular magnetic field. When the magnetic field is perpendicular to the direction of the ion flow and is oriented such that $\vec{B} = (0,B,0)$, then the force term of Newton's law is, in component form,

$$F = \frac{1}{\beta}(E_x - wB); \quad G = \frac{1}{\beta} E_y ; \quad H = \frac{1}{\beta} (E_z + uB).$$

$\vec{E}$ and $\vec{B}$ are constant over a volume cell. At $t = 0$, $u = u_o$, $v = v_o$, and $w = w_o$. By integration of Newton's equation, the dimensionless velocity vector is

$$u = -(w_o - E_x/B) \sin \omega_{gi} t + (u_o + E_z/B) \cos \omega_{gi} t - E_z/B,$$

$$v = (E_y/\beta)t + v_o,$$

$$w = (w_o - E_x/B) \cos \omega_{gi} t + (u_o + E_z/B) \sin \omega_{gi} t + E_x/B,$$

where $\omega_{gi} = B/\beta$.

In this case, the velocity component v parallel to the magnetic field is independent of the magnetic field. The velocity components u and w in the x and z directions, respectively, depend explicitly on both the magnetic field and the velocity w_o in the z direction. In this case with a perpendicular magnetic field, the electric field E_z in the z direction is not zero. Since the electric field is measured in the satellite frame of reference, an induced electric field arises from the motion of the reference frame through the stationary magnetic field. This induced field is the Lorentz transformation of the magnetic field and is $E_z = u_s B$, where u_s is the satellite speed. If this uniform electric field were ignored, the ions would not appear to stream past the satellite as in the case where no magnetic field is present; the ions would, in fact, circle the lines of magnetic field indefinitely.

The equation for the velocity component w in the z direction is retained since the x component u of velocity depends upon it. The equations for u and v are integrated in order to determine the locus y = y(x) of the ion trajectory. At t = 0, $x = x_o$ and $y = y_o$. Then the trajectory equations are

$$x = x_o + (1/\omega_{gi})(w_o - E_x/B)(\cos \omega_{gi} t - 1) + (1/\omega_{gi})(u_o + E_z/B) \times \sin \omega_{gi} t - (E_z/B)t,$$

$$y = y_o + v_o t + E_y t^2/2\beta.$$

If the electric field component E_z is set equal to the value of the induced electric field $u_s B$ and if the trigonometric

functions are expanded about the small parameter $\omega_{gi}t$, the trajectory equations become:

$$x = x_o + [u_o - (u_o + u_s)\frac{\omega_{gi}^2 t^2}{6}]t + (\frac{E_x}{\beta} - \omega_{gi}w_o)\frac{t^2}{2}(1 - \frac{\omega_{gi}^2 t^2}{12}),$$

$$y = y_o + v_o t + E_y t^2/2\beta.$$

In addition,

$$w = w_o(1 - \frac{\omega_{gi}^2 t^2}{2}) + (u_o + u_s)\omega_{gi}t(1 - \frac{\omega_{gi}^2 t^2}{6}) + \frac{E_x}{\beta}\, t(\frac{\omega_{gi}t}{2}).$$

If the ion trajectory leaves the cell via the horizontal wall defined by the line $y = y_1$, then the time of flight t_1 across the cell can be calculated by means of the expansion given in Eq. (2.11). On the other hand, if the ion leaves via the vertical wall, then the time of flight first must be estimated by neglecting the magnetic field. This estimat t_1^* is obtained by inverting the following equation:

$$x = x_o + u_o t_1^* + (E_x/\beta)(t_1^{*2}/2).$$

The value for u_o is replaced by an altered value u_o^* which accounts for the influence of the magnetic field; similarly, the value for E_x/β is replaced by an altered value E_x^*/β where

$$u_o^* = u_o - (u_o + u_s)\,(\omega_{gi}\, t_1^*)^2/6, \tag{4.3}$$

and

$$E_x^*/\beta = (E_x/\beta - \omega_{gi}w_o)[1 - (\omega_{gi}t_1^*)^2/12].$$

It should be noted that the corrections to u_o and E_x/β are small not only because $\omega_{gi}t$ is small but also because u_o is

approximately equal to u_s in value and opposite in sign. Thus in Eq. (4.3) the term which contains the factor $(u_o + u_s)$ is small. Thus, the time of flight t_1 is obtained from the modified equation

$$x_1 = x_o + u^*_o t_1 + E^*_x/\beta \ (t_1^2/2) .$$

With this value of t_1, the values of y, u, v, and w are calculated. These values of the exit parameters from one cell become the values of the entrance parameters for the next cell. As the ion moves from cell to cell, the entire ion trajectory is constructed.

B. Numerical Results

Depending upon the altitude and latitude, the magnitude of the earth's magnetic field in the ionosphere varies from 0.15 to 0.44 G. At an altitude of 1500 km, for example, where the electron density is about 1.6×10^{10} m^{-3}, the dimensionless magnetic field [in terms of the unit magnetic field $B_o = (n_e m_e/\varepsilon_o)^{\frac{1}{2}}$] is as high as 2. At this field value, the gyrofrequency of an average thermal electron equals twice the plasma frequency, and its gyroradius is equal to one half of the Debye length. Since the ion gyrofrequency is less than the electron gyrofrequency by a factor of the ion mass ratio, the magnetic field influences the ion motion significantly only when the satellite and its wake are very much larger than the Debye length and, therefore, when the ion time of flight through the wake is of the same order of magnitude as one ion gyroperiod.

Negligible interaction of ions with perpendicular magnetic field. When the magnetic field is perpendicular to both the flow velocity and the invariant direction [i.e., $\vec{B} = (0, B, 0)$], the interaction of the cold ions with this field is negligible when compared with the electric interaction. This is due to the fact that the change in the x velocity of the ions is small and, consequently, the cross product of this velocity component and the magnetic field is also small. The magnetic field, of course, does not influence the motion of the ions in the y direction.

Using the method described above, the potential and ion-flow fields around a satellite can be solved for the case of a perpendicular magnetic field. The ionospheric parameters

are set equal to typical values, and the magnitude of the dimensionless magnetic field is increased from zero to a value as large as 500. No significant changes in the potential or ion-flow fields are observed. The change in the x velocity is so small that the ion behavior is identical to that with no magnetic field. Hence, it is reasonable to conclude that the influence of a perpendicular magnetic field on satellite current collection and wake behavior is negligible.

Interaction of satellite body with perpendicular magnetic field. A perpendicular magnetic field acts indirectly on the ions by altering the satellite potential itself. Along the invariant direction of a planar body, a constant electric field is induced in the satellite reference frame. If the satellite is a good electrical conductor, an equal and opposite electric field which cancels the induced field must arise in the satellite. As a result, a linear potential gradient appears along the length of the satellite. Since the satellite potential is part of the boundary condition for the solution of Poisson's equation, the problem is no longer invariant in the z direction. However, the induced electric field in the z direction is very weak compared to the electric fields in the x and y directions. At a 1500-km altitude, the dimensionless induced electric field $E_z = u_s B$ is equal to ≈ 0.04. Hence, the influence of E_z on the ion motion may be neglected.

When the length of a planar satellite is much longer than its half-width (e.g., an antenna), the total current to the satellite may be obtained by integration of the ion and electron currents (per unit length) along the length of the

satellite. Chu and Gross[10] assume that the ion current remains constant regardless of the satellite potential and that the electron current is an exponential function of the potential. They obtained the potential distribution for which the net current to the satellite is zero: The potential at one end of the satellite approximates the plasma value and decreases linearly to a very negative value at the other end. If their assumption concerning the constant ion current is not made, and instead the more accurate values for ion current presented in the previous chapter are used, the qualitative behavior of the antenna potential remains the same. Since Chu and Gross assume too little ion current collected over the entire antenna length, the overall antenna potential is predicted to be slightly more positive than their estimate. This correction to the antenna potential, however, is similar to the logarithmic correction made for the floating potential in the previous chapter and is, therefore, minor.

Plasma drag and induction drag of a satellite. It should be noted that the plasma drag arising from both the intercepted ions and the electric drag of the antenna is not constant along the length of the body. Since the satellite potential is a linearly varying function, the plasma drag is greater at the highly negative end than at the opposite end. Hence, a torque is created which tends to rotate the antenna until its axis is parallel to the flow direction.

The plasma drag on the antenna and the resulting plasma torque are distinctly different from the induction drag discussed by Chu and Gross.[10] The induction drag is the force which arises from the interaction between the net current flux

along the length of the satellite and the perpendicular magnetic field (i.e., the drag is equal to $\vec{J} \times \vec{B}$). However, the plasma drag occurs even if the antenna is a nonconductor with no current flowing along its length.

Influence of parallel magnetic field on ion flow. The disturbed ion flow interacts with the magnetic field when the field is oriented parallel to the flow direction. The change in the horizontal ion velocity is not influenced by the magnetic field, whereas the change in the vertical velocity is significant and interacts directly with the magnetic field. The ion gyroradius is inversely proportional to the magnetic field and for a dimensionless magnetic field of unity is many times larger than the Debye length. Hence, for satellites which are many times larger than the Debye length, the magnetic interaction with the ions is important.

The potential field for a large satellite ($r_{sat} = 25$) in a parallel magnetic field ($B_{\parallel} = 2$) was calculated. The ions had a mass ratio corresponding to that of hydrogen. It was seen that only far downstream ($\approx$ 100 Debye lengths) of the large satellite did the magnetic field influence the ion-flow field sufficiently to slightly alter the potential distribution obtained in the zero-magnetic-field case. The near wake and most of the midwake as well as the ion current and drag are not influenced by the field. The far wake region, however, far downstream of the satellite, is not accurately determined by the computer program because of the memory size limit. It was for this reason that the investigation of the expected influence of the field on the ion flow around even larger satellites was not carried out.

Influence of strong magnetic field on ion flow. If the magnetic field is increased to values which do not occur naturally in the ionosphere, the ion-flow field around a satellite with radius of the order of a Debye length is strongly affected. Examination of the behavior of the ion-flow field and the associated ion current and near wake in a strong magnetic field provides an understanding of the behavior of the ion flow for very large satellites in an ionospheric magnetic field.

As previously discussed, even when a perpendicular magnetic field is strong (as large as $B_{\perp} = 500$), it has no significant interaction with the ion-flow field. A strong parallel magnetic field, however, interacts significantly with the ions. When the ions are attracted either toward the satellite or into the wake, they must cross lines of magnetic force which retard their vertical motion and tend to diminish the effect of the attractive electric field around the satellite and in the wake.

Influence of strong magnetic field on ion current. An obvious result of the strong parallel magnetic field is the reduction of the ion current collected by a satellite having a negative potential. At plasma potential the satellite collects the same current with or without a magnetic field, namely, the "ram" current. When the potential is made negative, the ions, "stiffened" by the magnetic field, have straighter trajectories and are not collected so readily as in the case of no magnetic field.

In Fig. 4.1, the ion current as a function of satellite potential is shown for two values of parallel magnetic field, zero and 100. (The plate satellite parameters are $\hat{E}_{KE} = 6$,

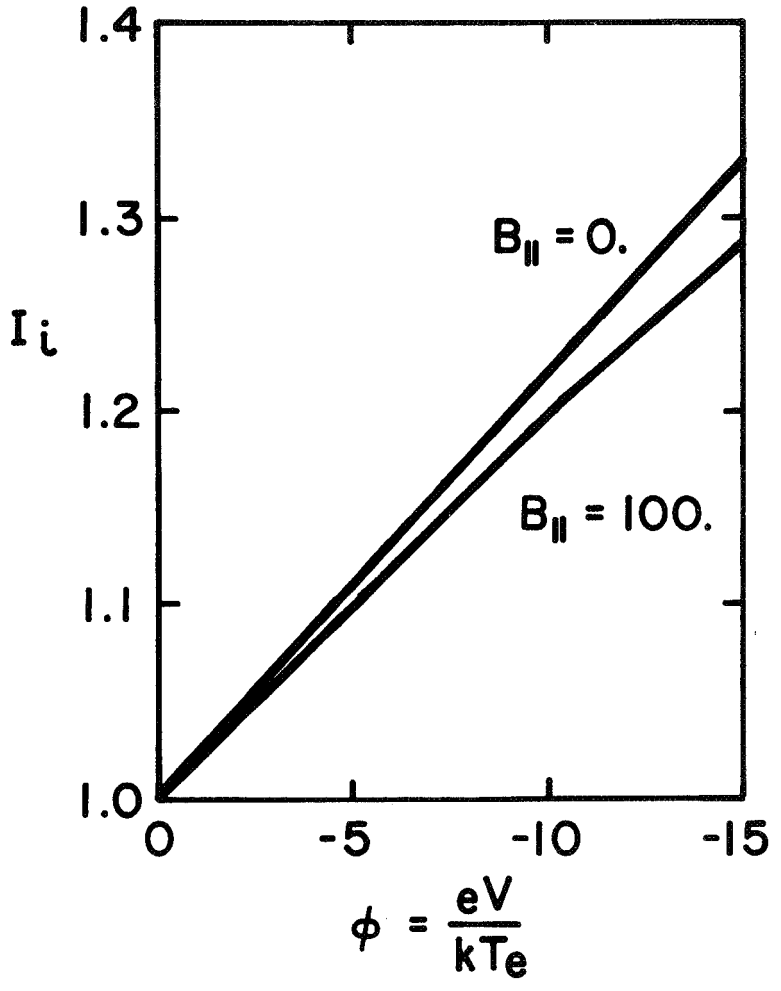

FIG. 4.1. ION CURRENT VS. POTENTIAL FOR PLATE SATELLITE IN MAGNETIC FIELD PARALLEL TO FLOW DIRECTION ($\hat{E}_{KE}$= 6, r_{sat}= 1).

and $r_{sat} = 1.$) The decrease from 2.2% to 1.9% in the rate of growth of the ion current per unit potential is not sufficient to significantly alter the value of the floating potential calculated previously for the case of no magnetic field. As the magnetic field is further increased, however, the value of ion current approaches that of the "ram" current.

Figure 4.2 shows the ion current to a plate satellite as a function of the parallel magnetic field. The satellite potential is fixed at a value of -10. Although that portion of the ion current which is collected by virtue of the negative potential is severely reduced by the magnetic field, the satellite continues to attract ions across the lines of magnetic force. In fact, when the figure is examined for the development of the ion current at the higher values of the magnetic field, it is estimated that the magnetic field must be an order of magnitude larger (i.e., $B \geq 1000$) if the ion current is to be reduced to the "ram" current. Hence, an assumption that the parallel magnetic field constrains the ions to have straight trajectories is valid only when the ion gyroradius is much less than the Debye length. Then the magnetic field is considered "infinite," and a negatively charged body collects only the "ram" current. Since the computer program assumes that the quantity $\omega_{gi}t = (B/\beta)t$ is small where t is the time of particle flight in a cell, the interesting case of a very large, parallel magnetic field has not been investigated.

Influence of strong magnetic field on satellite wake. When the parallel magnetic field is strong, the development of the wake region is influenced considerably. As in the zero-

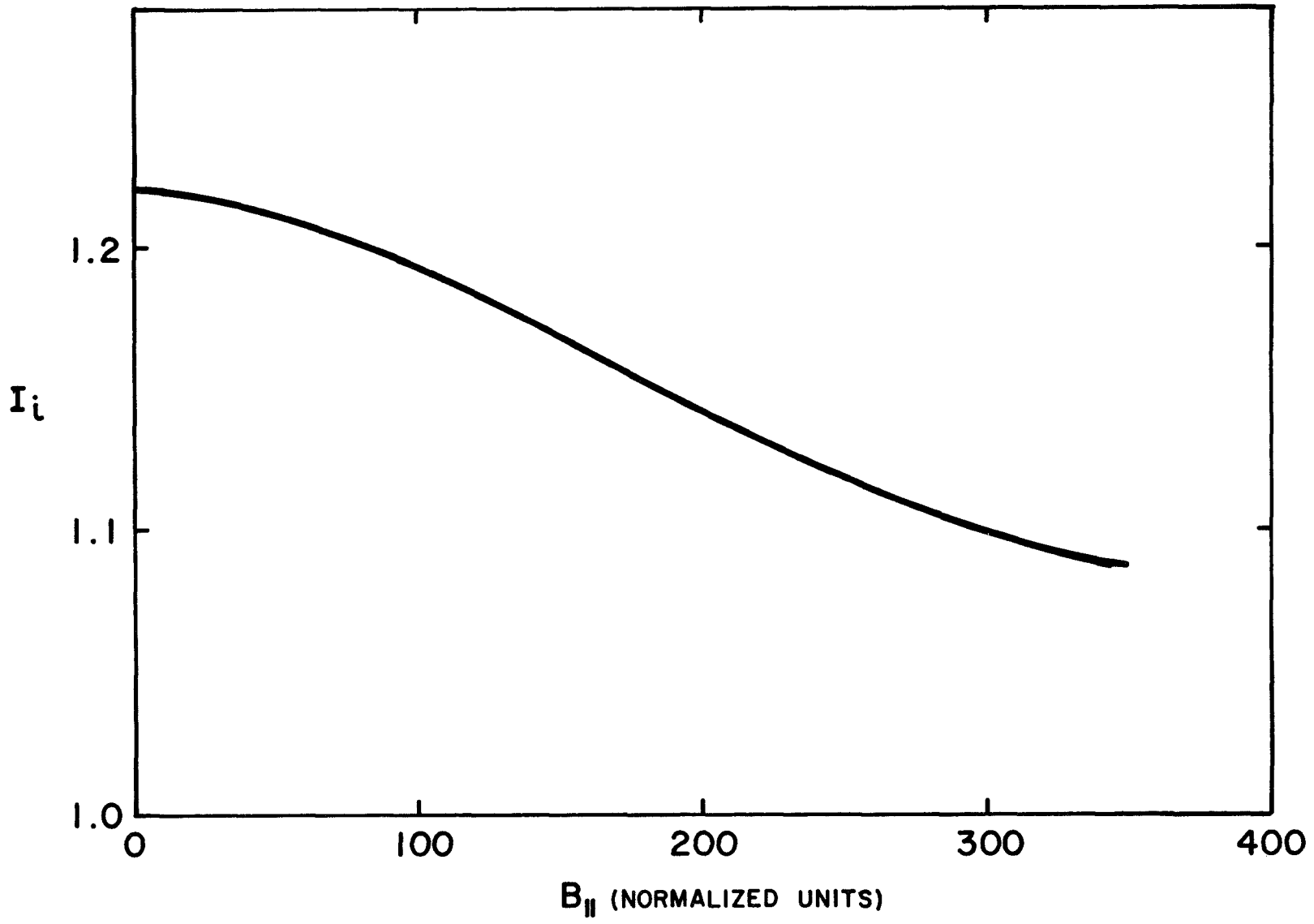

FIG. 4.2. ION CURRENT VS. PARALLEL MAGNETIC FIELD FOR PLATE SATELLITE ($\hat{E}_{KE}$= 6, ϕ_{sat}= -10, r_{sat}= 1).

magnetic-field case, the near wake is electron rich. Because of the magnetic field, however, the electrons in the wake enter it by moving along lines of magnetic force with helical trajectories originating far downstream of the satellite. These trajectories are assumed to be populated by electron-ion collisions in the far wake region. As a result, the electron density is proportional to the Boltzmann factor in the entire wake. The electric field which arises from the negative charge density attracts ions toward the wake in order to neutralize it. However, the magnetic field retards the ion motion across the lines of force. The ions instead of entering and crossing the wake have helical trajectories which wind about a line of magnetic force. The ions do not penetrate into the wake further than a distance of one ion gyroradius. As a result, if the satellite radius is larger than the ion gyroradius, a portion of the wake remains negatively charged for an indefinite distance downstream. Hence, the entire wake in a strong magnetic field retains the characteristic of a near wake for no magnetic field. In actuality, collisions provide the mechanism for neutralizing the far wake.[6] However, the collision lengths in the ionosphere are extremely large compared to the Debye length, and the disturbed region extends for distances much greater than those investigated by means of the computer program discussed here.

Figures 4.3 and 4.4 are the ion trajectory plot and the contour plot of potential, respectively, for a plate satellite in a parallel magnetic field ($B_{\parallel} = 200$ in dimensionless units). At this value of field, the gyroradius of the ions deflected into the wake by the attractive potential of the satellite is less than the satellite half-width of one Debye length. As a

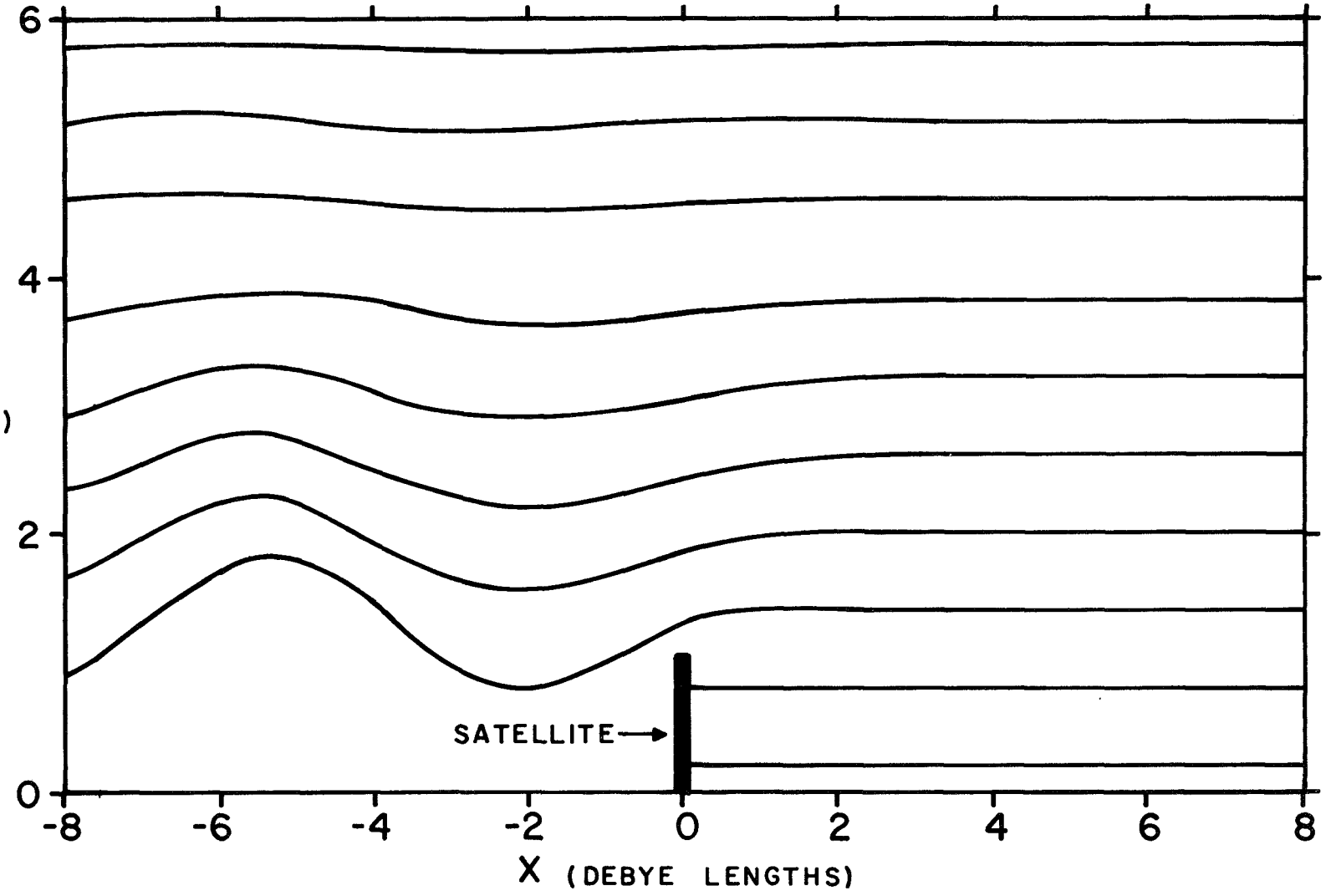

FIG. 4.3. ION TRAJECTORY PLOT FOR PLATE SATELLITE IN PARALLEL MAGNETIC FIELD ($\hat{E}_{KE}$= 6, ϕ_{sat}= -10, r_{sat}= 1, $B_{\parallel}$= 200).

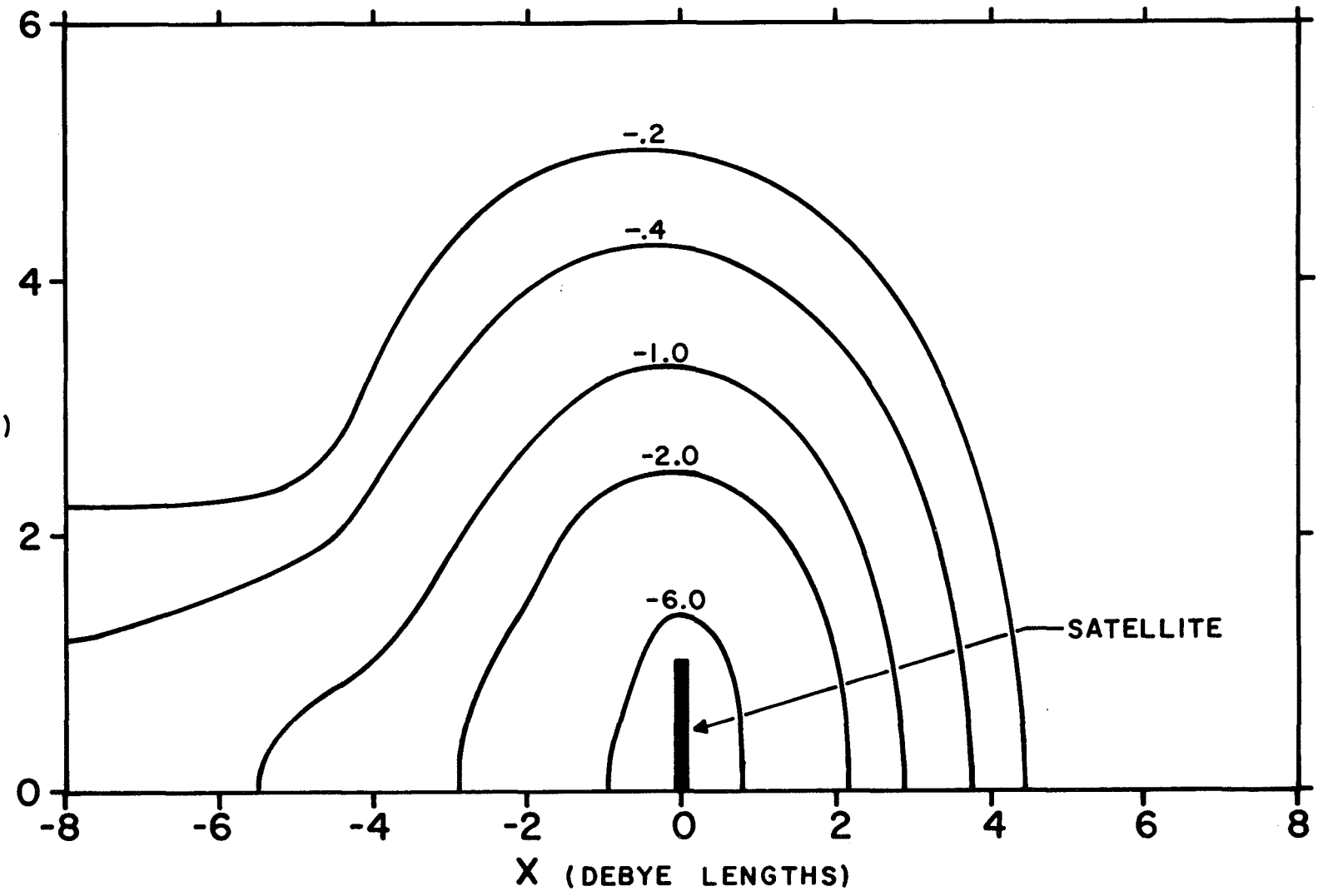

FIG. 4.4. CONTOUR PLOT OF POTENTIAL FOR PLATE SATELLITE IN PARALLEL MAGNETIC FIELD ($\hat{E}_{KE}$= 6, ϕ_{sat}= -10, r_{sat}= 1, $B_{\parallel}$= 200).

result, the ions do not completely fill in the wake, and the negative potential of the wake extends downstream without attenuation. The partially neutralized midwake found in the zero-magnetic-field case does not occur in this case. Furthermore, the ion beams are not created.

It is expected that in the case of very large satellites ($r_{sat} > 100$), the magnetic field of the earth, although its dimensionless value is of the order of unity, has an effect on the wake behavior similar to that of large fields and moderately sized bodies. The disturbed wake is extended very far downstream until collisions can provide sufficient ions which have wake-neutralizing trajectories. It is also possible that time-dependent phenomena such as Alfvén waves may occur, but such processes are not investigated in the present study.

CHAPTER V: CONCLUSIONS

The numerical results presented in this thesis demonstrate that the flow-field technique may be used in conjunction with the "alternating direction implicit" (ADI) method[30] to solve the Poisson-Vlasov system of equations and, thereby, to investigate the interaction of a satellite with the ionosphere. Since the flow-field technique permits efficient use to be made of the ion-trajectory data, the accuracy of the resulting ion density is an order of magnitude greater than that obtained with the "super-particle" technique[21] (for an equal number of ion trajectories). As a result, accurate predictions of the ion current, satellite drag, floating potential, and wake behavior have been made over a much wider range of ionospheric and satellite conditions than was previously possible. Furthermore, the flow-field technique has been shown to be applicable in the presence of a uniform magnetic field.

Plots of the ion current to the satellite as a function of potential for various satellite radii, satellite bodies, and ion kinetic energies have revealed that the ion current in all cases has a nearly linear dependence on the potential over a range of potential as negative as -25 times the electron thermal energy. For plate satellites with a radius greater than than 25 times the Debye length, the rate of growth of ion current is less than 0.1% per unit potential. For a smaller radius, however, the rate of growth may be as much as 7% per unit of potential (in the case of a sphere of radius one Debye length). The angular distribution of ion flux to the surface of a cylinder has the approximate functional dependence

on angle of a cosine curve incremented by a quantity which depends on the potential.

The drag on the satellite due to the ions has been shown to be dependent on the surface interaction as well as the potential. For satellites with radii large compared to the Debye length, the drag increases with increasingly negative potential if the ions undergo specular reflection at the surface. For moderately sized satellites ($r_{sat} \approx 1$), that portion of the drag which is due to the electric interaction may account for as much as 40% of the total drag.

In the case of satellites with the planar class of body shape, plots of potential and ion density clearly reveal a distinction between near wake and midwake. The ion-free near wake length is proportional to approximately the square root of the dimensionless satellite radius; as a result, the electric field extends for many Debye lengths in this region. In the midwake of moderately sized satellites, the formation of two symmetric ion beams has been observed in these numerical results. Their strength and angle with the flow direction increase with increasingly negative satellite potential. The formation of the beams is attributed to the wake potential which is distorted by the sharp ion-density gradient there. For large satellites ($r_{sat} > 10$), the ion beams have not been observed. For satellites of the axially symmetric class, the wake has a series of ion-free and ion-rich areas which decrease in strength with increasing distance downstream. The resulting potential field varies with distance over a range extending from -0.4 to 0.4 in units of electron thermal energy.

It has been demonstrated that a geomagnetic field which is perpendicular to the flow velocity has negligible direct influence on the ion motion. A perpendicular magnetic field, however, which is also perpendicular to the axis of a very long body will influence the ion motion indirectly by inducing a linear potential gradient on the body. If the geomagnetic field is parallel to the flow direction, the midwake of a large satellite is altered slightly. With a larger parallel field, the ion-free near wake is extended further downstream. In fact, for fields where $B > 500$ (in dimensionless units), the near wake may extend over distances in which collisional effects become important. At these large values of field, the collected ion current approaches the "ram" current.

APPENDIX A: DERIVATION OF ION DENSITY (FLOW-FIELD METHOD)

If one end of a flux tube is allowed to begin at a point in the undisturbed plasma where the ion density and the ion velocity are the known ambient values and the other end of the tube is extended into the disturbed region, then the ion density at any point can be calculated from the values of the ion velocity and tube area at that point. The tube walls are defined by individual ion trajectories; therefore, the velocity of the ions at any point can be estimated. However, in order to determine the area of the tube, the geometry of the problem must be considered. In the planar case, the "tube" of flux assumes the shape of a strip of flux bounded by two parallel sheets. In the axially symmetric case, the "tube" becomes a ring of flux bounded by two cylindrical walls. The locus of each cylindrical wall is given by an ion trajectory. As two adjacent trajectories are followed, the cross-sectional area $\vec{A}$ of the strip or ring varies. From the current conservation equation, (2.6), the ion current contained in the tube at any point is equal in value to the current at the source of the flux tube upstream in the undisturbed region. Therefore, the ion number density can be calculated at any point in the disturbed region. It is assumed that the ion density is approximately constant over the cross-sectional area of the tube and that the discontinuous change in the density of a neighboring tube is small compared to the magnitude of the density.

Figure A1 shows an "imaginary" flux tube of infinitesimal thickness. Surrounding that tube is a flux tube which is defined by two computed trajectories. The "imaginary" tube

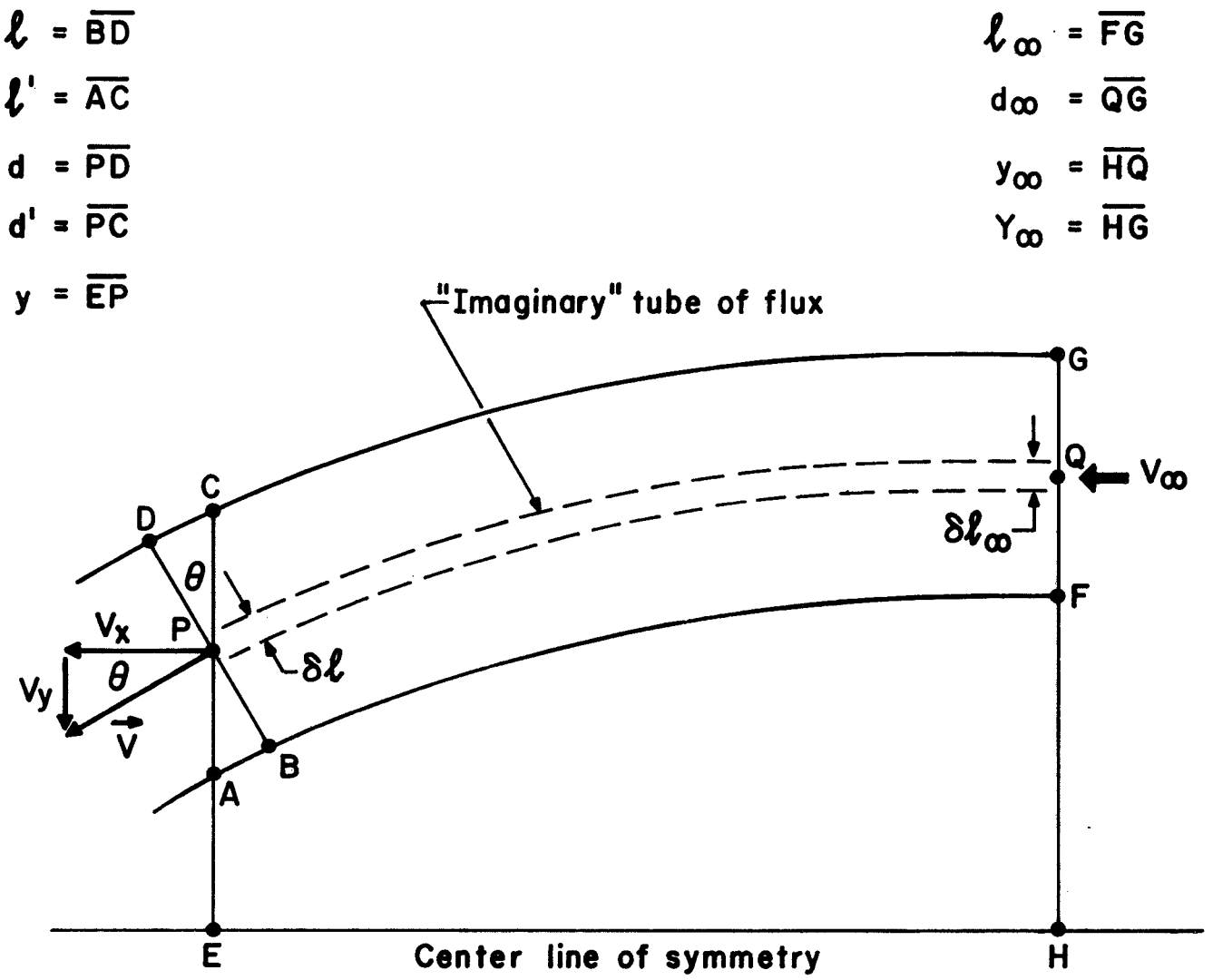

FIG. A1. GEOMETRY OF FLOW-FIELD METHOD. FLUX TUBE IS BOUNDED BY TWO CALCULATED TRAJECTORIES.

has been drawn to pass exactly through the (grid) point of interest P. The change in width of the imaginary tube along its length is assumed to be proportional to the change in width of the actual tube, that is,

$$\delta \ell_\infty / \delta \ell = \ell_\infty / \ell \ .$$

It is computationally convenient to measure the tube width as a distance ℓ' in the y-direction (rather than as a distance ℓ). The tube width ℓ_∞ in the undisturbed region is already in the y-direction; therefore, ℓ_∞ will be used as it is. From the geometry, and assuming that the width changes slowly, it follows that

$$\ell = \ell' \cos\theta, \text{ and } \delta \ell_\infty / \delta \ell' = \ell_\infty / \ell' \ . \tag{A1}$$

From Eqs. (2.6) and (2.7), the number density at the point of interest P is obtained:

$$n = n_\infty \frac{\vec{v}_\infty \cdot \vec{A}_\infty}{\vec{v} \cdot \vec{A}} = n_\infty \frac{v_\infty A_\infty}{|\vec{v}||\vec{A}|} \ .$$

Since $|\vec{v}| = v_x \sec\theta$ and $|\vec{A}| = A' \cos\theta$, the density is

$$n = n_\infty \frac{v_\infty A_\infty}{v_x A'} \ .$$

The area of the "imaginary" tube end is equal to the tube width $\delta \ell$ multiplied by a unit length L in the "invariant" direction, i.e.,

$$A_\infty = \delta \ell_\infty \, L_\infty, \text{ and } A' = \delta \ell' L.$$

If the geometry of the problem is planar, the unit length L is the same at both ends of the tube, and $L_\infty = L$. Thus, $A_\infty/A' = \delta\ell_\infty/\delta\ell'$, and from Eq. (A1)

$$n = n_\infty \frac{v_\infty \ell_\infty}{v_x \ell'} \quad . \tag{A2}$$

If, however, the geometry of the problem is axially symmetric, then $L_\infty = 2\pi y_\infty$ and $L = 2\pi y$. Therefore,

$$A_\infty = \delta\ell_\infty(2\pi y_\infty), \text{ and } A' = \delta\ell'(2\pi y),$$

where y_∞ and y are the radial distances from the axis of rotation. Although the distance y is known, the distance y_∞ must be estimated. It is assumed that the "imaginary" tube is situated between the walls of the actual tube in the same proportion throughout the length of the tube. From the geometry,

$$y_\infty = Y_\infty - d_\infty = Y_\infty - d' \frac{\ell_\infty}{\ell'} \quad .$$

Thus,

$$n = n_\infty \frac{v_\infty \ell_\infty}{v_x \ell'} \left[\frac{1}{y}\left(Y_\infty - d' \frac{\ell_\infty}{\ell'}\right)\right] \quad , \tag{A3}$$

which is identical to Eq. (A2) except for the factor in brackets. This factor is the radial compression or expansion which occurs in the axially symmetric geometry. Note that if the point of interest is on the axis, then $y=0$, and the density is singular at that point. To avoid singularities, the mesh will be located in such a way that no grid points will lie on the axis.

It should also be mentioned that in Eqs. (A2) and (A3) the velocity v_x (the x component of the ion velocity) is

not known at the point of interest. In fact, since the velocities of the two trajectories are approximately equal at the points directly above and below the point of interest, then either of these velocities is a good approximation for the velocity at the point of interest.

APPENDIX B: ACCURACY OF THE NUMERICAL SOLUTION

1. Grid Structure

Introduction. The region of interest which surrounds the satellite is partitioned into a mesh by means of a set of vertical and horizontal grid lines. The intersection of these lines are the grid points (also called mesh points or nodes). These grid lines and points form the structure upon which all of the approximations employed in the solution of the equations of the problem are based. Certain grid points are designated as the satellite surface. Poisson's equation is approximated by a set of coupled algebraic equations relating the value of potential at a given point to the values at neighboring points. The electric field calculated at each grid point is assumed constant over a cell, and the ion trajectory is approximated by parabolic arcs within cells. The ion density is calculated for each grid point by employing a flux-tube approximation for adjacent trajectories. Thus, each approximated equation is based on a common grid structure.

Grid-structure requirements. The main requirement for the grid structure is the accurate approximation of Poisson's equation both in the region neighboring the satellite and wake and in the region far away from the satellite. In general, the mesh spacing must not be greater than the Debye length for accurate approximation. In the region near the satellite, the potential gradients may be large and, as a result, the mesh size h may of necessity, be much less than a Debye length (e.g., $h = 0.1$). In the region far away from the satellite,

however, the potential gradients are weak and, as a result, the mesh size may be increased to a value of nearly a Debye length (e.g., $h \approx 0.75$). If the mesh size exceeds a Debye length in the weak-field region, it is possible that the iterates obtained by using the ADI method to solve Poisson's equation (minor iterates) will not converge. Since this upper limit on mesh size is not required for the convergence of the iterates of linear finite-difference operators, this limit may be attributed to that nonlinear portion of the operator which accounts for the Boltzmann factor.

If both the weak-field and strong-field areas of the disturbed region are to have a reasonable number of grid points, a variable mesh size must be employed. In the strong-field area, the mesh spacing is small; moving toward the weak-field area, the spacing becomes progressively larger. The variable spacing is chosen arbitrarily and depends on the parameters of the problem and the desired accuracy of the results; no coordinate transformation is used to provide an "automatically" varying mesh.

The mesh size must not be made unnecessarily small. Obviously, the smaller the mesh size, the greater the number of grid points to cover the same region of interest. Furthermore, the rate of convergence of the minor itnerates decreases with smaller mesh size, i.e., more iterates are necessary in order to obtain the same accuracy. Hence, the computation time needed for a solution increases rapidly. This inverse dependence of the number of minor iterates on the mesh size is characteristic of all finite-difference approximations to partial differential equations (see, for example, Ref. 30).

Model problem. Figure B1 shows the boundaries of the mesh structure for a typical plate-satellite problem which will be used as a model for error analysis. The horizontal mesh size is 0.25 Debye lengths in the neighborhood of the satellite, 0.5 in the wake, and 0.75 in the front. The vertical mesh size is 0.2 Debye lengths near the satellite and increases progressively to values of 0.4 and 0.75 until the side boundary is reached. Notice that no mesh points lie on the $y = 0$ line; therefore, this model grid may be used for axially symmetric satellite geometries. Furthermore, the satellite surface is defined to coincide with one of the vertical grid lines, and the upper edge of that surface ends on a horizontal grid line.

2. Iterate Convergence and Accuracy

Convergence of minor iterates. For the model and many other grid structures, it is found empirically that the optimum overrelaxation factor ω for the minor iterates (see Chap. II) is approximately 1.55. Apparently, the form of operator itself has more influence on the relaxation factor than the exact grid spacing, size of region, or location of the boundaries. In actuality, the overrelaxation value used is slightly less than the optimum value ($\omega^* = 1.58$) determined for the model case. The reason for this bias is that if ω is greater than the optimum value, the number of iterates required for a solution is much greater than if ω is less than the optimum value by a corresponding amount. Therefore, in order to insure that ω will never be greater than the optimum value for any case, a value smaller than the optimum value of the model case is used.

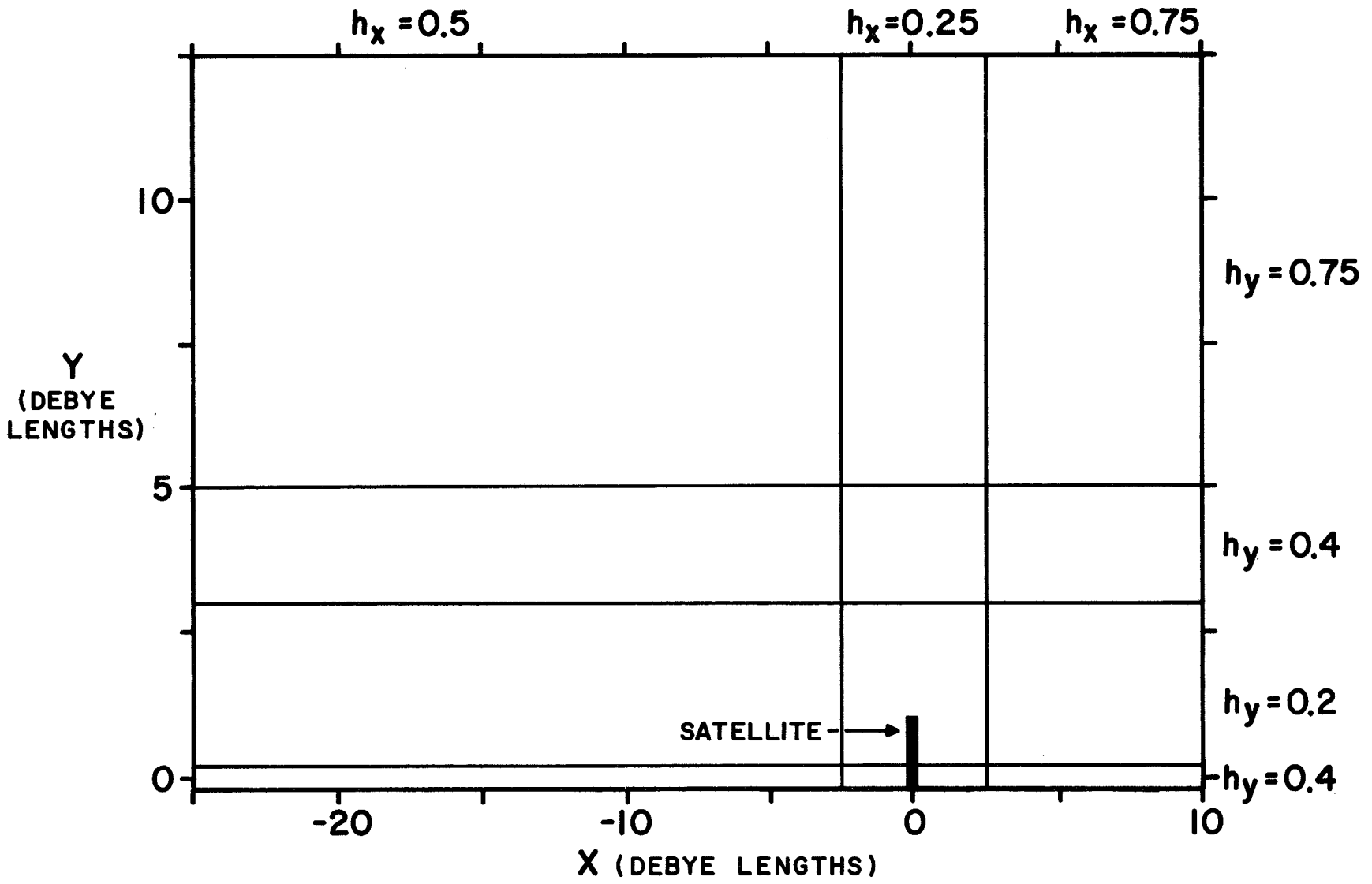

FIG. B1. BOUNDARIES AT WHICH GRID SIZE CHANGES IN SOLUTION OF MODEL PROBLEM (76×31 GRID POINTS).

The number of minor iterates necessary for the solution of Poisson's equation depends upon the degree of accuracy desired for the potential. Generally, there must be between 10 and 20 minor iterates in order to obtain a potential which is sufficiently accurate for computation of a new set of trajectories. Since at first the ion charge density record is not known accurately, it is not important that the potential be computed to a highly accurate value. When the accuracy of the ion density record is improved by recalculation of the ion trajectories, then the accuracy of the potential also will improve without an increase in the number of minor iterates.

Spacing between ion trajectories. Once the grid structure has been chosen, the choice of the spacing between ion trajectories follows in an obvious manner. Again, variable spacing is necessary in order to minimize the required computation time. As a rule, the distance between each trajectory must be slightly less than the vertical size of the cells which the trajectory will cross. This choice of spacing insures that variations in the ion charge density will occur smoothly for every grid point. The only exception to the spacing rule involves those trajectories which are known to intercept the satellite. Since the ion charge density varies slowly in front of the satellite, the spacing between trajectories may be made as large as a few cell widths without introducing serious error into the ion charge density record . It is understood that none of these trajectories will enter the wake where the charge density is likely to vary sharply.

Note that the spacing for those trajectories which enter the wake must be smaller than the wake mesh size even if those trajectories begin at points where the mesh size is large.

Underrelaxation factor for major iterates. After the record of the ion charge density has been obtained by use of the calculated ion trajectories, the potential is recomputed, and a new record for the ion charge density is obtained. The iterates which are the result of the alternate calculations for potential and charge density (called major iterates) converge when an underrelaxation factor for them is introduced. As in the case of the overrelaxation factor for minor iterates, the underrelaxation factor for major iterates must be obtained empirically. The factor for ion density iterates for planar geometries is approximately 0.75; for axially symmetric geometries where the ion density near the axis may be an order of magnitude larger than the ambient density, the factor may vary between 0.5 and 0.6. The factor for the major potential iterates may be nearer unity since the potential does not have such large variations as the ion density. Generally, a factor of 0.75 is sufficiently low to insure convergence. The underrelaxation factors for both the ion density and potential iterates should be unity for the first iterate since the initial guess is usually a very poor approximation of the solution. The remaining iterates may have an underrelaxation factor which is independent of the iterate number.

Definition of major iterate error. The number of major iterates controls the accuracy of the solution of the finite-difference equations which approximate the Poisson-Vlasov system of equations. In order to measure that accuracy, an

error norm must be defined. The most frequently used norm--the root mean square of the values of the difference matrix between one iterate and the next--is not so useful in this problem as in other finite-difference problems. Since a great many of the grid points lie in the region where the electric field is weak, this error norm would fail to reflect any serious errors in the near wake region where the field is strong. The root mean square of the relative values of the difference matrix between iterates is also unsatisfactory since the near zero values of potential (and, possibly, zero values) in the far field region would inflate and distort the error norm. Therefore, an error norm equal to the maximum absolute value of the difference matrix between iterates was chosen. Since this choice of norm reflects the iterate error at only one point--namely the point with the largest error--the error appears to be much larger than is customarily expected in this type of problem. However, this norm has proved to be much more useful than the other norms for the error analysis of the finite-difference techniques employed in the satellite-ionosphere interaction problem.

The accuracy of the solution to the finite-difference equation is obtained by calculation of the norm of the differences of two consecutive major iterates. As the major iterates converge to the solution, the norm of the difference decreases toward a value of zero. The error between any iterate and the true solution, therefore, is approximated by the norm of the difference between that iterate and the preceding iterate. Only in the case where the underrelaxation factors are very small (i.e., less than 0.25) is this estimate for the iterate error excessively low.

Major iterate error of model problem. Table III lists the error associated with the sequence of major iterates obtained in the solution of the problem with typical satellite parameters ($\hat{E}_{KE}$= 12, r_{sat}= 1) and the model grid structure. Since the error decreases with the increase in the iterate number, the iterates are convergent toward the solution. The error for the potential iterates is, of course, smaller than for the corresponding ion charge density iterates since the potential is the result of "double integration" of the ion charge density. In order to compare the iterate error for a satellite with zero potential and one with a negative potential, a relative error is defined by division of the absolute error by the absolute maximum value of the grid points. (The maximum absolute difference between two iterates does not occur necessarily at the same grid point as the maximum absolute value.)

In practice, six to eight major iterates are required for a satisfactory solution for the model problem. More iterates may be required for problems with very low ion kinetic energy or very negative satellite potential. Since the truncation error associated with finite mesh size is about 3% for the model problem (to be proved below), no improvement in the overall accuracy is gained by calculating a large number of major iterates.

Intersection of adjacent trajectories. An additional criterion on the number of major iterates required for solution of the problem is that large numbers of adjacent ion trajectories should not cross each other. Any two adjacent trajectories which intersect fail to satisfy the approximations

TABLE III

Major iterate error of the potential field of the model problem as a function of iterate number ($\hat{E}_{KE} = 12$, $r_{sat} = 1$).

Major iterate number	$\varpi_{sat} = 0$ Abs. error	$\varpi_{sat} = 0$ % rel. error	$\varpi_{sat} = -5$ Abs. error	$\varpi_{sat} = -5$ % rel. error
1	0.577	77.	4.32	97.
2	0.256	33.	0.243	5.6
3	0.0592	7.9	0.127	2.9
4	0.0736	9.8	0.0964	2.2
5	0.0350	4.7	0.0877	2.0
6	0.0114	1.5	0.0480	1.1
7	0.0156	2.1	0.0480	1.1
8	0.0082	1.1	0.0259	0.60
9	0.0274	3.7	0.0102	0.23
10	0.0242	3.2	0.0042	0.097
11	0.0118	1.5	0.0021	0.047
12	0.0044	0.60	0.0008	0.018

invoked in the flow-field method of calculating the ion density. Then, at grid points in the vicinity of the intersection, abnormally high values for the ion density arise. These high values create a local electric field which is not self-consistent. In succeeding iterates when the electric field is obtained more accurately, the number of trajectory crossings decreases. Therefore, for an accurate solution the number of major iterates should be extended until no adjacent trajectories intersect. However, in certain cases where the remaining one or two crossings are not near grid points, the results obtained for a small number of iterates are little different from those obtained for a larger number of iterates when no adjacent trajectories cross.

3. Truncation Error

Source of truncation error. The preceding discussion concerning the error of the major iterates considers only the error arising during the solution of the set of finite-difference equations. The discussion now concerns the error associated with the replacement of the Poisson-Vlasov system of differential equations by the finite-difference set of algebraic equations. In other words, even if the number of major iterates were extended until the difference between two consecutive iterates became zero, an error originating from the approximations invoked in the employment of the finite-difference scheme would remain in the solution. For example, in Chap. II the differential operator given by Eq. (2.12) is approximated by the finite-difference operator of Eq. (2.13). The error of this approximation is proportional

to the second power of the mesh spacing and is called the truncation error since the Taylor series expansion of the differential operator has been truncated in order to obtain a simple approximation for the operator. Other sources of error include the approximations invoked by assuming the constancy of the electric field over a volume cell and the finite spacing between particle trajectories necessary to obtain the ion-flow field. Both of these errors are dependent on the mesh size in such a manner that increasing the mesh size results in increased error; these errors also may be considered truncation errors.

The influence of the truncation error on the accuracy of the solution may be estimated by a comparison of the solutions for identical problems based on grid structures of different sizes. Any calculated "solution" has truncation error. If the identical problem is solved on a grid with smaller mesh size, the new "solution" contains less truncation error than, and hence is different from, the first "solution." Each time the mesh size is reduced, the resulting "solution" contains less truncation error and approaches the actual solution more closely. Hence, when two "solutions" based on grid structures with different mesh sizes are obtained, it is assumed that the difference is approximately the truncation error of the "solution" based on the larger mesh size.

Truncation error of model problem. In order to determine the truncation error of the solution obtained for the model problem, two other solutions were obtained based on coarse and fine grid structures with a mesh spacing twice as large and half as large, respectively, as that of the model

problem. While the model problem has 2356 grid points (76 x 31), the problem with a coarse mesh has 1173 (51 x 23); the problem with a fine mesh has 9211 (151 x 61). Note that although the fine structure has four times as many grid points as has the model problem, the structure with the coarse mesh has only about 40% fewer grid points than the model problem. The reason for this lack of balance between the three grid structures is that the minor iterates do not converge if a large part of the mesh spacing is near to the Debye length. Hence, for the coarse structure, all mesh sizes are double those of the model problem except where the size would exceed 0.75 Debye lengths.

The maximum absolute difference in the potential values between solutions based on the coarse and fine grid structures is 0.11; when divided by the maximum absolute potential value to obtain a relative error, this difference is 15%. On the other hand, the maximum absolute difference in the potential values between solutions based on the model and fine grid structures is 0.024 or 3.3%. This accuracy of the potential values for the model problem is sufficient to insure the accuracy of the detailed results on current, drag, and wake behavior presented in the main portion of the text.

Neglect of roundoff error. Roundoff errors which sometimes arise in problems of numerical analysis are due to the fact that the computer word length is finite and can hold only numbers with a limited number of significant digits. Since the roundoff error is proportional to the square root of the number of grid points times the accuracy of the computer word, the roundoff error is controlled in this problem by

employing a computer with words which will hold a sufficiently large number of digits. In the cases where the IBM 7094 computer is used, a word holds eight significant digits; where the IBM 360 is used, a double-word holds 16 to 18 significant digits. Therefore, these considerations show that round-off error is not a significant source of error in this problem.

4. Influence of the Boundary Location on the Numerical Accuracy

Front-boundary location. The locations of the boundaries of the disturbed region have an influence on the accuracy of the potential and ion-flow fields within the boundaries. Ideally, the boundaries where the potential is set equal to zero should be infinitely far from the satellite in order to duplicate the boundary conditions of the Poisson-Vlasov system of equations; practically, they must be a finite distance from the satellite. Since the disturbing electric field of the wake and the satellite is attenuated considerably over distances of the order of several Debye lengths, the boundaries can be located in most instances within ten Debye lengths of the satellite and wake. For example, when the front boundary is located ten Debye lengths upstream of the satellite, the values of the ion density of the grid points in the vicinity of the boundary remain at ambient. Even for satellite potentials as negative as -40, the front boundary must be only about ten Debye lengths away from the satellite to satisfy this criterion.

Side-boundary location. The distance between the side boundary and the satellite has an important effect on the behavior of the wake downstream. As the electric field of the near wake spreads out into the surrounding plasma of the midwake, the field perturbs the ions located far from the satellite, and they are attracted toward the wake. If the outermost ion trajectory is attracted for a sufficiently long distance, it moves below the downstream portion of the outermost horizontal line of grid points adjacent to the boundary line. Since no ion trajectory exists above that line of grid points, the ion density cannot be estimated for the remainder of the line. Hence, in order to avoid this difficulty during the investigation of very long wakes, the side boundary must be located as much as 15 or 20 Debye lengths away from the satellite.

It should be emphasized that the location of the side boundary, as in the case of the front boundary, does not affect the potential field in the near wake or in the vicinity of the satellite. Figure B2 is a semilogarithmic plot of the potential as a function of the vertical distance for the fixed position ($x = -4$) downstream of the satellite. Only the potential within two Debye lengths of the boundary is dependent upon the location of the boundary. The potential in the remainder of the distance is "locked" onto the solution values.

Downstream-boundary location. The downstream-boundary location has a similar effect on the potential in its vicinity. Since the potential there is no longer nearly zero, however, the change of the potential as a result of the downstream-boundary location is significant. Within a few Debye lengths

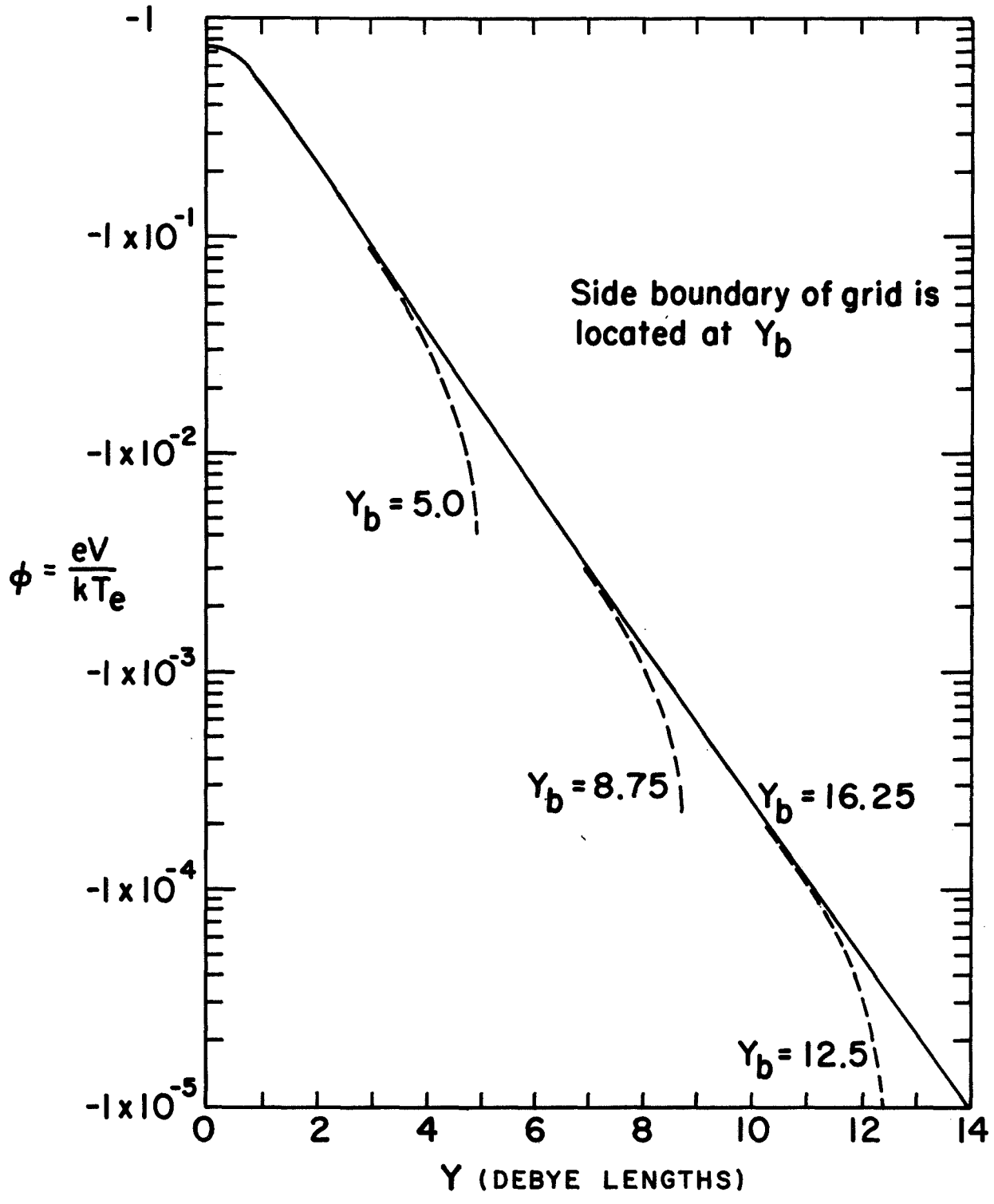

FIG. B2. POTENTIAL VS. VERTICAL DISTANCE FOR VARIOUS SIDE-BOUNDARY LOCATIONS ($\hat{E}_{KE}$= 12, ϕ_{sat}= 0, r_{sat}= 1, X= 4). NOTE THAT POTENTIAL IS INDEPENDENT OF Y_b EXCEPT WITHIN TWO DEBYE LENGTHS OF Y_b.

of the boundary location, therefore, the values of the potential and ion-flow fields are not accurate.

The results obtained in that area not in the vicinity of the downstream boundary are unaffected by location of the downstream boundary. Since the ions are assumed to have zero temperature, none travel upstream, and, as a result, no information about the downstream conditions can be carried upstream by the ions. Only the electric field influences the ion behavior in the upstream direction, and its effect is limited to distances of a few Debye lengths. Hence, the results obtained in the region "shielded" from the downstream boundary condition are accurate.

A problem with similar conditions to those of the model problem was run a number of times with the downstream boundary located further downstream for each run. The potential field was compared for each run and was found constant from run to run in that part of the region at least five Debye lengths from the downstream boundary. It is suggested, therefore, that the length of the region of investigation is limited only by the memory size of the computer employed and the corresponding time of computation necessary for an accurate solution.

5. Computation Time of the Model Problem

In order to compare the speed of computation as a function of the computer model, the model problem was run for six major iterates on three different machines. On the IBM 7094, the problem runs for 229.8 sec; on the IBM 360/75 it runs for 87.31 sec; on the IBM 360/95 it runs for 13.56 sec.

The resulting speeds of computation of the benchmark are in the ratio of 1:2.6:17 for the three machines.

APPENDIX C: DESCRIPTION AND LISTING OF COMPUTER PROGRAM

The computer program, written in FORTRAN, consists of a short main program and 14 subprograms. The main program (SETUP) controls the amount of allocated memory space, permitting the program to fit into computers of various core sizes. Furthermore, SETUP calls the subprograms DREAD, which reads the input data, and DPOCO, which obtains the solution. The data is grouped into a single format-free packet and is read under control of the NAMELIST feature of FORTRAN. Since the NAMELIST feature allows the omission of any of the input variables, most of the input variables are preset to default values which may be overridden for the particular problem. In order to transfer the input values to the remaining subprograms, the input variables are located in labelled common blocks of core storage.

The subprogram DPOCO controls the solution of the major iterates. This subprogram invokes the "alternating direction implicit" method and the flow-field method through lower level subprograms until a convergent solution is obtained. DPOCO also directs both the printing of the solution matrices through DWRITE and the plotting of the important variables through CONTOU.

In order to solve the finite-differenced Poisson equation, the matrix which operates on the potential values is inverted by a series of alternate horizontal and vertical sweeps over the grid points. Subprograms ADIH and ADIV control the horizontal and vertical sweeps, respectively. Both subprograms use the tridiagonal solver in subprogram TRILIN.

After the minor iterates have converged satisfactorily, DPOCO calls upon subroutine RHO which obtains the electric field, solves for the ion trajectories, and then obtains the ion-density record. As an ion trajectory passes through each cell, RHO calls upon ORBIT to calculate the exit parameters. ORBIT uses the lower-level subprogram TIME to obtain the time of flight from a point to a line. The two subprograms ROTATE and ILOC are service routines for ORBIT and RHO, respectively.

When the ion density has been determined, DPOCO returns to the matrix inversion routines and recomputes a new set of potential values. In this manner, DPOCO controls the cycling of the major iterates until satisfactory convergence is obtained.

Using the two subprograms ERRC and ERROR, a high degree of error control is maintained throughout the program. At the point where an error is about to occur, the program notes the type of error and attempts to take corrective action. In those few cases where the error is uncorrectable, an appropriate change in the initial data is generally sufficient to eliminate it.

Following the listing of the program is the sample data packet and the printed output for the model problem. The less frequently varied data are not specified in the packet and, as a result, their values are given by default options in the subprogram DREAD. The more frequently varied data are explicitly stated (overriding the default options) and are defined as follows:

&INPUT	Indicates beginning of data packet.
IMAX	Number of grid points in x direction.
ISAT	Horizontal grid point at which satellite body is located.
G	Matrix of horizontal mesh sizes (from left to right).
XLEFT	The leftmost x coordinate.
JMAX	Number of grid points in y direction.
JSAT	Vertical grid point at which top edge of satellite body is located.
H	Matrix of vertical mesh sizes (from bottom to top and starting at y coordinate = -H(1)/2.).
DTR	Matrix of trajectory spacing from top to bottom.
TR	Matrix of y coordinates at which trajectory spacing changes value according to DTR (e.g., ΔTR=.54 from top to y=4.81; ΔTR=.24 from y=4.81 to y=2.81; etc.).
NPMAJ	The potential and ion density matrices are printed every major iterate whose number is a multiple of NPMAJ.
NWSKIP	The potential and ion density matrix elements, when printed, are printed such that if a row or column is not a multiple of NWSKIP, that row or column is not printed.
MPASS	Maximum number of major iterates.
OMEGA	Overrelaxation factor ω for minor iterates.
ROTINV	If "T," geometry is axially symmetric; if "F," geometry is planar.
ERRADI	Matrix of maximum error bounds for each minor iterate.
MITER	Maximum number of minor iterates.
ERMPAR	Maximum error of ion density matrix (unless MPASS would be exceeded in order to obtain this accuracy).
ERMPAU	Maximum error of potential matrix (unless MPASS would be exceeded in order to obtain this accuracy).
RHISTA	Initial value of ion density for grid points which lie in triangular region behind satellite (see RHIX).

MINITE Minimum number of minor iterates.

ALPHAR Matrix of the ion-density underrelaxation factors for each major iterate.

ALPHAU Matrix of the potential underrelaxation factors for each major iterate.

RHIMAX Matrix of the maximum ion-density value for each major iterate.

UMAX Maximum potential value for all major iterates.

VXST Satellite velocity u_s.

POTSAT Satellite potential φ_{sat}.

RHIX Value of x coordinate of apex of triangle in which ion-density values are specified initially by RHISTA.

BETA Ion mass ratio β.

XP1 Leftmost x coordinate of potential plot.

XP2 Rightmost x coordinate of potential plot.

XPDEL Spacing of x coordinate per unit of print spacing.

YP1, YP2, and YPDEL Corresponds to XP1, XP2, and XPDEL for y coordinate.

NUG Number of possible potential contour lines whose values are specified by UG.

UG Values of the potential contour lines.

PLOTU If "T," potential is plotted for the respective major iterate (e.g., PLOTU(6)=T indicates that a contour plot of potential is produced only on iterate No.6).

NRG Number of possible ion-density contour lines whose values are specified by RG.

RG Values of the ion-density contour lines.

PLOTR Corresponds to PLOTU for ion-density plot.

XT1, XT2, XTDEL Corresponds to XP1, XP2, XPDEL for trajectory plot.

YT1, YT2, YTDEL Corresponds to YP1, YP2, YPDEL for trajectory plot.

PLOTTR Corresponds to PLOTU for trajectory plot.

DYTRPL Value of spacing between plotted trajectories.

NGTRPL Number of ion-trajectory groups to be plotted (usually equals one).

&END Indicates end of data packet.

```
      SUBROUTINE ADIH(*)
      IMPLICIT REAL*8 (A-H, O-Z), INTEGER*4 (I-N)
      INTEGER TRAN 1
      REAL*8 K
      DIMENSION W(1), Z(1)
      EQUIVALENCE (C(1), W(1)), (K(1), Z(1))
      COMMON /CAP/ X(500), Y(200), G(500), H(200), BETA, POTSAT,
     1 IMAX,JMAX, IMAX1, JMAX1, ISAT, JSAT,IIN, IO, IPU, ROTINV
      LOGICAL*1 ROTINV
      COMMON /CTRI/ A(500), B(500), C(500), K(500), NMIN, NMAX
      COMMON /CADI/ C2(500), C3(200),C4(500), C5(200), UMIN, UMAX,
     1 CMEGA, ERRTRI, NMEXP
      GO TO 1
      ENTRY     CADIH(U, RHOI, C1, LX, LY)
      DIMENSION U(LX, LY), RHOI(LX, LY), C1(LX, LY)
      RETURN
1     NMIN = 2
      NMAX = IMAX1
      NEXP= 0
      ERRTRI= 0.
      DO 32 J = 2, JMAX1
      DO 28 I = 2, IMAX1
      RHOE= 0.
      IF(U(I,J) .LE. UMAX) GO TO 22
      U(I, J)= UMAX
      CALL ERRC(NEXP, NMEXP, 622, 6201, 8HADI   22)
22    IF (U(I, J) .GE. UMIN) RHOE=DEXP(U(I, J))
      K(I) = C5(J)*U(I,J-1) + C3(J)*U(I,J+1) - RHOE              +RHOI(I,J
     1)
      A(I) = -C2(I)
      B(I) = C1(I,J)
28    C(I) = -C4(I)
      IF(J.NE.2) GO TO 31
      DO 29 I = 2, IMAX1
      K(I) = -C5(2)*U(I,J-1) +K(I)
29    B(I) = B(I) -C5(2)
31    IF(J.GT. JSAT) GO TO 30
      A(ISAT) =0.
      A(ISAT+1) = 0.
      C(ISAT-1) = 0.
      C(ISAT) =0.
      K(ISAT) = B(ISAT) *U(ISAT, J)
      K(ISAT-1) = K(ISAT-1) + C4(ISAT-1)*U(ISAT,J)
      K(ISAT+1) = K(ISAT+1) + C2(ISAT+1) * U(ISAT,J)
30    CALL TRILIN
      DO 32 I = 2, IMAX1
      TEM = CMEGA * (Z(I)-U(I,J))
      ERRTRI = CMAX1(ERRTRI,DABS(TEM))
32    U(I,J) = TEM+U(I,J)
      RETURN
201   RETURN 1
      END
```



```
      SUBROUTINE ADIV(*)
      IMPLICIT REAL*8 (A-H, O-Z), INTEGER*4 (I-N)
      INTEGER TRAN 1
      REAL*8 K
      DIMENSION W(1), Z(1)
      EQUIVALENCE (C(1), W(1)), (K(1), Z(1))
      COMMON /CAP/ X(500), Y(200), G(500), H(200), BETA, POTSAT,
     1 IMAX,JMAX, IMAX1, JMAX1, ISAT, JSAT,IIN, IO, IPU, ROTINV
      LOGICAL*1 ROTINV
      COMMON /CTRI/ A(500), B(500), C(500), K(500), NMIN, NMAX
      COMMON /CADI/ C2(500), C3(200),C4(500), C5(200), UMIN, UMAX,
     1 CMEGA, ERRTRI, NMEXP
      GO TO 1
      ENTRY     CADIV(U, RHOI, C1, LX, LY)
      DIMENSION U(LX, LY), RHOI(LX, LY), C1(LX, LY)
      RETURN
1     NMIN = 2
      NMAX = JMAX1
      ERRTRI= 0.
      TRAN1 = 1
      DO 48 I=2, IMAX1
      IF (I .EQ. ISAT) TRAN1 = 2
      GO TO (37, 39), TRAN1
39    NMIN = JSAT+1
37    DO 38 J = NMIN, JMAX1
      RHOE= 0.
      IF(U(I,J) .LE. UMAX) GO TO 36
      U(I, J)= UMAX
      CALL ERRC(NEXP,NMEXP, 636,6201, 8HADI   36)
36    IF (U(I, J) .GE. UMIN) RHOE=DEXP(U(I, J))
      K(J)=C2(I)*U(I-1,J)+C4(I)*U(I+1,J)-RHOE              +RHOI(I,J)
      A(J)= -C5(J)
      B(J)= C1(I, J)
38    C(J)= -C3(J)
      B(2)= B(2) -C5(2)
      GO TO (40, 42), TRAN 1
42    K(JSAT +1)= K(JSAT +1) +C5(JSAT +1) *U(ISAT, JSAT)
40    CALL TRILIN
      DO 44 J= NMIN, JMAX1
      TEM= OMEGA *(Z(J) -U(I, J))
      ERRTRI= CMAX1 (ERRTRI,DABS(TEM))
44    U(I, J)= TEM +U(I, J)
      GO TO (48, 46), TRAN 1
46    TRAN 1= 1
      NMIN= 2
48    CONTINUE
      RETURN
201   RETURN 1
      END
```



```
      SUBROUTINE CONTOU (A, UG, NUG, M, WORDS, *)
      IMPLICIT REAL*8 (A-H, O-Z), INTEGER*4 (I-N)
      DIMENSION XPM(40), WORDS(1), IKEY(1), CHARAC(5), UG(1)
      EQUIVALENCE                    (IKEY(1), XPM(1) )
      LOGICAL*1 CHARAC        /1H1, 1H3, 1H5, 1H7, 1H9/,
     1 BLANK /1H /,ASTER /1H*/, XES /1HX/, AMINUS /1H-/, PLUS /1H+/,
     2 AIES /1HI/, CHAR, WORDS
      DIMENSION             A(LX, LY)
      COMMON /CCONT/          XP1, XP2, XPDEL, YP1, YP2, YPDEL
      COMMON /CPLTRA/ XT1, XT2, XTDEL, YT1, YT2, YTDEL, YMA1(500), I11
      COMMON /CAP/ X(500), Y(200), G(500), H(200), BETA, POTSAT,
     1 IMAX,JMAX, IMAX1, JMAX1, ISAT, JSAT,IIN, IO, IPU, ROTINV
      LOGICAL*1 ROTINV
      PO1(X, XO, X1, YO, Y1) = (YO *(X1 -X) -Y1 *(XO-X))/(X1 -XO)
      GO TO 1
      ENTRY      CCONT (    A, LX, LY, BL, LBX, LBY)
      LOGICAL*1 BL(LBX, LBY)
      RETURN
1     IF (NUG .EQ. 0) CALL ERRCR(6201, 8HCONTOU 6)
      DO 6 I1= 1,120
      DO 6 J1= 1, 57
6     BL(I1, J1)= BLANK
      NUMLX=IDINT((XP2-XP1) /XPDEL+1.00001)
      IF (NUMLX .GT. 120) NUMLX= 120
      NUMLY=IDINT((YP2 -YP1) /YPDEL +1.00001)
      IF (NUMLY .GT. 57) NUMLY= 57
      NUMLX1= NUMLX -1
      NUMLY1= NUMLY -1
      XP2= XP1+DFLOAT(NUMLX1) *XPDEL
      YP2= YP1+DFLOAT(NUMLY1) *YPDEL
      YP= YP1
      DO 30 J1= 2, NUMLY1
      XP= XP1
      YP= YP +YPDEL
      IF (YP .LT. Y(1) .OR. YP .GT. Y(JMAX)) GO TO 30
      J= JLOC(YP)
      DO 30 I1= 2, NUMLX1
      XP= XP +XPDEL
      IF (XP .LT. X(1) .OR. XP .GT. X(IMAX)) GO TO 30
      I= ILOC(XP)
      IF (XP .LT. X(2)) I= 1
      UP1= PO1(XP, X(I), X(I+1) , A(I,J), A(I+1, J))
      UP2= PO1(XP, X(I), X(I+1), A(I, J+1), A(I+1, J+1))
      UP= PO1(YP, Y(J), Y(J+1) , UP1, UP2)
      DO 10 K= 2, NUG
      IF (UP .LE. UG(K-1) .AND. UP .GT. UG(K)) GO TO 14
      IF (UP .GE. UG(K-1) .AND. UP .LT. UG(K)) GO TO 14
10    CONTINUE
      CHAR= XES
      GO TO 12
14    K= MOD(K-2, 10)
      IF (MOD(K, 2) .EQ. 0) GO TO 30
      K= K/2 +1
      CHAR= CHARAC(K)
      GO TO 12
12    BL(I1, J1)= CHAR
```



```
30    CONTINUE
      IF (X(ISAT) .LT. XP1 .OR. X(ISAT) .GT. XP2 .OR. Y(JSAT) .LT. YP1)
     1 GO TO 22
      I1=IDINT((X(ISAT)-XP1) /XPDEL +1.5)
      J0= 1
      IF(-Y(JSAT) .GT. YP1) J0= IDINT((-Y(JSAT) -YP1) /YPDEL +1.5)
      J1= NUMLY
      IF (Y(JSAT) .LT. YP2) J1= IDINT(( Y(JSAT) -YP1) /YPDEL +1.5)
26    DO 16 J2=J0, J1
16    BL(I1, J2)= AIES
22    DO 18 I1= 1, NUMLX
      CHAR= AMINUS
      IF (MOD(I1 -1, 10) .NE. 0) GO TO 17
      CHAR= PLUS
      K1=(I1-1) /10 +1
      XPM(K1)= XP1+DFLOAT(I1-1) *XPDEL
17    BL(I1, NUMLY1)= CHAR
18    BL(I1, 1)= CHAR
      DO 20 J1= 2, NUMLY1
      BL(1, J1)= AMINUS
20    BL(NUMLX, J1)= AMINUS
      WRITE (IO,100) (WORDS(I), I= 1,M)
      WRITE (IO, 106)
      DO 24 J1= 1, NUMLY
      J2= NUMLY -J1 +1
      IF (MOD(J2-1, 10) .EQ. 0) GO TO 23
      WRITE (IO,101) (BL(I, J2), I= 1,120)
      GO TO 24
23    YP= YP1+DFLOAT(J2-1) *YPDEL
      WRITE (IO,102) YP, (BL(I, J2), I= 1,120)
24    CONTINUE
      WRITE (IO,103) (XPM(K), K= 1, K1)
      DO 32 I= 1, NUG
32    IKEY(I)= I-1
      WRITE (IO,104) (IKEY(I), UG(I), I= 1, NUG)
      RETURN
201   RETURN 1
      ENTRY PLTRA1
      DO 50 I1= 1,120
      DO 50 J1= 1, 57
50    BL(I1, J1)= BLANK
      NUMLX=IDINT((XT2 -XT1) /XTDEL +1.00001)
      IF (NUMLX .GT. 120) NUMLX= 120
      NUMLY=IDINT(( YT2 -YT1) /YTDEL +1.00001)
      IF(NUMLY .GT. 57) NUMLY= 57
      NUMLX1= NUMLX -1
      NUMLY1= NUMLY -1
      XT2= XT1+DFLOAT(NUMLX1) *XTDEL
      YT2= YT1+DFLOAT(NUMLY1) *YTDEL
      RETURN
      ENTRY PLTRA2
      DO 52 I= I11, IMAX
      IF (X(I) .LT. XT1 .OR. X(I) .GT. XT2 .OR. YMA1(I) .LT. YT1 .OR.
     1 YMA1(I) .GT. YT2) GO TO 52
      I1=IDINT((X(I) -XT1) /XTDEL +1.5)
      J1=IDINT((YMA1(I) -YT1) /YTDEL +1.5)
      BL(I1, J1)=ASTER
```

```
52    CONTINUE
      RETURN
      ENTRY PLTRA3
      IF (X(ISAT) .LT. XT1 .OR. X(ISAT) .GT. XT2 .OR. Y(JSAT) .LT. YT1)
     1 GO TO 42
      I1=IDINT((X(ISAT)-XT1) /XTDEL +1.5)
      J0= 1
      IF(-Y(JSAT) .GT. YT1) J0= IDINT((-Y(JSAT) -YT1) /YTDEL +1.5)
      J1= NUMLY
      IF (Y(JSAT) .LT. YT2) J1= IDINT(( Y(JSAT) -YT1) /YTDEL +1.5)
46    DO 36 J2=J0, J1
36    BL(I1, J2)= AIES
42    DO 38 I1= 1, NUMLX
      CHAR= AMINUS
      IF (MOD(I1 -1, 10) .NE. 0) GO TO 37
      CHAR= PLUS
      K1=(I1-1) /10 +1
      XPM(K1)= XT1+DFLOAT(I1-1) *XTDEL
37    BL(I1, NUMLY)= CHAR
38    BL(I1, 1)= CHAR
      DO 40 J1= 2, NUMLY1
      BL(1, J1)= AMINUS
40    BL(NUMLX, J1)= AMINUS
      WRITE (IO,105)
      DO 44 J1= 1, NUMLY
      J2= NUMLY -J1 +1
      IF (MOD(J2-1, 10) .EQ. 0) GO TO 43
      WRITE (IO,101) (BL(I, J2), I= 1,120)
      GO TO 44
43    YP= YT1+DFLOAT(J2-1) *YTDEL
      WRITE (IO,102) YP, (BL(I, J2), I= 1,120)
44    CONTINUE
      WRITE (IO,103) (XPM(K), K= 1, K1)
      RETURN
100   FORMAT (1H1 49X 16HCONTOUR PLOT OF   48A1 //)
101   FORMAT (7X120A1)
102   FORMAT (1X F5.1, 1X120A1)
103   FORMAT (12( 4X F5.1, 1X))
104   FORMAT (1HO 49X 11HKEY TO PLOT / 10(1X I4, 1H= F6.2))
105   FORMAT (1H1 49X 15HTRAJECTORY PLOT   //)
106   FORMAT (1HO /)
      END
```



```
      SUBROUTINE DPOCC (U, RHOI, TE, C1, LX, LY)
      IMPLICIT REAL*8 (A-H, O-Z), INTEGER*4 (I-N)
      DIMENSION U(LX, LY), RHOI(LX, LY), TE(LX, LY), C1(LX, LY)
      LOGICAL*1 WRMAJ
      COMMON /DPOCC/ ERRADI(20), RHIMAX(20),ALPHAU(20), ALPHAR(20),
     1 FACITE, ERMPAR, ERMPAU, UG(40), RG(40), RTG(40),
     2 NUG, NRG, NRTG, MPASS,MITER, MINITE, NPITER,
     2 NPMAJ,    WRITEF(20), PUNCH(20), TRACC(20), PLOTU(20), PLOTR(20),
     3 PLOTTR(20), TESADI, WRCHDE, PLOTRT(20)
      LOGICAL*1 WRITEF, PUNCH, TRACC, PLOTU, PLOTR, PLOTTR, TESADI,
     1 WRCHDE, PLOTRT
      COMMON /CAP/ X(500), Y(200), G(500), H(200), BETA, POTSAT,
     1 IMAX,JMAX, IMAX1, JMAX1, ISAT, JSAT,IIN, IO, IPU, ROTINV
      LOGICAL*1 ROTINV
      COMMON /CRHO/ DTR(10), TR(10), VXITEM(20), CURR, UNCURR, WC,
     1 VZNM, DYTRPL, DRAG(2), UNDRAG(2),
     2                    NCROSS, NTRAJ, NPTRAJ, NTSKIP, NGRP,
     2 NGTRPL,          WRFLOW, ACCTRA, TRPLCT
      LOGICAL*1 WRFLOW, ACCTRA, TRPLCT
      COMMON /CADI/ C2(500), C3(200),C4(500), C5(200), UMIN, UMAX,
     1 OMEGA, ERRTRI, NMEXP
      COMMON /CWRI/ NPASS, NWSKIP, ITIME
      RETURN
      ENTRY PDCO
      DO 80 NPASS= 1, MPASS
      ERMTRI=  ERRADI(NPASS)
      WRFLOW= WRITEF(NPASS)
      ACCTRA= TRACC(NPASS)
      TRPLCT= PLOTTR(NPASS)
      WRMAJ= .FALSE.
      IF(MOD(NPASS-1, NPMAJ) .EQ. NPMAJ-1) WRMAJ= .TRUE.
      DO 26 I= 2, IMAX1
      DO 26 J= 2, JMAX1
26    C1(I, J)= 2. /H(J) / H(J -1) +2. /G(I) /G(I -1)
      ASSIGN 28 TO LRET
      DO 55 ITER= 1, MITER
      GO TO LRET, (29, 30)
28    CALL ADIH(&1)
      ASSIGN 30 TO LRET
      GO TO 50
30    CALL ADIV(&1)
      ASSIGN 29 TO LRET
      GO TO 50
50    IF (ERRTRI .LE. ERMTRI .AND. ITER .GT. MINITE) GO TO 58
      IF ( MOD(ITER -1, NPITER) .NE. NPITER -1) GO TO 55
      WRITE (IO,103) ERRTRI, ERMTRI, OMEGA, ITER
      CALL WRITEM (U,35, 35HPOTENTIAL MATRIX PARTIALLY COMPUTED )
55    CONTINUE
      IF (ERRTRI .GT. FACITE *ERMTRI) CALL ERROR(&1, 8HPDCO  55)
      WRITE (IO, 114)
58    ERRPAU= 0.
      DO 60 I= 2, IMAX1
      DO 60 J= 2, JMAX1
      TEM= ALPHAL(NPASS) *(U(I, J) -TE(I, J))
      ERRPAU= DMAX1 (ERRPAU,DABS(TEM))
      U(I, J)= TEM +TE(I, J)
```



```
60    TE(I, J)= RHOI(I, J)
      WRITE  (IC,100) ERRTRI, ERMTRI, OMEGA, ITER
      WRITE (IO,107) ERRPAU, ERMPAU, ALPHAU(NPASS)
      DO 61 I= 2, IMAX1
61    U(I, 1)= U(I, 2)
      IF ( PLOTU(NPASS)) CALL CONTOU (U, UG, NUG, 9, 9HPOTENTIAL, &64)
64    IF( .NOT. WRMAJ) GO TO 63
      CALL WRITEM (U,16, 16HPOTENTIAL MATRIX )
63    IF(TESADI) GO TO 1
      IF (.NOT. WRCHDE .AND. .NOT. PLOTRT(NPASS)) GO TO 62
      DO 53 I= 2, IMAX1
      DO 53 J= 2, JMAX1
53    RHOI(I, J)= RHOI(I, J)-DEXP(U(I, J))
      IF (WRCHDE) CALL WRITEM (RHOI, 21,21HCHARGE DENSITY MATRIX )
      IF (PLOTRT(NPASS)) CALL CONTOU (RHOI, RTG, NRTG, 14,
     1 14HCHARGE DENSITY, &62)
62    IF (ERRPAU .LT. ERMPAU) GO TO 1
      CALL RHO (&1)
      ERRPAR= 0.
      DO 65 I= 2, IMAX1
      DO 65 J= 2, JMAX1
      TEM= ALPHAR(NPASS) *(DMIN1(RHIMAX(NPASS), RHOI(I, J)) -TE(I, J))
      ERRPAR= DMAX1 (ERRPAR,DABS(TEM))
      RHOI(I, J)= TEM +TE(I, J)
65    TE(I, J) = U(I, J)
      IF (PUNCH(NPASS)) WRITE(IPU,110) IMAX, JMAX, ISAT, JSAT, MXYMAT,
     1 X(1),  BETA, VXST, ROTINV, (G(I), I= 1, IMAX), (H(J), J= 1,JMAX),
     2 ((U(I, J), I= 1, IMAX), J= 1, JMAX), ((RHOI(I, J),  I= 1, IMAX),
     3 J= 1, JMAX)
      WRITE(IC,101)UNCURR,NTRAJ, NCROSS, VZNM, CURR, ERRPAR,
     1 ALPHAR(NPASS), ERMPAR, DRAG, UNDRAG(1)
      IF ( PLOTR(NPASS)) CALL CONTOU (RHOI, RG, NRG, 11, 11HION DENSITY,
     1 &67)
67    IF( .NOT. WRMAJ) GO TO 66
      CALL WRITEM (RHOI,18, 18HION DENSITY MATRIX)
66    IF (ERRPAR .LT. ERMPAR) GO TO 1
80    CONTINUE
      WRITE (IO,113) MPASS
1     RETURN
100   FORMAT (// 5X 10HPDE ERROR= 1PE11.4, 5X 18HMAXIMUM PDE ERROR=
     1 E8.1, 5X 25HPDE RELAXATION PARAMETER=  0PF6.3, 5X 21HNUMBER OF IT
     2ERATIONS= I3)
101   FORMAT(/5X8HCURRENT= F 9.5,  9X I4, 13H TRAJECTORIES  8X I4,
     1 10H CROSSINGS10X 19HMAXIMUM Z-VELOCITY= 1PE11.4/ 5X
     2 14HNORM. CURRENT= 0PF9.5,                5X 10HRHO-ERROR= 1PE11.4,
     3 5X 10HRHO-ALPHA= 0PF5.2,   6X 18HMAXIMUM RHO-ERROR= 1PE8.1/
     4 5X 14HNORM. DRAG(R)=  0PF9.5,   5X 14HNORM. DRAG(A)= 0PF9.5,
     5 3X 5HDRAG= 1PE11.4)
107   FORMAT                    ( 5X 8HU-ERROR= 1PE11.4, 7X 16HMAXIMUM
     1U-ERROR= E8.1, 7X 8HU-ALPHA= 0PF5.2)
110   FORMAT ( 5I3, 1P3E11.4, L2 / (20(1PF8.4))
113   FORMAT ( //  1X I3,26H MAJOR ITERATES COMPLETED.  // )
114   FORMAT (// 1HO 4X 31HMINOR ITERATION LIMIT EXCEEDED.   //)
      END
```



```
      SUBROUTINE DREAD (U, RHOI, TE, C1, LX, LY)
      IMPLICIT REAL*8 (A-H, O-Z), INTEGER*4 (I-N)
      DIMENSION U(LX, LY), RHOI(LX, LY), TE(LX, LY), C1(LX, LY)
      LOGICAL*1 CARDS, ZERO, PRCOE
      DIMENSION VGROUP(20), LDATE(2)
      EQUIVALENCE (X(1), XLEFT)
      COMMON /CAP/ X(500), Y(200), G(500), H(200), BETA, POTSAT,
     1 IMAX,JMAX, IMAX1, JMAX1, ISAT, JSAT,IIN, IO, IPU, ROTINV
      LOGICAL*1 ROTINV
      COMMON /DPOCC/ ERRADI(20), RHIMAX(20),ALPHAU(20), ALPHAR(20),
     1 FACITE, ERMPAR, ERMPAU, UG(40), RG(40), RTG(40),
     2 NUG, NRG, NRTG, MPASS,MITER, MINITE, NPITER,
     2 NPMAJ,    WRITEF(20), PUNCH(20), TRACC(20), PLOTU(20), PLOTR(20),
     3 PLOTTR(20), TESADI, WRCHDE, PLOTRT(20)
      LOGICAL*1 WRITEF, PUNCH, TRACC, PLOTU, PLOTR, PLOTTR, TESADI,
     1 WRCHDE, PLOTRT
      COMMON /CILCC/ XVMAT, YVMAT, IMAT(500), JMAT(500)
      COMMON /CRHO/ DTR(10), TR(10), VXITEM(20), CURR, UNCURR, WC,
     1 VZNM, DYTRPL, DRAG(2), UNDRAG(2),
     2                    NCROSS, NTRAJ, NPTRAJ, NTSKIP, NGRP,
     2 NGTRPL,          WRFLOW, ACCTRA, TRPLCT
      LOGICAL*1 WRFLOW, ACCTRA, TRPLCT
      COMMON /CADI/ C2(500), C3(200),C4(500), C5(200), UMIN, UMAX,
     1 OMEGA, ERRTRI, NMEXP
      COMMON /CWRI/ NPASS, NWSKIP, ITIME
      COMMON /CCONT/        XP1, XP2, XPDEL, YP1, YP2, YPDEL
      COMMON /CPLTRA/ XT1, XT2, XTDEL, YT1, YT2, YTDEL, YMA1(500), I11
      NAMELIST /INPUT/ G, H, IMAX, JMAX,  ISAT, JSAT, TESADI, MXYMAT,
     1 ALPHAU,ROTINV, ERRADI, NWSKIP, RHIMAX, NMEXP, BETA, POTSAT, VXST,
     2 RHISTA, MPASS, TRACC, DTR, TR, ZERO,  MITER, NPITER, NTSKIP,
     3 UMIN, OMEGA, ERMPAU, WRCHDE, XLEFT, WRITEF, ALPHAR, RHIX,
     4 ERMPAR, PUNCH, CARDS, NPMAJ, NPTRAJ, TRATIO, NGRP, VGROUP,
     5UG, NUG, XP1, XP2, XPDEL, YP1, YP2, YPDEL, PLOTU, PLOTR, BFIELD,
     6 PLOTTR, NGTRPL, DYTRPL, XT1, XT2, XTDEL, YT1, YT2, YTDEL, UMAX,
     7 MINITE, FACITE, PRCOE, RG, NRG, RTG, NRTG, PLOTRT
      NAMELIST/OUTPUT/              CARDS, ZERO, TESADI, ROTINV, WRCHDE,
     1 MITER, NPITER, MINITE, FACITE, OMEGA, MPASS,
     2               ERMPAR, ERMPAU, NMEXP, UMIN, UMAX, NWSKIP, NTSKIP,
     3 BFIELD, WC, RHIX, RHISTA,    NPMAJ, NPTRAJ, TRATIO, NGRP, MXYMAT
      NAMELIST /OUTPLO/ NUG, XP1, XP2, XPDEL, YP1, YP2, YPDEL, NRG,NRTG
      NAMELIST /OUTPTR/ NGTRPL, DYTRPL, XT1, XT2, XTDEL, YT1, YT2, YTDEL
      RETURN
      ENTRY READ
      REAL*4 ITIME
      CALL CLOCK (D)
      ITIME= 0.
      IIN= 5
      IO=6
      IPU= 7
1     MXYMAT=399
      NPASS= 0
      TESADI= .FALSE.
      ZERO= .TRUE.
      NTSKIP= 1
      NWSKIP= 1
      RHISTA= 0.
```

```
      NMEXP= 10
      TRATIO= 1.
      NGRP= 1
      NGTRPL= 0
      VXST= .036323
      BETA= +29376.
      BFIELD= 0.
      NPTRAJ= 1
      POTSAT= 0.
      MPASS= 1
      NUG= 0
      NRG= 0
      NRTG=0
      DO 3 I= 1, 20
      VGROUP(I)= 0.
      ALPHAU(I)= 1.
      ALPHAR(I)= 1.
      RHIMAX(I)= 2.
      ERRADI(I)= .0001
      PUNCH(I)= .FALSE.
      PLOTU(I)= .FALSE.
      PLOTR(I)= .FALSE.
      PLOTRT(I)= .FALSE.
      TRACC(I)= .FALSE.
      PLOTTR(I)= .FALSE.
    3 WRITEF(I)= .FALSE.
      WRCHOE= .FALSE.
      CARDS= .FALSE.
      PRCOE= .FALSE.
      NPMAJ= 1
      MITER= 75
      NPITER=75
      MINITE= 10
      FACITE= 10.
      UMIN= -10.
      UMAX= 3.
      READ(IIN,INPUT, ERR= 1, END= 202)
      IF (IMAX .LE. 0 .OR. JMAX.LE. 0) GO TO 202
      IF (CARDS) READ(IIN, 110, ERR= 1, END= 202)
     1                                IMAX, JMAX, ISAT, JSAT, MXYMAT,
     1 XLEFT, BETA, VXST, ROTINV, (G(I), I= 1, IMAX), (H(J), J= 1,JMAX),
     2 ((U(I, J), I= 1, IMAX), J= 1, JMAX), ((RHOI(I, J),  I= 1, IMAX),
     3 J= 1, JMAX)
      IF (IMAX.GT. LX .OR. JMAX .GT. LY) CALL ERROR(61, 8HREAD   4)
      IMAX1= IMAX -1
      JMAX1= JMAX -1
      Y(1)= -H(1)/2.
      DO 4 I= 2, IMAX
    4 X(I)= X(I -1) +G(I-1)
      DO 6 J= 2, JMAX
    6 Y(J)= Y(J -1) +H(J-1)
      DO 8 I= 2, IMAX1
      C2(I)= 2. /G(I -1) /(G(I -1) +G(I))
    8 C4(I)= 2. /G(I) /(G(I -1) +G(I))
      TEM= 0.
      DO 10 J= 2, JMAX1
      IF (ROTINV) TEM= 1. /Y(J)
```



```
      C3(J)= (2. /H(J) +TEM) /(H(J) + H(J -1))
      C5(J)= (2. /H(J-1)-TEM)/(H(J) + H(J -1))
      DO 10 I= 2, IMAX1
   10 C1(I, J)= 2. /H(J) / H(J -1) +2. /G(I) /G(I -1)
      XYMAT=DFLOAT(MXYMAT) /(X(IMAX) -X(1))
      YYMAT=DFLOAT(MXYMAT) /Y(JMAX)
      IMAT(MXYMAT +1)= IMAX
      JMAT(MXYMAT +1)= JMAX
      I1= 1
      J1= 1
      DO 12 I= 1, MXYMAT
      IF (X(I1 +1) .LE.DFLOAT(I) /XYMAT +X(1)) I1= I1 +1
      IMAT(I)= I1
      IF (Y(J1 +1) .LE.DFLOAT(I) /YYMAT) J1= J1 +1
   12 JMAT(I)= J1
      VXI= OSCRT( DABS(TRATIO /BETA))
      DO 13 K= 1, NGRP
   13 VXITEM(K)= VXI *VGROUP(K) +VXST
      WC= BFIELD /BETA
      ENERGY= BETA* VXST *VXST /2.
      IF (CARDS) GO TO 20
      IF (.NOT. ZERO) GO TO 20
      DO 14 I= 1, IMAX
      DO 14 J= 1, JMAX
      U(I, J)= 0.
   14 RHOI(I, J)= 1.
      J1= JSAT -1
      IRHSTA= ILOC(RHIX)
      DO 17 J= 2, J1
      DO 17 I= 2, ISAT
   17 RHOI(I, J)= RHISTA
      DO 18 I= IRHSTA, ISAT
      JRH= JLOC((X(I) -RHIX) *Y(JSAT) / (X(ISAT) -RHIX) -.001)
      DO 18 J= 2, JRH
   18 RHOI(I, J)= 0.
   20 DO 16 J= 1, JSAT
   16 U(ISAT, J)= POTSAT
      DO 19 I= 2, IMAX1
      DO 19 J= 2, JMAX1
   19 TE(I, J)= U(I, J)
      CALL DATE (LDATE(1))
      WRITE (IO, 108) LDATE,
     1              (I, WRITEF(I), ERRADI(I), ALPHAU(I), ALPHAR(I),
     1 RHIMAX(I), PUNCH(I), PLOTU(I), PLOTR(I), PLOTTR(I), TRACC(I),
     2 I= 1, MPASS)
      WRITE (IO,112) IMAX, JMAX, ISAT, JSAT, X(1), X(IMAX), Y(JMAX),
     1 X(ISAT),Y(JSAT), VXST, BETA, ENERGY, POTSAT
      WRITE (IO,102) (I, X(I), I= 1, IMAX)
      WRITE (IO,103) (J, Y(J), J= 1, JMAX)
      DO 21 J= 1, 10
      DTR(J)= DTR(J) *.9991147?
      IF (TR(J) .LE. 0.) GO TO 22
   21 CONTINUE
   22 WRITE (IO,109) (I, DTR(I), TR(I), I= 1, J )
      WRITE (IO,111) (K, VGROUP(K), VXITEM(K), K= 1, NGRP)
      WRITE (IO,OUTPUT)
      IF (NUG .NE. 0 .OR. NRG .NE. 0 .OR. NRTG .NE. 0) WRITE (IO,OUTPLO)
```



```
      IF (NGTRPL .NE. 0) WRITE (IO,OUTPTR)
      IF (.NOT. PRCOE) GO TO 11
      J= MXYMAT +1
      WRITE(IO,104) (I, IMAT(I), JMAT(I), I= 1, J)
      WRITE (IO,105) (X(I), C2(I), C4(I), I= 2, IMAX1)
      WRITE (IO,106) (Y(J), C3(J), C5(J), J= 2, JMAX1)
      CALL WRITEM (C1,20, 20HDIAGONAL COEFFICIENT )
   11 RETURN
  202 CALL EXIT
  102 FORMAT (// 50X 8HX MATRIX / 13( 1X I3, F6.1))
  103 FORMAT (// 50X 8HY MATRIX / 13( 1X I3, F6.2))
  104 FORMAT (// 50X 22HTABLE LOOK-UP MATRICES / 13( I3, 2I3, 1H/))
  105 FORMAT (// 50X 23HHORIZONTAL COEFFICIENTS / 5( 0PF6.1, 1P2E10.2))
  106 FORMAT (// 50X 21HVERTICAL COEFFICIENTS  / 5(0PF6.2, 1P2E10.2 ))
  108 FORMAT (1H1 49X 7HPOCO 11 50X 2A4 ///
     1            7X 4HPASS 6X 5HWRITE 6X 3HADI 9X 2HU~ 7X 4HRHO~ 5X
     2 7HMAXIMUM 5X 5HPUNCH 4X 6HPLCT U 3X 8HPLOT RHO 5X 4HPLOT 6X
     3 8HIMPROVED /          6X 6HNUMBER 5X 4HFLOW 6X 5HERROR 6X
     45HALPHA 5X 5HALPHA 7X 3HRHO 7X 6HOPTION 3X 6HOPTION 4X 6HOPTION 2X
     5 12HTRAJECTORIES 3X
     6 6HORBITS          //(5X I5, 5X L5, 5X 1PE8.1, 5X 0PF5.2, 5X F5.2,
     7 5X 1PE8.1,2X L5, 3(5X L5), 7X L5))
  109 FORMAT (// 50X 18HTRAJECTORY SPACING /  8(I3, F6.3, F7.3))
  110 FORMAT ( 5I3, 1P3E11.4, L2 / (0P10F8.4))
  111 FORMAT (// 50X 19HION VELOCITY GROUPS // 38X 6HNUMBER 4X
     1 16HTHERMAL VELOCITY 4X 14HTOTAL VELOCITY / (40X I2, 8X F10.5,
     2 9X F10.6))
  112 FORMAT (// 35X 5HIMAX= I4, 3X 5HJMAX= I3, 3X 5HISAT= I4, 3X
     1 5HJSAT= I3// 1X 24HHORIZONTAL COORDINATES (  F5.1, 1H,  F5.1,
     2 1H)  7X 28HVERTICAL COORDINATES (  0.0,   F5.1, 1H)  7X
     3 28HSATELLITE EDGE COORDINATES (  F5.1, 1H,  F5.1, 1H)   /
     4 1X 19HSATELLITE VELOCITY= F8.5, 16X 15HION MASS RATIO= F7.0,
     5 19X 19HION KINETIC ENERGY= F7.3/1X 20HSATELLITE POTENTIAL= F6.1)
      END
```



```
      SUBROUTINE DWRITE (A, LX, LY)
      IMPLICIT REAL*8 (A-H, O-Z), INTEGER*4 (I-N)
      DIMENSION A(LX, LY)
      RETURN
      ENTRY WRITEM (A, NWRD, M)
      LOGICAL*1 M(1)
      COMMON /CWRI/ NPASS, NWSKIP, ITIME
      COMMON /CAP/ X(500), Y(200), G(500), H(200), BETA, POTSAT,
     1 IMAX,JMAX, IMAX1, JMAX1, ISAT, JSAT,IIN, IO, IPU, ROTINV
      LOGICAL*1 ROTINV
      REAL*4 ITIME,JTIME
      CALL CLOCK (1, JTIME)
      TIME= JTIME -ITIME
      ITIME= JTIME
      WRITE (IO,100) NPASS, TIME, (M(I), I= 1, NWRD)
      DO 10 J= 2, JMAX1, NWSKIP
   10 WRITE (IO,101) Y(J), (X(I),A(I,J),I= 2, IMAX1, NWSKIP)
      RETURN
  100 FORMAT (13HOPASS NUMBER= I2,  8X F7.2, 8H SECONDS 12X 60A1)
  101 FORMAT (/10X 2HY= 0PF6.2 / 7( 0PF6.1, 1PE12.4))
      END
```

LISTING OF SUBROUTINE ERRC PAGE 13

```
      SUBROUTINE ERRC (N, NMAX, *, *, ALOC)
      IMPLICIT REAL*8 (A-H, O-Z), INTEGER*4 (I-N)
      COMMON /CAP/ X(500), Y(200), G(500), H(200), BETA, POTSAT,
     1 IMAX,JMAX, IMAX1, JMAX1, ISAT, JSAT,IIN, IO, IPU, ROTINV
      LOGICAL*1 ROTINV
      LOGICAL*1 ALOC(8)
      N= N+1
      IF (N .LT. NMAX) RETURN 1
      WRITE (IO, 101) ALOC
      RETURN 2
101   FORMAT (32HOMAXIMUM ERROR COUNT EXCEEDED AT 1X8A1, 31H.  ALTERNATE
     1 LOGIC ROUTE TAKEN.  //)
      END
```

LISTING OF SUBROUTINE ERRCR PAGE 14

```
      SUBROUTINE ERRCR (*, ALOC)
      IMPLICIT REAL*8 (A-H, O-Z), INTEGER*4 (I-N)
      COMMON /CAP/ X(500), Y(200), G(500), H(200), BETA, POTSAT,
     1 IMAX,JMAX, IMAX1, JMAX1, ISAT, JSAT,IIN, IO, IPU, ROTINV
      LOGICAL*1 ROTINV
      LOGICAL*1 ALOC(8)
      WRITE (IO, 100) ALOC
      RETURN 1
100   FORMAT (18HOPOSSIBLE ERRCR AT 1X8A1, 31H.  ALTERNATE LOGIC ROUTE T
     1AKEN.  //)
      END
```

LISTING OF FUNCTION ILOC PAGE 15

```
      FUNCTION ILOC(XP)
      IMPLICIT REAL*8 (A-H, O-Z), INTEGER*4 (I-N)
      LOGICAL *1 S1 /.TRUE./
      COMMON /CAP/ X(500), Y(200), G(500), H(200), BETA, POTSAT,
     1 IMAX,JMAX, IMAX1, JMAX1, ISAT, JSAT,IIN, IO, IPU, ROTINV
      LOGICAL*1 ROTINV
      COMMON /CILOC/ XVMAT, YVMAT, IMAT(500), JMAT(500)
      IF (XP .LT. X(IMAX1)) GO TO 45
      I= IMAX1
      GO TO 52
45    IF (XP .GE. X(3)) GO TO 46
      I= 2
      GO TO 52
46    I= (XP- X(1)) *XVMAT +1.C00001
      I= IMAT(I)
      GO TO 51
50    I= I-1
51    IF (XP .LT. X(I)) GO TO 50
      IF (XP .LT. X(I+1)) GO TO 52
      I= I +1
      GO TO 51
52    ILOC= I
      RETURN
      ENTRY JLOC(YQ)
      IF (YQ .LT. 0.) S1= .FALSE.
      YP=DABS(YQ)
      IF (YP .LT. Y(JMAX1)) GO TO 48
      I= JMAX1
      GO TO 57
48    I= YP *YVMAT +1.000001
      I= JMAT(I)
      GO TO 56
54    I= I-1
56    IF (YP .LT. Y(I))GO TO 54
      IF (YP .LT. Y(I +1)) GO TO 57
      I= I+1
      GO TO 56
57    IF (S1) GO TO 52
      ILOC= 2-I
      S1= .TRUE.
      JLOC= ILOC
      RETURN
      END
```

LISTING OF SUBROUTINE ORBIT PAGE 16

```
      SUBROUTINE ORBIT(*)
      IMPLICIT REAL*8 (A-H, O-Z), INTEGER*4 (I-N)
      COMMON /COMORB/ XC, YC, VXC, VYC, FX, FY, XC, HX, HY, T, FACE
      INTEGER*4 FACE
      INTEGER*4 ERR
      ERR= 0
      X1= XC- HX*.5
      IF (VYC .LE. 0.) CALL ERROR (680, 8HORBIT 50)
      R= VXC/ VYC
      D= X1- XC
      IF ( R .LT. D/ HY) GO TO 60
      IF (R .GT. (D+ HX)/ HY) GO TO 70
50    CALL TIM(HY, VYC, FY, &75)
      FACE= 2
      YF= HY+ YC
53    ERR= ERR+ 1
      IF(ERR. GE. 2) CALL ERROR (&80, 8HORBIT 53)
      XF= (FX *T *.5          +VXC) *T +XC
      IF (XF. LT. X1) GO TO 60
      IF (XF. GT. X1+HX) GO TO 70
55    VXC= FX *T              +VXC
      VYC= FY *T              +VYC
      XC= XF
      YC= YF
      RETURN
60    CALL TIM  (X1 -XC, VXC, FX, &50)
      FACE= 1
      XF= X1
65    YF=(FY *T *.5           +VYC) *T +YC
      IF (YF. GT. YC+ HY) GO TO 50
      IF (YF. LT. YC) GO TO 75
      GO TO 55
70    CALL TIM(X1+ HX- XC, VXC, FX, &50)
      FACE= 3
      XF= X1+ HX
      GO TO 65
75    T= -2.* VYC/ FY
      FACE= C
      YF= YC
      GO TO 53
80    RETURN 1
      END
```

```
      SUBROUTINE RHO(*)
      IMPLICIT REAL*8 (A-H, O-Z), INTEGER*4 (I-N)
      PO1(X, X0, X1, Y0, Y1) = (Y0 *(X1 -X) -Y1 *(X0-X))/(X1 -X0)
      POD2(X, X0, X1, X2, Y0, Y1, Y2) = Y0* ((2. *X) -X2 -X1) /(X0 -X2)
     1 /(X0 -X1) -Y1 *((2. *X) -X2 -X0) /(X1 -X2) /(X0-X1) + Y2 *((2.
     2 *X) -X1 -X0) /(X1 -X2) /(X0- X2)
      GO TO 1
      ENTRY       CRHO (U, RHOI, DX, DY, LX, LY)
      DIMENSION U(LX, LY), RHOI(LX, LY), DX(LX, LY), DY(LX, LY)
      LOGICAL*1 S1, S2, S3, S4, S5, WRTRAJ, CORR, REDO, TRPL1
      INTEGER EXIT, RTR, IBAC
      DIMENSION YMA2(500), VTEM(500), VEND(2)
      COMMON /CAP/ X(500), Y(200), G(500), H(200), BETA, POTSAT,
     1 IMAX,JMAX, IMAX1, JMAX1, ISAT, JSAT,IIN, IO, IPU, ROTINV
      LOGICAL*1 ROTINV
      COMMON /COMORB/ XN, YN, VXN, VYN, FX, FY, COX, G1, H1, T, EXIT
      COMMON /CRHO/ DTR(10), TR(10), VXITEM(20), CURR, UNCURR, WC,
     1 VZNM, DYTRPL, DRAG(2), UNDRAG(2),
     2                        NCROSS, NTRAJ, NPTRAJ, NTSKIP, NGRP,
     2 NGTRPL,          WRFLOW, ACCTRA, TRPLOT
      LOGICAL*1 WRFLOW, ACCTRA, TRPLOT
      COMMON /CPLTRA/ XT1, XT2, XTDEL, YT1, YT2, YTDEL, YMA1(500), I11
      REAL*8 PI/3.14159/
      RETURN
1     DO 4 I= 1, IMAX
      DO 4 J= 1, JMAX
      RHOI(I, J)= 0.
      DX(I, J)= 0.
4     DY(I, J)= 0.
      DO 10 I= 2, IMAX1
      DO 10 J= 2, JMAX1
      DX(I, J)= POD2(X(I), X(I-1), X(I), X(I+1), U(I-1,J), U(I,J),
     1 U(I+1,J))
10    DY(I, J)= POD2(Y(J), Y(J-1), Y(J), Y(J+1), U(I, J-1), U(I,J),
     1 U(I,J+1))
      I= ISAT
      DO 12 J= 2, JSAT
      DX(I,J)=POD2(X(I), X(I), X(I+1), X(I+2), U(I, J), U(I+1, J),
     1 U(I+2, J))
12    DY(I,J)= 0.
      J= JSAT
      DY(I, J)= POD2(Y(J), Y(J), Y(J+1), Y(J+2), U(I,J), U(I, J+1),
     1 U(I,J+2))
      DO 14 I= 2, IMAX1
      DO 14 J= 2, JMAX1
      DX(I, J)= -DX(I, J) /BETA
14    DY(I, J)= -DY(I, J) /BETA
      DO 6 I= 2, IMAX1
      DX(I, 1)= DX(I, 2)
6     DY(I, 1)= -DY(I, 2)
      MCELL= 6 *IMAX
      JS2= JMAX1 +JMAX
      CURR= 0.
      DRAG(1)= 0.
      DRAG(2)= 0.
      NCROSS= 0
```



```
      VZNM= 0.
      CORR= .FALSE.
      IF (WC .NE. 0. .OR.ACCTRA) CORR= .TRUE.
      DO 61 K= 1, NGRP
      IF(TRPLOT .AND. NGTRPL .GE. K) CALL PLTRA1
      S1= .FALSE.
      S2= .FALSE.
      S4= .TRUE.
      ICH= 1
      MAX= IMAX1
      YN= .95 *Y(JMAX) +.05*Y(JMAX1)
      YTRPL= YN
      DO 59 NTRAJ= 1, 500
      XN= X(IMAX)
      VXN= -VXITEM(K)
      VYN= 0.
      VZN= 0.
      I= IMAX
      J= JLOC(YN)
      EXIT= 1
      RTR= 0
      TRPL1= .FALSE.
      IF (YN .GT. YTRPL) GO TO 71
      YTRPL= YN     -DYTRPL
      IF (TRPLOT .AND. NGTRPL .GE. K) TRPL1= .TRUE.
71    WRTRAJ= .FALSE.
      IF (.NOT. WRFLOW) GO TO 67
      IF (MOD(NTRAJ-1, NPTRAJ) .EQ. NPTRAJ-1) WRTRAJ= .TRUE.
67    S3= .FALSE.
      REDO= .FALSE.
      IF (CORR) REDO= .TRUE.
      DO 40 ICEL= 1, MCELL
      IF (.NOT. CORR) GO TO 65
      REDO= .NOT. REDO
      IF (REDO .AND. .NOT. ACCTRA) GO TO 75
65    RTR= MOD(EXIT +RTR +2, 4)
      IF (RTR .NE. 3) GO TO 62
      FX= PO1(YN, Y(J), Y(J+1), DX(I, J), DX(I, J+1))
      FY= PO1(YN, Y(J), Y(J+1), DY(I, J), DY(I, J+1))
      IF(REDO) GO TO 75
      YMA1(I)= YN
      VTEM(I)= VXN
      IF (S3) YMA1(I) = -YMA1(I)
      I= I-1
      GO TO 68
62    IF (RTR .NE. 2) GO TO 64
      FX= PO1(XN, X(I), X(I+1), DX(I, J), DX(I+1,J))
      FY= PO1(XN, X(I), X(I+1), DY(I, J), DY(I+1,J))
      IF(REDO) GO TO 75
      J= J-1
      GO TO 68
64    IF(RTR .NE. 3) CALL ERROR (&2C1, 8HRHO   64)
      J= J+1
      FX= PO1(XN, X(I), X(I+1), DX(I, J), DX(I+1,J))
      FY= PO1(XN, X(I), X(I+1), DY(I, J), DY(I+1,J))
      IF (.NOT. REDO) GO TO 68
      J= J-1
```



```
      GO TO 75
75    XN= XN1
      YN= YN1
      VXN= VXN1
      VYN= VYN1
      RTR= IRTR
      IF(ACCTRA) GO TO 76
      FX= FX1
      FY= FY1
      GO TO 77
76    FX= (FX1 +FX) *.5
      FY= (FY1 +FY) *.5
77    IF (WC .EQ. 0.) GO TO 66
      WCT2=(WC*T) **2
      FY= (FY +VZN *WC) *(1. -WCT2 /12.)
      FY2= FY
      VYN= VYN *(1. -WCT2/6.)
      GO TO 66
68    IF (I .LE. 1) GO TO 50
      IF (I .EQ.ISAT-1.AND. YN .LT. Y(JSAT)) GO TO 13
      IF(J .EQ. JMAX) GO TO 51
      IF (J .NE. 0) GO TO 63
      YN= -YN
      VYN= -VYN
      RTR= 0
      J= 2
      S3= .NOT. S3
63    IF (.NOT. CORR) GO TO 66
      XN1= XN
      YN1= YN
      VXN1= VXN
      VYN1= VYN
      FX1= FX
      FY1= FY
      IRTR= RTR
66    G1= G(I)
      H1= H(J)
      COX= (X(I) +X(I+1)) /2.
      COY= (Y(J) +Y(J+1)) /2.
      IBAC= MOD (4-RTR, 4)
      IF (IBAC .EQ. 0) GO TO 70
      CALL ROTATE (XN, YN, IBAC)
      CALL ROTATE (VXN, VYN, IBAC)
      CALL ROTATE (FX, FY, IBAC)
      CALL ROTATE (COX,  COY, IBAC)
      CALL ROTATE (G1, H1, IBAC)
      G1=DABS(G1)
      H1=DABS(H1)
70    CALL ORBIT (&19)
      CALL ROTATE(XN, YN, RTR)
      CALL ROTATE(VXN, VYN, RTR)
      IF (WC .EQ. 0. .OR. .NOT. REDO) GO TO 40
      WCT= WC *T
      WCT2= WCT *WCT
      VZN= -VYN1 *(1. -WCT2/6.) *WCT +VZN *(1. -WCT2/2.)-FY2 *T *WCT/2.
      VZNM= DMAX1(VZNM,DABS(VZN))
40    CONTINUE
```



```
      CALL ERROR(&2C1, 8HRHO   40)
51    I1= I
      DO 72 I= 2, I1
      VTEM(I)= VTEM(I1+1)
72    YMA1(I)= PO1(X(I), X(I1+1), X(I1+2), YMA1(I1+1), YMA1(I1+2))
      GO TO 50
50    IF (WRTRAJ) WRITE (IO,10C) (X(I),YMA1(I), VTEM(I), I= 2, IMAX,
     1 NTSKIP)
      VEND(1)= VTEM(2)
      VEND(2)= VEND(1)
      IF (.NOT. TRPL1) GO TO 73
      III= 2
      CALL PLTRA2
73    IF (.NOT. S4) GO TO 9
      S4= .FALSE.
      DO 8 I= 2, IMAX
      IF    (YMA1(I) .LT. Y(JMAX1)) CALL ERROR(&8, 8HRHO    8)
8     YMA2(I)= YMA1(I)
      GO TO 19
9     DO 11 I= 2, IMAX1
      IF (YMA1(I) .GE. YMA2(I)) GO TO 17
11    CONTINUE
      GO TO 15
17    NCROSS= NCROSS +1
15    TRH= YMA2(IMAX) -YMA1(IMAX)
      DO 36 I1= 2, MAX
      I= IMAX -I1 +1
      AL= YMA2(I) -YMA1(I)
      Y4= DMIN1(YMA1(I), YMA2(I))
      Y5=DMAX1 (YMA1(I), YMA2(I))
      JS1= JLOC(Y4) +1 +JMAX
      DO 31 JS= JS1, JS2
      J= JS -JMAX
      IF (J .GT. 1) GO TO 28
      J= 3-J
      Y3= -Y(J)
      GO TO 29
28    Y3= Y(J)
29    IF (Y3 .GT. Y5) GO TO 35
33    TEM=DABS(TRH /AL *VTEM(IMAX) /VTEM(I))
      IF (ROTINV) TEM=DABS (TEM *(YMA2(IMAX) -TRH/ AL *(YMA2(I) -Y3))
     1 /Y3)
31    RHOI(I, J)= RHOI(I, J) +TEM
35    YMA2(I) = YMA1(I)
36    CONTINUE
      DO 41 L=1,2
      TDRAG= TRH* (VEND(L)  -VTEM(IMAX))
      IF(ROTINV) TDRAG= TDRAG *(TRH + 2. *YMA1(IMAX))
41    DRAG(L)= TDRAG + DRAG(L)
      YMA2(IMAX)= YMA1(IMAX)
      GO TO 19
13    IF (WRTRAJ) WRITE (IO,10C) (X(I), YMA1(I), VTEM(I), I= ISAT, IMAX,
     1 NTSKIP)
      VEND(1)= -VTEM(ISAT)
      VEND(2)= 0.
      IF (.NOT. TRPL1) GO TO 74
      III= ISAT
```

```
      CALL PLTRA2
74    IF (S1) GO TO 15
      CUR = PO1(Y(JSAT), YMA1(ISAT), YMA2(ISAT), YMA1(IMAX), YMA2(IMAX))
     1 /Y(JSAT)
      IF (RCTINV) CUR = CUR  *CUR
      CURR= CURR +CUR
      TRHEL= PO1( Y(JSAT), YMA1(ISAT), YMA2(ISAT), TRH, 0.)
      DO 42 L= 1,2
      TDRAG= TRHEL *(VTEM(2) -VEND(L))
      IF (ROTINV) TDRAG= TDRAG *(2. *YMA2(IMAX) -TRHEL)
42    DRAG(L)= TDRAG +DRAG(L)
      S1= .TRUE.
      MAX= IMAX -ISAT
      GO TO 15
19    IF (S2) GO TO 60
      YN= YMA1(IMAX) -DTR(ICH)
      IF (YN .GT. 0.) GO TO 21
      S2= .TRUE.
      DO 20 I1= 1, MAX
      I= IMAX -I1 +1
20    YMA1(I)= 0.
      VEND(1)= DSQRT (VTEM(IMAX) *VTEM(IMAX) -2. *POTSAT /BETA )
      VEND(2)= 0.
      GO TO 15
21    IF (YN .GT. TR(ICH))  GO TO 59
      YN= TR(ICH)
      ICH= ICH +1
59    CONTINUE
      CALL ERROR(6201, 8HRHO   59)
60    IF (TRPLOT .AND. NGTRPL .GE. K) CALL PLTRA3
61    CONTINUE
      GRP=CFLOAT(NGRP)
      VAVE = 0
      DO   89   K = 1, NGRP
89    VAVE = VXITEM (K) + VAVE
      UNCURR = CURR*VAVE * Y(JSAT)*2./GRP
      IF (RCTINV) UNCURR = UNCURR * Y(JSAT) * PI/2.
      DO 43 L= 1,2
      UNDRAG(L)= BETA *VAVE /GRP *DRAG(L) *2.
      IF (ROTINV) UNDRAG(L)= UNDRAG(L) *PI /2.
      DRAG(L)= DRAG(L)      /Y(JSAT) /VAVE *GRP
43    IF (RCTINV) DRAG(L) =DRAG(L) /Y(JSAT)
      DO 58 I= 2, IMAX1
      DO 58 J= 2, JMAX1
58    RHOI(I, J)= RHOI(I, J) /GRP
      RETURN
201   RETURN 1
100   FORMAT ( /4(6X 1HX 5X 1HY 6X 10HX-VELOCITY   ) / 4(4X 0PF6.2,
     1 F11.6, 1PE12.4))
      END
```



```
      SUBROUTINE ROTATE (L,V,I)
      IMPLICIT REAL*8 (A-H, O-Z), INTEGER*4 (I-N)
      X=U
      Y=V
      IF (I. NE. 1) GO TO 1
      TEM= Y
      Y= -X
      X= TEM
      GO TO 10
1     IF(I. NE. 2) GO TO 2
      X= -X
      Y= -Y
      GO TO 10
2     IF (I. NE. 3)GO TO 12
      TEM= Y
      Y= X
      X= -TEM
10    U= X
      V= Y
      RETURN
12    IF (I. EQ. 0) RETURN
      CALL ERROR (614, 8HROTAT 12)
14    RETURN
      END
```



```
C     SETUP PROGRAM
      IMPLICIT REAL*8 (A-H, O-Z), INTEGER*4 (I-N)
      COMMON /CMAIN/ A(200000)
      LOGICAL*1 PAGE(120, 57)
      LX= 80
      LY= 50
      LXY= LX *LY
1     CALL DREAD (A(1), A(LXY +1), A(2 *LXY +1), A(3* LXY +1), LX, LY)
      CALL DWRITE (A(1), LX, LY)
      CALL READ
      CALL DPOCO (A(1), A(LXY +1), A(2 *LXY +1), A(3* LXY +1), LX, LY)
      CALL DRHO  (A(1), A(LXY +1), A(3 *LXY +1), A(4* LXY +1), LX, LY)
      CALL DACIH(A(1), A(LXY +1), A(3 *LXY +1), LX, LY)
      CALL DACIV(A(1), A(LXY +1), A(3 *LXY +1), LX, LY)
      CALL DCONT(              A(1), LX, LY, PAGE(1, 1), 120, 57)
      CALL PCCO
      GO TO 1
201   CALL EXIT
      END
```



```
      SUBROUTINE TIM(DIF, VEL, FORCE, *  )
      IMPLICIT REAL*8 (A-H, O-Z), INTEGER*4 (I-N)
      COMMON /CCMORB/ XC, YC, VXO, VYO, FX, FY, XC, HX, HY, TIME, FACE
      INTEGER*4 FACE
      REAL*8 VMIN /1.D-6/, RATMX /.95DC/, FMIN /1.D-6/
      IF(DABS(VEL).LT. VMIN) GC TO 20
      RAT= FORCE* DIF/ VEL/ VEL
      IF(DABS(RAT). GT. RATMX) GC TC 20
      TIME= DIF/ VEL* ((RAT- 1.)* .5* RAT+ 1.)
      IF ( TIME .LT. 0.) GO TO 20
      RETURN
20    IF(DABS(FORCE).LE. FMIN) GO TC 40
      TEM= VEL* VEL +FORCE* DIF *2.
      IF (TEM .LT. 0.) RETURN 1
      SQR=DSQRT(TEM)
      T1  = ( -VEL + SQR) /FORCE
      T2  = ( -VEL - SQR) /FORCE
      TIME= DMIN1 (T1, T2)
      IF (TIME .GE. 0.) RETURN
      TIME= DMAX1 (T1, T2)
      IF (TIME .GE. 0.) RETURN
      RETURN 1
40    TIME= DIF/ VEL
      RETURN
      END
```

```
      SUBROUTINE TRILIN
      IMPLICIT REAL*8 (A-H, O-Z), INTEGER*4 (I-N)
      REAL*8 K
      DIMENSION W(1), Z(1)
      EQUIVALENCE (C(1), W(1)), (K(1), Z(1))
      COMMON /CTRI/ A(500), B(500), C(500), K(500), NMIN, NMAX
      M= NMIN
      N= NMAX
      W(M)= C(M) /B(M)
      Z(M)= K(M) /B(M)
      M1= M +1
      N1= N -1
      DO 10 J= M1, N1
      TEM= B(J) -A(J) *W(J -1)
      W(J)= C(J) /TEM
10    Z(J)= (K(J) -A(J) *Z(J -1)) /TEM
      Z(N)= (K(N) -A(N) *Z(N -1)) /(B(N) -A(N) *W(N -1))
      DO 20 J= M1, N
      I= N -J +M
20    Z(I)= Z(I) -W(I) *Z(I +1)
      RETURN
      END
```



```
     SAMPLE DATA PACKET FOR MODEL PROBLEM
&INPUT
IMAX= 076, ISAT= 056, G(1)= 45*.5, 20*.25, 10*.75,  XLEFT=-25.,
JMAX=31, JSAT=06,H(1)= .4, 14*.2, 5*.4, 20*.75,
CTR(1)= .54, .24, .08, .16,          TR(1)= 4.81, 2.81, .98, 0.0,
NPMAJ=6,  NWSKIP=3, MPASS=6,
OMEGA= 1.55, RCTINV=F,
ERRADI(1)= .2, .08, 4*.05, 12*.03,         MITER= 19,
ERMPAR=.001,ERMPAU= .0001,RHISTA= 0.80, MINITE= 11,
ALPHAR= 1., 19*.75,  ALPHAU= 1., 19*.75,  RHIMAX(1)=20*5., UMAX= 5.,
VXST=.05710, PCTSAT= -0.0, RHIX= -12., BETA=07344.,
XP1= -20., XP2= 5., XPDEL= .25,
YP1=   0., YP2=10., YPDEL= .20,
NUG= 26,   UG(1)= 5., .2, .05, -.01, -.05, -.1, -.2, -.4, -.6, -1.,
-2., -3., -4., -6., -8., -10., -12., -14., -16., -18., -20., -22.,
-24., -26., -28., -30.,
PLCTU(6)= T,
NRG= 15, RG(1)= -1., -.1, .1, .55, .65, .75, .85, .95, .99, 1.05,
1.10, 1.101, 1.2, 1.201, 3.,
PLCTR(6)=  T,
XT1= -20., XT2= 5., XTDEL= .25,
YT1= -10., YT2=10., YTDEL= .4,
PLCTTR(6)= T,     CYTRPL= 1.,  NGTRPL=1,
&END
```

PASS NUMBER	WRITE FLOW	ADI ERROR	U-ALPHA	RHO-ALPHA	MAXIMUM RHO	PUNCH OPTION	PLOT U OPTION	PLOT RHO OPTION	PLOT TRAJECTORIES	IMPROVED ORBITS
1	F	2.0D-01	1.00	1.00	5.0D 00	F	F	F	F	F
2	F	8.0D-02	0.75	0.75	5.0D 00	F	F	F	F	F
3	F	5.0D-02	0.75	0.75	5.0D 00	F	F	F	F	F
4	F	5.0D-02	0.75	0.75	5.0D 00	F	F	F	F	F
5	F	5.0D-02	0.75	0.75	5.0D 00	F	F	F	F	F
6	F	5.0D-02	0.75	0.75	5.0D 00	F	T	T	T	F

IMAX= 76 JMAX= 31 ISAT= 56 JSAT= 6

HORIZONTAL COORDINATES (-25.0, 10.0) VERTICAL COORDINATES (0.0, 12.5) SATELLITE EDGE COORDINATES (0.0, 1.0)
SATELLITE VELOCITY= 0.05710 ION MASS RATIO= 7344. ION KINETIC ENERGY= 11.972
SATELLITE POTENTIAL= -2.5

X MATRIX

1	-25.0	2	-24.5	3	-24.0	4	-23.5	5	-23.0	6	-22.5	7	-22.0	8	-21.5	9	-21.0	10	-20.5	11	-20.0	12	-19.5	13	-19.0
14	-18.5	15	-18.0	16	-17.5	17	-17.0	18	-16.5	19	-16.0	20	-15.5	21	-15.0	22	-14.5	23	-14.0	24	-13.5	25	-13.0	26	-12.5
27	-12.0	28	-11.5	29	-11.0	30	-10.5	31	-10.0	32	-9.5	33	-9.0	34	-8.5	35	-8.0	36	-7.5	37	-7.0	38	-6.5	39	-6.0
40	-5.5	41	-5.0	42	-4.5	43	-4.0	44	-3.5	45	-3.0	46	-2.5	47	-2.2	48	-2.0	49	-1.7	50	-1.5	51	-1.2	52	-1.0
53	-0.8	54	-0.5	55	-0.3	56	0.0	57	0.3	58	0.5	59	0.8	60	1.0	61	1.2	62	1.5	63	1.7	64	2.0	65	2.2
66	2.5	67	3.2	68	4.0	69	4.7	70	5.5	71	6.2	72	7.0	73	7.7	74	8.5	75	9.2	76	10.0				

Y MATRIX

1	-0.20	2	0.20	3	0.40	4	0.60	5	0.80	6	1.00	7	1.20	8	1.40	9	1.60	10	1.80	11	2.00	12	2.20	13	2.40
14	2.60	15	2.80	16	3.00	17	3.40	18	3.80	19	4.20	20	4.60	21	5.00	22	5.75	23	6.50	24	7.25	25	8.00	26	8.75
27	9.50	28	10.25	29	11.00	30	11.75	31	12.50																

TRAJECTORY SPACING

1 0.540 4.810 2 0.240 2.810 3 0.080 0.980 4 0.160 0.0

ION VELOCITY GROUPS

NUMBER	THERMAL VELOCITY	TOTAL VELOCITY
1	0.0	0.057100

```
&OUTPUT
CARDS=F,ZERO=T,TESADI=F,POTINV=F,WRCHGE=F,MITER=          19,NPITER=          75,MINITE=          11,FACITE=  9.999999999999999     ,
OMEGA=  1.549999999999999     ,MPASS=           6,ERMPAR= 0.99999999999999998D-03,ERMPAU= 0.99999999999999990D-04,NMEXP=          10,
UMIN= -9.999999999999999     ,LMAX=  4.999999999999999     ,NWSKIP=           3,NTSKIP=           1,PFIELD= 0.0                    ,WC=
 0.0                    ,RHIX= -11.999999999999999     ,RHISTA= 0.7999999999999999     ,NPMAJ=           6,NPTRAJ=           1,TRATIO=
 0.9999999999999990     ,NGRP=           1,MXYMAT=         399
&END
&OUTPLO
NUG=          26,XP1= -19.999999999999999     ,XP2=  4.999999999999999     ,XPDEL= 0.2500000000000000     ,YP1= 0.0
YP2=  9.999999999999999     ,YPDEL= 0.1999999999999999     ,NRG=          15,NRTG=           0
&END
&OUTPTR
NGTRPL=           1,DYTRPL= 0.9999999999999990     ,XT1= -19.99999999999999     ,XT2=  4.999999999999999     ,XTDEL=
 0.2500000000000000     ,YT1= -9.999999999999999     ,YT2=  9.999999999999999     ,YTDEL= 0.3999999999999999
&END
```

PDE ERROR= 3.1027D-02 MAXIMUM PDE ERROR= 2.0D-01 PDE RELAXATION PARAMETER= 1.550 NUMBER OF ITERATIONS= 12
U-ERROR= 2.1987D 00 MAXIMUM U-ERROR= 1.0D-04 U-ALPHA= 1.00

```
CURRENT=  0.11712          54 TRAJECTORIES          2 CROSSINGS          MAXIMUM Z-VELOCITY= 0.0
NORM. CURRENT=  1.02555    RHO-ERROR= 4.0000D 00    RHO-ALPHA= 1.00      MAXIMUM RHO-ERROR= 1.0D-03
NORM. DRAG(R)=  2.14832    NORM. DRAG(A)=  1.03583  DRAG= 1.0288D 02

PDE ERRLR= 4.3839D-03    MAXIMUM PDE ERROR= 8.0D-02    PDE RELAXATION PARAMETER= 1.550    NUMBER OF ITERATIONS= 12
U-ERROR= 2.1224D-01      MAXIMUM U-ERROR= 1.0D-04      U-ALPHA= 0.75

CURRENT=  0.11712          54 TRAJECTORIES          1 CROSSINGS          MAXIMUM Z-VELOCITY= 0.0
NORM. CURRENT=  1.02558    RHO-ERROR= 3.3327D 00    RHO-ALPHA= 0.75      MAXIMUM RHO-ERROR= 1.0D-03
NORM. DRAG(R)=  2.13888    NORM. DRAG(A)=  1.02612  DRAG= 1.0243D 02

PDE ERRLR= 1.6910D-03    MAXIMUM PDE ERROR= 5.0D-02    PDE RELAXATION PARAMETER= 1.550    NUMBER OF ITERATIONS= 12
U-ERROR= 1.1009D-01      MAXIMUM U-ERROR= 1.0D-04      U-ALPHA= 0.75

CURRENT=  0.11712          54 TRAJECTORIES          1 CROSSINGS          MAXIMUM Z-VELOCITY= 0.0
NORM. CURRENT=  1.02561    RHO-ERROR= 2.2705D 00    RHO-ALPHA= 0.75      MAXIMUM RHO-ERROR= 1.0D-03
NORM. DRAG(R)=  2.13482    NORM. DRAG(A)=  1.02195  DRAG= 1.0223D 02

PDE ERRLR= 9.1236D-04    MAXIMUM PDE ERROR= 5.0D-02    PDE RELAXATION PARAMETER= 1.550    NUMBER OF ITERATIONS= 12
U-ERROR= 7.4867D-02      MAXIMUM U-ERROR= 1.0D-04      U-ALPHA= 0.75

CURRENT=  0.11713          54 TRAJECTORIES          1 CROSSINGS          MAXIMUM Z-VELOCITY= 0.0
NORM. CURRENT=  1.02563    RHO-ERROR= 1.5409D 00    RHO-ALPHA= 0.75      MAXIMUM RHO-ERROR= 1.0D-03
NORM. DRAG(R)=  2.13152    NORM. DRAG(A)=  1.01860  DRAG= 1.0208D 02

PDE ERRLR= 7.0063D-04    MAXIMUM PDE ERROR= 5.0D-02    PDE RELAXATION PARAMETER= 1.550    NUMBER OF ITERATIONS= 12
U-ERROR= 5.5306D-02      MAXIMUM U-ERROR= 1.0D-04      U-ALPHA= 0.75

CURRENT=  0.11713          54 TRAJECTORIES          1 CROSSINGS          MAXIMUM Z-VELOCITY= 0.0
NORM. CURRENT=  1.02564    RHO-ERROR= 1.2194D 00    RHO-ALPHA= 0.75      MAXIMUM RHO-ERROR= 1.0D-03
NORM. DRAG(R)=  2.13103    NORM. DRAG(A)=  1.01809  DRAG= 1.0205D 02

PDE ERRLR= 6.1961D-04    MAXIMUM PDE ERROR= 5.0D-02    PDE RELAXATION PARAMETER= 1.550    NUMBER OF ITERATIONS= 12
U-ERROR= 3.9574D-02      MAXIMUM U-ERROR= 1.0D-04      U-ALPHA= 0.75
```

CONTOUR PLOT OF POTENTIAL

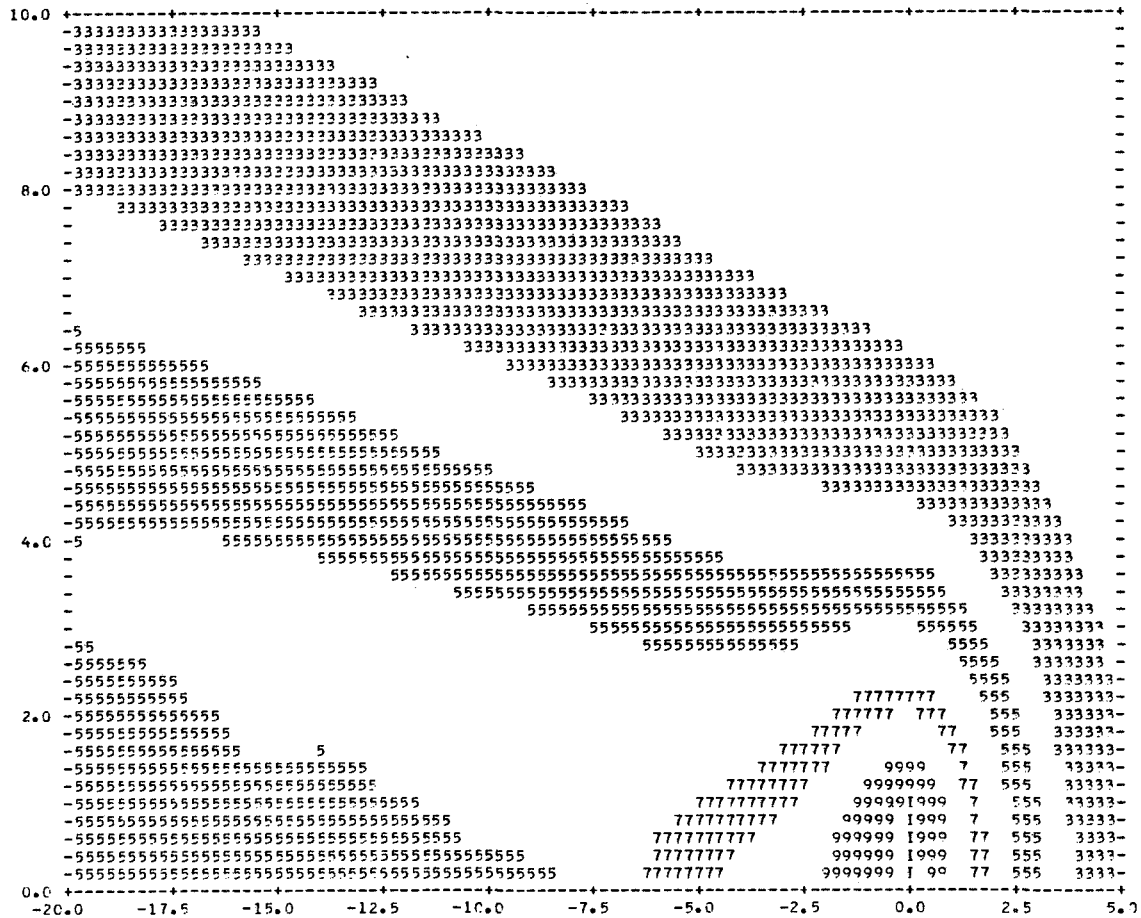

KEY TO PLOT

0= 5.00 1= 0.20 2= 0.05 3= -0.01 4= -0.05 5= -0.10 6= -0.20 7= -0.40 8= -0.60 9= -1.00
10= -2.00 11= -3.00 12= -4.00 13= -6.00 14= -8.00 15=-10.00 16=-12.00 17=-14.00 18=-16.00 19=-18.00
20=-20.00 21=-22.00 22=-24.00 23=-26.00 24=-28.00 25=-30.00

PASS NUMBER= 6 83.07 SECONDS POTENTIAL MATRIX

```
        Y=  0.20
-24.5 -6.4928D-02 -23.0 -1.2948D-01 -21.5 -1.4488D-01 -20.0 -1.5169D-01 -18.5 -1.4535D-01 -17.0 -1.4489D-01 -15.5 -1.4565D-01
-14.0 -1.2010D-01 -12.5 -1.2187D-01 -11.0 -1.4807D-01  -9.5 -1.5845D-01  -8.0 -2.9635D-01  -6.5 -3.5989D-01  -5.0 -5.2043D-01
 -3.5 -7.1396D-01  -2.2 -9.4866D-01  -1.5 -1.2308D 00  -0.8 -1.7226D 00   0.0 -2.5000D 00   0.8 -1.2373D 00   1.5 -5.6250D-01
  2.2 -2.4606D-01   4.0 -3.7811D-02   6.2 -3.6407D-03   8.5 -3.4206D-04

        Y=  0.80
-24.5 -5.3391D-02 -23.0 -1.2041D-01 -21.5 -1.4055D-01 -20.0 -1.4762D-01 -18.5 -1.4572D-01 -17.0 -1.4899D-01 -15.5 -1.5557D-01
-14.0 -1.2059D-01 -12.5 -1.4798D-01 -11.0 -1.9786D-01  -9.5 -2.4521D-01  -8.0 -3.1623D-01  -6.5 -3.6454D-01  -5.0 -4.2841D-01
 -3.5 -5.6635D-01  -2.2 -7.6444D-01  -1.5 -1.0322D 00  -0.8 -1.4816D 00   0.0 -2.5000D 00   0.8 -1.1013D 00   1.5 -5.0090D-01
  2.2 -2.2314D-01   4.0 -3.5375D-02   6.2 -3.4773D-03   8.5 -3.3010D-04

        Y=  1.40
-24.5 -4.7311D-02 -23.0 -1.1093D-01 -21.5 -1.3197D-01 -20.0 -1.4113D-01 -18.5 -1.4443D-01 -17.0 -1.5691D-01 -15.5 -1.8908D-01
-14.0 -1.5930D-01 -12.5 -2.2349D-01 -11.0 -2.6463D-01  -9.5 -2.8665D-01  -8.0 -3.1088D-01  -6.5 -3.2763D-01  -5.0 -3.5017D-01
 -3.5 -4.1223D-01  -2.2 -5.3994D-01  -1.5 -7.0299D-01  -0.8 -9.7628D-01   0.0 -1.2714D 00   0.8 -7.6800D-01   1.5 -3.8271D-01
  2.2 -1.8008D-01   4.0 -3.0616D-02   6.2 -3.1462D-03   8.5 -3.0602D-04

        Y=  2.00
-24.5 -4.7446D-02 -23.0 -1.1074D-01 -21.5 -1.3479D-01 -20.0 -1.5074D-01 -18.5 -1.4598D-01 -17.0 -1.8949D-01 -15.5 -2.3625D-01
-14.0 -2.3759D-01 -12.5 -2.5692D-01 -11.0 -2.7330D-01  -9.5 -2.7850D-01  -8.0 -2.8015D-01  -6.5 -2.7626D-01  -5.0 -2.7535D-01
 -3.5 -2.9822D-01  -2.2 -3.6623D-01  -1.5 -4.5095D-01  -0.8 -5.6465D-01   0.0 -6.0953D-01   0.8 -4.4717D-01   1.5 -2.5574D-01
  2.2 -1.3087D-01   4.0 -2.4653D-02   6.2 -2.7035D-03   8.5 -2.7229D-04

        Y=  2.60
-24.5 -4.6774D-02 -23.0 -1.1400D-01 -21.5 -1.4519D-01 -20.0 -1.8063D-01 -18.5 -1.9218D-01 -17.0 -2.2392D-01 -15.5 -2.4697D-01
-14.0 -2.4940D-01 -12.5 -2.5118D-01 -11.0 -2.5168D-01  -9.5 -2.4577D-01  -8.0 -2.3522D-01  -6.5 -2.2092D-01  -5.0 -2.0828D-01
 -3.5 -2.1004D-01  -2.2 -2.3970D-01  -1.5 -2.7627D-01  -0.8 -3.1508D-01   0.0 -3.1520D-01   0.8 -2.4718D-01   1.5 -1.5707D-01
  2.2 -8.7681D-02   4.0 -1.8626D-02   6.2 -2.2138D-03   8.5 -2.3276D-04

        Y=  3.40
-24.5 -5.2932D-02 -23.0 -1.3135D-01 -21.5 -1.8172D-01 -20.0 -2.0650D-01 -18.5 -2.1527D-01 -17.0 -2.2184D-01 -15.5 -2.2489D-01
-14.0 -2.2235D-01 -12.5 -2.1310D-01 -11.0 -2.0173D-01  -9.5 -1.8767D-01  -8.0 -1.7174D-01  -6.5 -1.5264D-01  -5.0 -1.3484D-01
 -3.5 -1.2589D-01  -2.2 -1.3099D-01  -1.5 -1.3903D-01  -0.8 -1.4456D-01   0.0 -1.3676D-01   0.8 -1.1096D-01   1.5 -7.7008D-02
  2.2 -4.7305D-02   4.0 -1.1805D-02   6.2 -1.5853D-03   8.5 -1.7985D-04

        Y=  4.60
-24.5 -7.1155D-02 -23.0 -1.5441D-01 -21.5 -1.7659D-01 -20.0 -1.7999D-01 -18.5 -1.7614D-01 -17.0 -1.7329D-01 -15.5 -1.6354D-01
-14.0 -1.5071D-01 -12.5 -1.3659D-01 -11.0 -1.2155D-01  -9.5 -1.0641D-01  -8.0 -9.2012D-02  -6.5 -7.7041D-02  -5.0 -6.3561D-02
 -3.5 -5.4075D-02  -2.2 -5.0098D-02  -1.5 -4.8530D-02  -0.8 -4.6153D-02   0.0 -4.1456D-02   0.8 -3.4042D-02   1.5 -2.5247D-02
  2.2 -1.7036D-02   4.0 -5.2246D-03   6.2 -8.4680D-04   8.5 -1.0879D-04

        Y=  6.50
-24.5 -4.4962D-02 -23.0 -9.5594D-02 -21.5 -1.0110D-01 -20.0 -9.6920D-02 -18.5 -8.8115D-02 -17.0 -7.8227D-02 -15.5 -6.8197D-02
-14.0 -5.8464D-02 -12.5 -4.9427D-02 -11.0 -4.1493D-02  -9.5 -3.6172D-02  -8.0 -2.9903D-02  -6.5 -2.3535D-02  -5.0 -1.8068D-02
 -3.5 -1.3813D-02  -2.2 -1.1174D-02  -1.5 -9.8454D-03  -0.8 -8.5723D-03   0.0 -7.2565D-03   0.8 -5.8761D-03   1.5 -4.5016D-03
  2.2 -3.2504D-03   4.0 -1.2280D-03   6.2 -2.5761D-04   8.5 -3.9361D-05

        Y=  8.75
-24.5 -1.6982D-02 -23.0 -3.6064D-02 -21.5 -3.6690D-02 -20.0 -3.2759D-02 -18.5 -2.8009D-02 -17.0 -2.3440D-02 -15.5 -1.9303D-02
-14.0 -1.5655D-02 -12.5 -1.2528D-02 -11.0 -9.9331D-03  -9.5 -7.8282D-03  -8.0 -6.0464D-03  -6.5 -4.5360D-03  -5.0 -3.3149D-03
 -3.5 -2.3735D-03  -2.2 -1.7785D-03  -1.5 -1.4864D-03  -0.8 -1.2313D-03   0.0 -1.0038D-03   0.8 -7.9849D-04   1.5 -6.1549D-04
  2.2 -4.5771D-04   4.0 -1.9666D-04   6.2 -4.7305D-05   8.5 -1.0649D-05

        Y= 11.00
-24.5 -4.2642D-03 -23.0 -9.1075D-03 -21.5 -9.0843D-03 -20.0 -7.8868D-03 -18.5 -6.5099D-03 -17.0 -5.2414D-03 -15.5 -4.1632D-03
-14.0 -3.2713D-03 -12.5 -2.5203D-03 -11.0 -1.9167D-03  -9.5 -1.4440D-03  -8.0 -1.0694D-03  -6.5 -7.7118D-04  -5.0 -5.3765D-04
 -3.5 -3.7473D-04  -2.2 -2.6806D-04  -1.5 -2.1612D-04  -0.8 -1.7290D-04   0.0 -1.3729D-04   0.8 -1.0765D-04   1.5 -8.3318D-05
  2.2 -6.3580D-05   4.0 -3.0279D-05   6.2 -8.2542D-06   8.5  2.2305D-06

POSSIBLE ERROR AT CONTOU 6.  ALTERNATE LOGIC ROUTE TAKEN.
```

TRAJECTORY PLOT

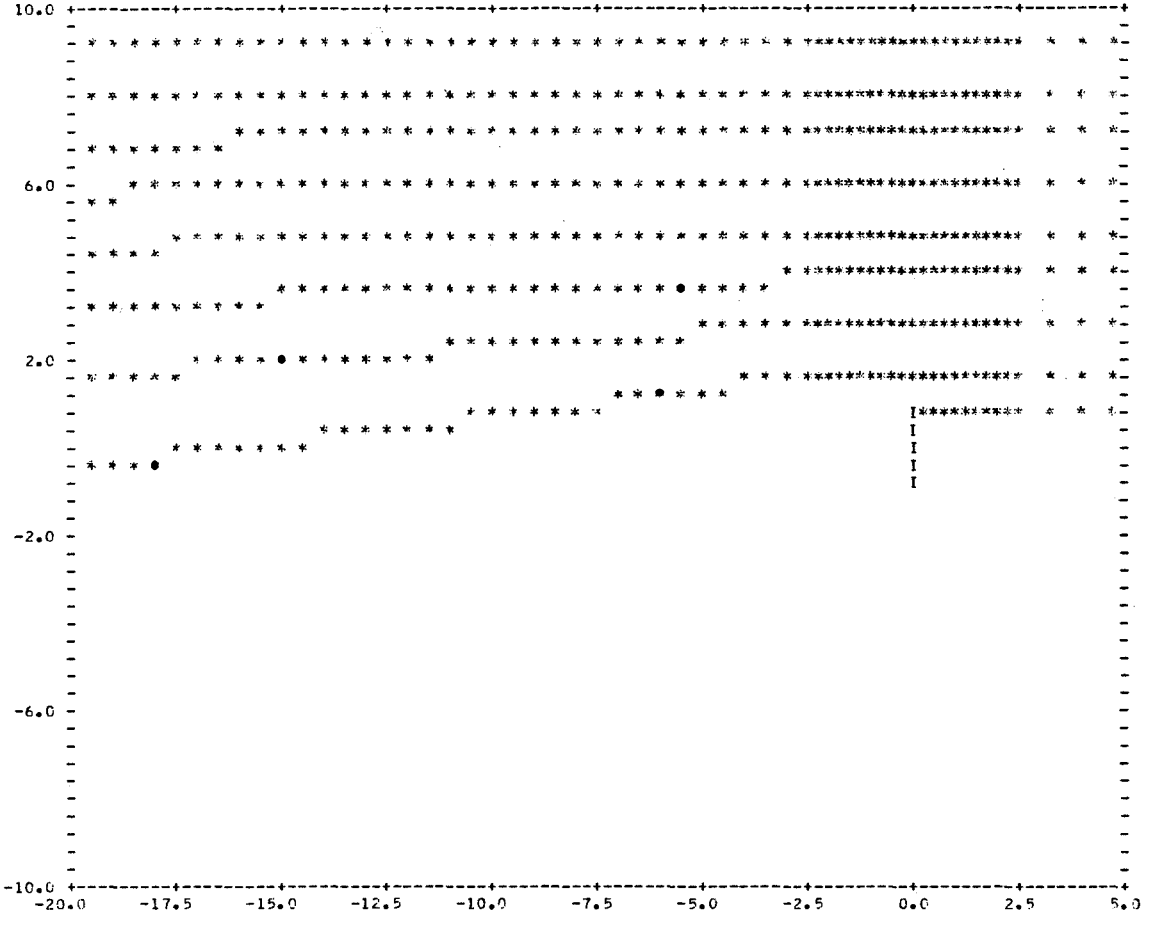

CURRENT= 0.11713 54 TRAJECTORIES 1 CROSSINGS MAXIMUM Z-VELOCITY= 0.0
NORM. CURRENT= 1.02564 RHO-ERROR= 1.7547D 00 RHO-ALPHA= 0.75 MAXIMUM RHO-ERROR= 1.00-03
NORM. DRAG(R)= 2.13080 NORM. DRAG(A)= 1.01785 DRAG= 1.0204D 02

CONTOUR PLOT OF ION DENSITY

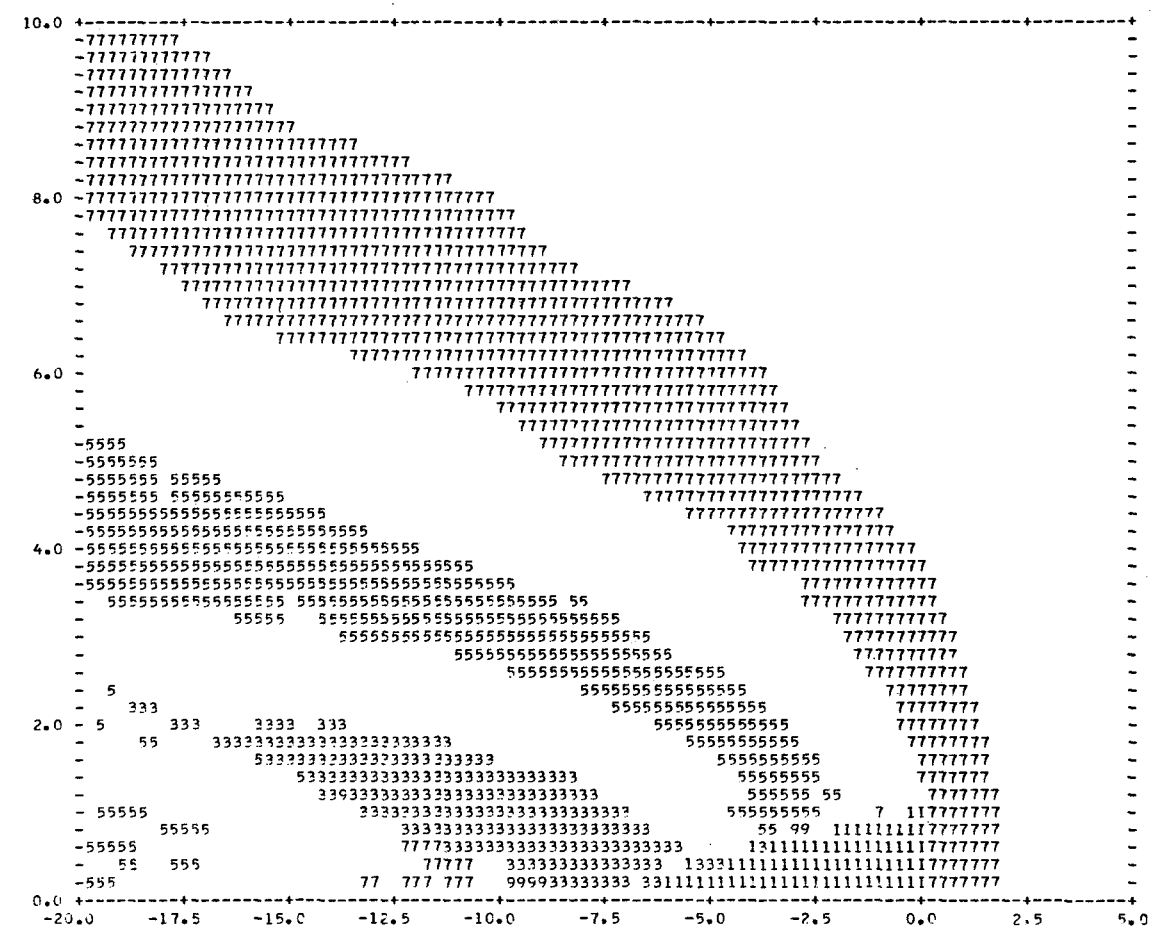

KEY TO PLOT

0= -1.00 1= -0.10 2= 0.10 3= 0.55 4= 0.65 5= 0.75 6= 0.85 7= 0.95 8= 0.99 9= 1.05
10= 1.10 11= 1.10 12= 1.20 13= 1.20 14= 3.00

PASS NUMBER= 6 11.20 SECONDS ION DENSITY MATRIX

Y= 0.20

-24.5	7.3239D-01	-23.0	8.7271D-01	-21.5	8.5849D-01	-20.0	8.2119D-01	-18.5	8.7764D-01	-17.0	8.8492D-01	-15.5	8.6698D-01
-14.0	9.1898D-01	-12.5	9.3689D-01	-11.0	9.6889D-01	-9.5	1.0833D 00	-8.0	5.6844D-01	-6.5	1.2306D 00	-5.0	0.0
-3.5	0.0	-2.2	0.0	-1.5	0.0	-0.8	0.0	0.0	0.0	0.8	9.6782D-01	1.5	9.8453D-01
2.2	9.9350D-01	4.0	9.9901D-01	6.2	9.9990D-01	8.5	9.9999D-01						

Y= 0.80

-24.5	9.2700D-01	-23.0	9.2889D-01	-21.5	8.4148D-01	-20.0	8.5111D-01	-18.5	8.8132D-01	-17.0	8.4732D-01	-15.5	8.9003D-01
-14.0	8.9092D-01	-12.5	9.3957D-01	-11.0	5.7653D-01	-9.5	5.6917D-01	-8.0	6.1614D-01	-6.5	6.4748D-01	-5.0	6.7055D-01
-3.5	7.9687D-01	-2.2	1.0310D 00	-1.5	0.0	-0.8	0.0	0.0	0.0	0.8	9.6927D-01	1.5	9.8526D-01
2.2	9.9377D-01	4.0	9.9904D-01	6.2	9.9990D-01	8.5	9.9999D-01						

Y= 1.40

-24.5	8.4998D-01	-23.0	8.9303D-01	-21.5	9.1252D-01	-20.0	9.4086D-01	-18.5	9.1291D-01	-17.0	8.9949D-01	-15.5	8.8645D-01
-14.0	6.0873D-01	-12.5	6.1174D-01	-11.0	6.2793D-01	-9.5	6.3251D-01	-8.0	6.5156D-01	-6.5	6.8777D-01	-5.0	7.2347D-01
-3.5	8.0113D-01	-2.2	8.5485D-01	-1.5	8.9359D-01	-0.8	9.2950D-01	0.0	9.5231D-01	0.8	9.7454D-01	1.5	9.8774D-01
2.2	9.9468D-01	4.0	9.9914D-01	6.2	9.9991D-01	8.5	9.9999D-01						

Y= 2.00

-24.5	9.0779D-01	-23.0	9.0152D-01	-21.5	8.5509D-01	-20.0	8.8812D-01	-18.5	8.6942D-01	-17.0	6.6815D-01	-15.5	6.4631D-01
-14.0	6.4577D-01	-12.5	6.6080D-01	-11.0	6.8326D-01	-9.5	6.9378D-01	-8.0	7.0754D-01	-6.5	7.4576D-01	-5.0	7.9514D-01
-3.5	8.3611D-01	-2.2	8.8823D-01	-1.5	9.1851D-01	-0.8	9.4332D-01	0.0	9.6525D-01	0.8	9.8104D-01	1.5	9.9043D-01
2.2	9.9568D-01	4.0	9.9926D-01	6.2	9.9992D-01	8.5	9.9999D-01						

Y= 2.60

-24.5	8.8539D-01	-23.0	9.1172D-01	-21.5	8.7174D-01	-20.0	7.1348D-01	-18.5	7.1319D-01	-17.0	6.8460D-01	-15.5	6.9315D-01
-14.0	7.0766D-01	-12.5	7.2756D-01	-11.0	7.2936D-01	-9.5	7.5926D-01	-8.0	7.9336D-01	-6.5	8.0803D-01	-5.0	8.3923D-01
-3.5	8.8641D-01	-2.2	9.2430D-01	-1.5	9.4517D-01	-0.8	9.6040D-01	0.0	9.7592D-01	0.8	9.8660D-01	1.5	9.9313D-01
2.2	9.9674D-01	4.0	9.9939D-01	6.2	9.9993D-01	8.5	1.0000D 00						

Y= 3.40

-24.5	8.7133D-01	-23.0	7.4462D-01	-21.5	7.4632D-01	-20.0	7.4730D-01	-18.5	7.5513D-01	-17.0	7.6757D-01	-15.5	7.8309D-01
-14.0	7.5865D-01	-12.5	7.8059D-01	-11.0	8.0590D-01	-9.5	8.3296D-01	-8.0	8.4773D-01	-6.5	8.7805D-01	-5.0	9.0859D-01
-3.5	9.3774D-01	-2.2	9.5946D-01	-1.5	9.7066D-01	-0.8	9.8000D-01	0.0	9.8728D-01	0.8	9.9250D-01	1.5	9.9590D-01
2.2	9.9791D-01	4.0	9.9957D-01	6.2	9.9995D-01	8.5	1.0000D 00						

Y= 4.60

-24.5	7.9959D-01	-23.0	8.0649D-01	-21.5	8.1776D-01	-20.0	8.3147D-01	-18.5	8.4646D-01	-17.0	8.2678D-01	-15.5	8.4546D-01
-14.0	8.6471D-01	-12.5	8.8073D-01	-11.0	8.9976D-01	-9.5	9.1812D-01	-8.0	9.3534D-01	-6.5	9.5116D-01	-5.0	9.6524D-01
-3.5	9.7727D-01	-2.2	9.8545D-01	-1.5	9.8945D-01	-0.8	9.9270D-01	0.0	9.9522D-01	0.8	9.9704D-01	1.5	9.9827D-01
2.2	9.9904D-01	4.0	9.9977D-01	6.2	9.9997D-01	8.5	1.0000D 00						

Y= 6.50

-24.5	8.8217D-01	-23.0	8.9414D-01	-21.5	9.0738D-01	-20.0	9.2051D-01	-18.5	9.3312D-01	-17.0	9.4477D-01	-15.5	9.5522D-01
-14.0	9.6435D-01	-12.5	9.7211D-01	-11.0	9.7849D-01	-9.5	9.7272D-01	-8.0	9.7931D-01	-6.5	9.8490D-01	-5.0	9.8954D-01
-3.5	9.9326D-01	-2.2	9.9568D-01	-1.5	9.9684D-01	-0.8	9.9777D-01	0.0	9.9850D-01	0.8	9.9903D-01	1.5	9.9940D-01
2.2	9.9965D-01	4.0	9.9990D-01	6.2	9.9999D-01	8.5	1.0000D 00						

Y= 8.75

-24.5	9.5989D-01	-23.0	9.6570D-01	-21.5	9.7149D-01	-20.0	9.7675D-01	-18.5	9.8133D-01	-17.0	9.8523D-01	-15.5	9.8851D-01
-14.0	9.9121D-01	-12.5	9.9341D-01	-11.0	9.9517D-01	-9.5	9.9654D-01	-8.0	9.9760D-01	-6.5	9.9839D-01	-5.0	9.9896D-01
-3.5	9.9936D-01	-2.2	9.9960D-01	-1.5	9.9971D-01	-0.8	9.9979D-01	0.0	9.9985D-01	0.8	9.9990D-01	1.5	9.9993D-01
2.2	9.9996D-01	4.0	9.9999D-01	6.2	1.0000D 00	8.5	1.0000D 00						

Y= 11.00

-24.5	9.9134D-01	-23.0	9.9276D-01	-21.5	9.9414D-01	-20.0	9.9536D-01	-18.5	9.9638D-01	-17.0	9.9722D-01	-15.5	9.9790D-01
-14.0	9.9844D-01	-12.5	9.9887D-01	-11.0	9.9919D-01	-9.5	9.9944D-01	-8.0	9.9962D-01	-6.5	9.9975D-01	-5.0	9.9984D-01
-3.5	9.9990D-01	-2.2	9.9994D-01	-1.5	9.9996D-01	-0.8	9.9997D-01	0.0	9.9998D-01	0.8	9.9998D-01	1.5	9.9999D-01
2.2	9.9999D-01	4.0	1.0000D 00	6.2	1.0000D 00	8.5	1.0000D 00						

6 MAJOR ITERATES COMPLETED.

REFERENCES

1. F.S. Johnson, Ed., Satellite Environment Handbook, (Stanford University Press, Stanford, California, 1965).

2. Ya.L. Al'pert, A.V. Gurevich, and L.P. Pitaevskii, Space Physics with Artificial Satellites (Consultants Bureau, New York, 1965).

3. H.A. Taylor Jr., H.C. Brinton, M.W. Pharo III, and N.K. Rahman, "Thermal Ions in the Exosphere", J. Geophys. Res. 73, 5521 (1968).

4. H.G. Mayr, L.H. Brace, and G.S. Dunham, "Ion Composition and Temperature in the Topside Ionosphere", J. Geophys. Res. 72, 4391 (1967).

5. S.A. Schaaf and P.L. Chambré, Flow of Rarefied Gases, (Princeton University Press, Princeton, New Jersey 1961).

6. Y.S. Pan, and R. Vaglio-Laurin, "Trail of an Ionospheric Satellite I, AIAA J. 5, 1801 (1967).

7. R. Jastrow and C.A. Pearse, "Atmospheric Drag on the Satellite", J. Geophys. Res. 62, 413 (1957).

8. R. E. Kiel, F.C. Gey, and W.A. Gustafsen, "Electrostatic Potential Fields of an Ionospheric Satellite", AIAA J. 6, 690 (1968).

9. U. Samir and A.P. Willmore, "The Equilibrium Potential of a Spacecraft in the Ionosphere", Planet. Space Sci. 14, 1131 (1966).

10. C.K. Chu and R.A. Gross, "Alfvén Waves and Induction Drag on Long Cylindrical Satellites", Columbia University, New York, Plasma Laboratory Report 25 (1965).

11. U. Samir and A. P. Willmore, "The Distribution of Charged Particles Near a Moving Spacecraft", Planet. Space Sci. 13, 285 (1965).

12. S. Chapman and T.G. Cowling, The Mathematical Theory of Non-Uniform Gases, (Cambridge University Press, London, 1960).

13. D.B. Beard and F.S. Johnson, "Charge and Magnetic Field Interaction with Satellites", J. Geophys. Res. 65, 1 (1960).

14. S.D. Drell, H.M. Foley, and M.A. Ruderman, "Drag and Propulsion of Large Satellites in the Ionosphere", Phys. Rev. Letters 14, 171 (1965).

15. F. Hohl and G.P. Wood, "The Electrostatic and Electromagnetic Drag Forces on a Spherical Satellite in a Rarefied Partially Ionized Atmosphere", in Rarefied Gas Dynamics, J.A. Laurmann, Ed. (Academic Press, Inc., New York, 1963), Vol. II, p. 45.

16. L.W. Parker, "Analytic and Computer Studies of Electron Collection by a Spherical Satellite in the Earth's Magnetic Field", NASA Contract Report 618 (1966).

17. J.J. Shea, "Collisionless Plasma Flow Around a Conducting Sphere in a Magnetic Field", in Rarefied Gas Dynamics, C.L. Brundin, Ed. (Academic Press, Inc., New York, 1967), Vol. II, p. 1671.

18. A.H. Davis and I. Harris, "Interaction of a Charged Satellite with the Ionosphere", in Rarefied Gas Dynamics, L. Talbot, Ed. (Academic Press, Inc., New York, 1961), p. 691.

19. S.H. Lam and M. Greenblatt, "On the Interaction of a Solid Body with a Flowing Collisionless Plasma", Gas Dynamics Laboratory, Princeton University, Princeton, New Jersey, Report 699 (1965).

20. S.H. Lam and M. Greenblatt, "Flow of a Collisionless Plasma Over a Cone", AIAA J. 3, 1850 (1965).

21. M.V. Maslennikov and Yu.S. Sigov, "A Discrete Model for the Study of the Flow of a Rarefied Plasma About a Body", Dokl. Akad. Nauk SSSR 159, 1013 (1964), [English transl.: Soviet Phys.—Doklady 9, 1063 (1965)].

22. M.V. Maslennikov and Yu.S. Sigov, "Discrete Model of Medium in a Problem on Rarefied Plasma Stream Interaction with a Charged Body", in Rarefied Gas Dynamics, C.L. Brundin, Ed. (Academic Press, Inc., New York, 1967), Vol. II, p. 1657.

23. M.V. Maslennikov, Yu.S. Sigov, and G.P. Churkina, "Numerical Experiments for Objects of Various Form in a Flowing Rarefied Gas", Kosmicheskie Issledovaniya 6, 220 (1968).

24. R.W. Hockney, "Computer Experiment of Anomolous Diffusion", Phys. Fluids 9, 1826 (1966).

25. R.P. Wadhwa, O. Buneman, and D.F. Bauch, "Two-Dimensional Computer Experiments of Ion-Beam Neutralization", AIAA J. 3, 1076 (1965).

26. L.W. Parker, "Theory of Electrostatic Planar and Spherical Probes", Mt. Auburn Research Associates, Inc., Cambridge, Mass., Technical Report No. 3-16-66(LWR-TR) (1966).

27. L.W. Parker, "A Computer Program for Calculating Charge Distribution about a Space Vehicle", NASA Contract Report 401 (1966).

28. J.C. Taylor, "Disturbance of a Rarefied Plasma by a Supersonic Body on the Basis of the Poisson-Vlasov Equations, I — The Heuristic Method", Planet. Space Sci. 15, 155 (1967).

29. J.C. Taylor, "Disturbance of a Rarefied Plasma by a Supersonic Body on the Basis of the Poisson-Vlasov Equations, II — The Formal Method", Planet. Space Sci. 15, 463 (1967).

30. R.S. Varga, Matrix Iterative Analysis, (Prentiss-Hall, Englewood Cliffs, New Jersey, 1962).

31. J.W. Cooley and J.W. Tukey, "An Algorithm for the Machine Calculation of Complex Fourier Series", Math. Comput. 19, 297 (1965).

32. W.A. Clayden and C.V. Hurdle, "An Experimental Study of Plasma-Vehicle Interaction", in Rarefied Gas Dynamics, C.L. Brundin, Ed. (Academic Press, Inc., New York, 1967), Vol. II, p. 1717.

33. W.C. Pitts and E.D. Knechtel, "Experimental Investigation of Electric Drag on Satellites", Aerospace Sciences Meeting, New York, AIAA Preprint 64-32 (1964).

34. S.D. Hester and A.A. Sonin, "Some Results from a Laboratory Study of Satellite Wake Structure and Probe Response in Collisionless Plasma Flows", (to be published).

35. Yu. M. Kagan and V.I. Perel', "Probe Methods in Plasma Research", Usp. Fiz. Nauk 81, 409 (1963), [English transl.: Soviet Phys. — Usp. 6, 767 (1964)].

36. K.M. Watson, "Use of the Boltzmann Equation for the Study of Ionized Gases of Low Density", Phys. Fluids 102, 12 (1956).

37. P.T. Kirstein, G.S. Kino, and W.E. Waters, Space-Charge Flow, (McGraw-Hill Book Co., Inc., New York, 1967), Chap. 8.

38. L.W. Parker, "Boundary Conditions and Iterative Procedures for Plasma Sheath Problems", (to be published).

39. G.K. Medicus, "Theory of Electron Collection of Spherical Probes", J. App. Phys. 32, 2512 (1961).

40. C.L. Brundin, "Effects of Charged Particles on the Motion of an Earth Satellite", AIAA J. 1, 2529 (1963).

41. A.A. Sonin, "The Free Molecule Langmuir Probe and Its Use in Flow Field Studies", Aerospace Sciences Meeting, New York, AIAA Paper 66-5 (1966).

42. E.D. Knechtel and W.C. Pitts, "Experimental Momentum Accommodation on Metal Surfaces of Ions Near and Above Earth-Satellite Speeds", (to be published).